MODELING AND HISTOGENESIS OF SOFT TISSUE SARCOMAS ASSOCIATED WITH P53 AND RB DEFICIENCY

A Dissertation

Presented to the Faculty of the Graduate School

of Cornell University

In Partial Fulfillment of the Requirement for the Degree of

Doctor of Philosophy

by

Jin Hyang Choi

May 2010

MODELING OF AND HISTOGENESIS OF SOFT TISSUE SARCOMAS ASSOCIATED WITH P53 AND RB DEFICIENCY

Jin Hyang Choi, Ph. D.

Cornell University 2010

Human soft tissue sarcomas (STS), particularly their most common type, undifferentiated pleomorphic sarcoma (UPS), also known as malignant fibrous histiocytoma (MFH), frequently carry mutations in *P53* and *RB* tumor suppressor genes. We have established mouse model of STS by using Cre-*loxP*-mediated conditional inactivation of *p53* and *Rb* tumor suppressor genes in the connective tissue cells of the dermis. Similar to human STS, the majority of sarcomas in this model are UPS and overexpress Cxcr4, which contributes to their invasive properties. By using irradiation chimeras that have been generated by transplanting bone marrow cells from mice carrying the *Rosa26Stop*^{loxP}*LacZ* or the *Z/EG* reporter, as well as floxed *p53* and *Rb* genes, to irradiated *p53*$^{loxP/loxP}$*Rb*$^{loxP/loxP}$ mice, we have determined that sarcomas originate from the local resident cells. Notably, isolated mesenchymal multipotent cells characterized by strict plastic adherence and low levels of Sca-1 expression have shown enhanced potential for malignant transformation according to invasion, soft agar and tumorigenicity assay following conditional inactivation of *p53* and *Rb*. Taken together, our results indicate that local Sca-1^{low} dermal mesenchymal stem/progenitor cells may be a preferential target for malignant transformation associated with *p53* and *Rb* deficiency.

As the next step towards imaging of STS formation, we have evaluated applicability of highly fluorescent core-shell silica nanoparticles, known as C dots, for *in vivo* applications. We have demonstrated C dots are not toxic and can be used in a

broad range of imaging applications including intravital visualization of capillaries and macrophages, sentinel lymph node mapping, and peptide-mediated multi-color cell labeling for real-time imaging of tumor metastasis and tracking of injected bone marrow cells in mice. These results demonstrate that fluorescent core-shell silica nanoparticles represent a powerful novel imaging tool within the field of nanomedicine and will be invaluable for future studies of STS pathogenesis.

BIOGRAPHICAL SKETCH

The author was born and raised in Korea. Her childhood was spent living in Daegu, Korea. In 1997, she graduated from high school and entered Kyungpook National University in Daegu, Korea with major in Veterinary Medicine. In 2001, the author graduated with a Bachelor of Science degree and a Doctor of Veterinary Medicine and then entered Seoul National University in Seoul, Korea with major of Biochemistry in a Master of Sciences program. After finishing her coursework in M.S. program in 2003, the author received a scholarship to study abroad for 1 year from BK21 program in Korea. With this program, she came to USA and joined the laboratory of Dr. Alexander Yu. Nikitin, who works on modeling and targeting cancer associated with deficiency for *p53* and *Rb* tumor suppressor genes in genetically modified mice in the Department of Biomedical Sciences, College of Veterinary Medicine at Cornell University. After receiving her M.S. in Biochemistry in 2004, Dr. Choi continued her work in the laboratory of Dr. Nikitin and enrolled into the Ph. D program at Cornell University in the field of Comparative Biomedical Sciences in 2005. Her project is mainly focused on studying pathogenesis of soft tissue sarcomas.

ACKNOWLEDGMENTS

I would like to express my appreciation to my adviser, Dr. Alexander Yu. Nikitin for accepting and supporting me during my studies in his laboratory at Cornell University for the past seven years. In particular, I want to thank him for his intellectual guidance and unfailing encouragement throughout my study and for training me as an independent researcher which I believe would be especially helpful my future career.

I am also grateful to other members of my thesis committee, Dr. Tudorita Tumbar, Dr. Warren R. Zipfel, and Dr. Robert S. Weiss for their full support for my study. Their achievements and spirit in science have been ironed in my mind to idolize.

I would also like to thank Dr. Ulrich Wiesner and Andrew A. Burns for their kind cooperation in our study of core-shell silica nanoparticles (C dots). I want to thank Dr. Rebecca M. Williams for her support of our study of C dots.

I am thankful to Stephen J. Curtis and David M. Roy, undergraduate students who worked with me, for their help in my project. I want to thank my colleagues, Dr. Zongxiang Zhou, Andrea Flesken-Nikitin, Dave Corney, Le Chang, Dr. Chang-il Hwang for their advice, help and collaboration of my project. I would also like to thank all past and current members of the Nikitin laboratory, including Chieh-Yang Cheng, Gaofeng Jiang, and Urmi Chatterji for their friendship, help and cooperation.

I would also like to thank Dr. Mun Han Lee in College of Veterinary Medicine, Seoul National University for his generous support during my externship period in Cornell University.

Finally, I want to thank my parents and my brothers for their love and support. They have always been, and will continue to be a source of courage to me.

TABLE OF CONTENTS

Biographical Sketch		iii
Acknowledgement		iv
Table of Contents		v
List of Figures		vi
List of Tables		viii
Chapter 1	Introduction	1
	1.1 Soft tissue sarcoma	2
	1.2 Role of CXCR4 expression in sarcomas	7
	1.3 Cellular origin of soft tissue sarcomas and mesenchymal stem cell	8
	1.4 The status of animal sarcoma model	14
	1.5 Fluorescence nanoparticles as tools for biomedical imaging	18
	1.6 Project overview	20
	1.7 References	22
Chapter 2	Local mesenchymal stem/progenitor cells are a preferential target for initiation of adult soft tissue sarcomas associated with p53 and Rb deficiency	
	2.1 Abstract	35
	2.2 Introduction	36
	2.3 Material and Methods	38
	2.4 Results	47
	2.5 Discussion	70
	2.6 References	78
Chapter 3	Core-shell silica particles as fluorescent labels for nanomedicine	
	3.1 Abstract	90
	3.2 Introduction	90
	3.3 Material and Methods	94
	3.4 Results	100
	3.5 Discussion	111
	3.6 References	116
Chapter 4	Conclusion and future prospects	
	4.1 Mouse model of soft tissue sarcoma and its applications for histogenesis and pathogenesis studies	122
	4.2 Applications of core-shell silica nanoparticles in biomedicine and for in vivo imaging study of sarcoma origin	126
	4.3 References	129

LIST OF FIGURES

Figure 1.1	Cancer stem cell hypothesis	13
Figure 1.2	Structure of the floxed alleles of *p53* and *Rb* genes	17
Figure 2.1	Induction of soft tissue sarcomas by conditional inactivation of *p53* and/or *Rb*	48
Figure 2.2	Characterization of soft tissue sarcomas	51
Figure 2.3	CXCR4 overexpression contributes to invasive properties of STS	54
Figure 2.4	Identification of connective tissue cells infected with Ad*CMVCre-EGFP* adenovirus	59
Figure 2.5	Identification of soft tissue sarcomas cellular origin in irradiation chimeras	61
Figure 2.6	Assessment of bone marrow rescue in irradiation chimeras	62
Figure 2.7	Detection of bone-marrow derived cells in soft tissue sarcomas	65
Figure 2.8	Neoplastic potential of dermal mesenchymal stem cells (MSC) after conditional inactivation of p53 and Rb	68
Figure 2.9	EGFP and Sca-1 expression in one week cultured murine dermal cells after adenovirus-induced EGFP expression	74
Figure 3.1	C dot core-shell fluorescent silica nanoparticles	93
Figure 3.2	Biodistribution of C dots following tail vein injection	101
Figure 3.3	Concentration dependent biodistribution of C dots injected Intravenously	102
Figure 3.4	Time dependent biodistribution of 30 nm C dot in the liver after intravenous injection	103
Figure 3.5	Labeling of capillaries and macrophage and sentinel lymph node mapping	104
Figure 3.6	The stability of C dot fluorescence intensity	105
Figure 3.7	Sentinel lymph node mapping with C dots	107

Figure 3.8 Labeling and tracing cells with C dots 109

LIST OF TABLES

Table 2.1	Soft tissue sarcomas induced by a single subcutaneous administration of Ad*CMVCre* into mice carrying floxed *p53* and/or *Rb*	49
Table 2.2	Expression of CXCR4 in human soft tissue tumors	56
Table 2.3	Percentage of EGFP-expressing cells in dermal cells populations 3 days after Ad*CMVCre-eGFP* infection	58

CHAPTER 1

Introduction

I attempted to develop a mouse model of soft tissue sarcoma (STS) associated with inactivation of *p53* and *Rb*, tumor suppressor genes. Since p53-deficient mice succumb to rapidly progressing lymphomas and germline biallelic inactivation of *Rb* cause embryonic lethality, I used a conditional inactivation of *p53* and/or *Rb* by a single subcutaneous injection of adenovirus carrying Cre-recombinase into adult genetically modified mice with floxed copies of *p53* and/or *Rb* genes in order to induce a development of sarcomas. I characterized induced STS and evaluated their cellular origin with a particular attention to mesenchymal stem cells. Next, I focused on a development of biomedical tools for future studies of STS origin and pathogenesis with recently introduced silica nanoparticles, C dots. Towards visualizing sarcoma development, I tested toxicity of C dots in cell culture and *in vivo* and evaluated several possible applications of these particles for future biological and biomedical studies.

In this chapter, I will describe the current status of soft tissue sarcomas including their definitions, common genetic alterations, presumed histogenesis and treatment. I will describe in detail the mesenchymal origin hypothesis in STS and increasing evidence supporting this hypothesis. Additionally, I will outline a current mouse model of STS and discuss the advantage of our mouse model induced by an inactivation of two major tumor suppressor genes, *p53* and *Rb*, as compared with other models. Following these, C dots will be introduced as a new useful biomedical tool for a rapidly increasing field of nanobiotechnology. Finally, I will provide my conclusions about project and outline future directions.

1.1 Soft tissue sarcoma

Sarcomas are a large heterogeneous group of rare tumors that arise from derivates of mesenchymal tissues, which are derived from embryonic mesoderm with some contribution of neuroectoderm. They may occur anywhere in the body and at any age. Sarcomas include such types as bone sarcoma, Ewing's sarcoma, peripheral primitive neuroectodermal tumors, and soft tissue tumors, which are the most frequent. Soft tissues sarcomas (STS) are malignant neoplasms arising from nonepithelial and extraskeletal tissues, such as connective tissue, muscles, vessels and peripheral nerves. STS are classified on a histogenetic basis according to the adult tissue they resemble. Within the various histogenetic categories, soft tissue tumors are usually divided into benign and malignant forms. Benign tumors more closely resemble normal tissue and have a limited capacity for autonomous growth. They exhibit little tendency to invade locally and are characterized by a low rate of local recurrence following conservative therapy. On the other hand, malignant tumors, or sarcomas, are locally aggressive and are capable of invasion or destructive growth, recurrence, and distant metastasis (Enzinger and Weiss, 2001). Currently, more than 50 histologic groups of STS have been identified, with the most common type being undifferentiated high grade pleomorphic sarcoma (UPS), also known as malignant fibrous histiocytoma (MFH) in adults and a rhabdomyosarcoma in childhood (Cormier and Pollock, 2004). In 2009, new estimated STS diagnosed account for less than 1% of all cancers (Jemal et al., 2009). Diagnosis and treatment of STS have been challenging due to their rarity and diversity in genetics and phenotypes.

The etiology and pathogenesis of most STS are still poorly understood. Recognized causes include various physical and chemical factors, exposure to ionizing radiation, and inherited or acquired immunologic defects. Evaluation of the exact cause is often difficult because of the long latent period between the time of exposure

and the development of sarcoma, as well as the possible effect of multiple environmental and hereditary factors during the induction period.

Development of a useful, comprehensive histology classification of STS has been a relatively slow process. Until recently, the clinical importance of histological typing and subtyping of STS was minor, and their treatment depended more on grade, stage, and technical considerations in relation to the site. In some case, like fibrosarcomas, haemangiopericytomas, and MFH, poorly defined entities had a tendency to become diagnostic 'waste baskets'. The clinical management of these tumors was independent of their subclassification. However, with the advance in immunohistochemical (IHC) applications and the accumulating knowledge of molecular mechanisms of growth and oncogenesis, new treatment strategies are gradually becoming possible. The new WHO classification represents a summary of recent pathobiological advances and provides a new baseline for a clinical as well as laboratory research (Daugaard, 2004). In this classification, the importance of correct histotyping has been recognized by the incorporation of IHC into the diagnostic criteria, and in many cases cytogenetic data has also been included. For example, in the case of MFH, except the myxoid form, it is now considered to be 'undifferentiated pleomorphic sarcomas (UPS)' based on the absence of their characteristic IHC profile and specific cytogenetic aberrations. The myxoid MFH is synonymous with myxofibrosarcoma. The term of MFH was first proposed from an observation that cultured fibroblast adopted phagocytic qualities resembling histiocytes (Kauffman and Stout, 1961; O'Brien and Stout, 1964; Ozzello et al., 1963). However, this diagnostic category had brought many questions and considerations from following a careful analysis of tumors identified as MFH. The term UPS has remains of questionable validity and usefulness as a diagnostic category (Adrien et al., 2009).

The management of newly diagnosed sarcomas is complicated. The current treatment of sarcomas generally involves surgery in parallel with radiotherapy and chemotherapy dependent upon demands. Although surgical excision remains the dominant curative therapy, it has a blurry line between unresectable and resectable sarcomas. Radiation can be effective treatment to decrease local recurrence of STS. However, it is not surprising that many important issues are under debate. Those issues concern the relative merits of preoperative versus postoperative radiotherapy and a multitude of side effects. Overall, chemotherapy has been relatively unsuccessful for treating sarcomas. Use of doxorubicin or ifosfamide remains controversial because of the toxicity. Decision-making is more difficult in tumors considered high risk. The timing and order of wide local resection, preoperative or postoperative radiotherapy, and preoperative or postoperative chemotherapy require a multidisiciplinary approach. While advances have been made, the treatment of STS still has much room for improvement (Steen and Stephenson, 2008).

A variety of genetic alterations, which involve three broad types of cancer genes; oncogenes, tumor suppressor genes, and caretaker genes, occurs in the development of sarcomas. Currently, sarcomas can be separated into two classes by genetic analysis: one comprises of tumors that display multiple complex karyotypic abnormalities with no specific pattern: the other is composed of tumors that harbor relatively simple genetic mutations believed to underlie their pathogenesis. A majority of sarcomas including osteosarcoma, UPS, liposarcoma (other than myxoid type), angiosarcoma, leiomyosarcoma, fibrosarcoma and skeletal chondrosarcoma belonged to the first group. Mutations in oncogenes that are altered by gene amplification, translocation, or by a combination of both, may lead to sarcoma development. For examples, alterations in KIT and PDGFRA activated by mutations have been observed in gastrointestinal stromal tumor (GIST) (Helman and Meltzer, 2003). Translocations

that fuse the coding sequences of two genes to generate chimeric proteins are generally considered a special variety of oncogene, known as fusion oncogenes, of which there are numerous examples in sarcomas. Examples are representatively a EWS-FLI1 fusion in Ewing sarcoma, a PAX3-FKHR or PAX7-FKHR fusion in alveolar rhabdomyosarcomas, a FUS-CHOP or EWS-CHOP fusion in myxoid/round cell liposarcomas, and SYT-SSX1 or SYT-SSX2 fusion in synovial sarcomas (Enzinger and Weiss, 2001).

Mutations and deletions in two major tumor suppressor genes, *P53* and *RB*, are the most common genetic alteration in human STS (Cormier and Pollock, 2004). Mutations of *RB*, the first tumor suppressor gene, have been found in both inherited and sporadic retinoblastomas, which increase the risk of developing sarcomas later in life. RB is a regulator of cell proliferation which acts by binding to proteins of the E2F family of transcriptional factors that promote transition from the G1 phase to the S phase of the cell cycle (Classon and Harlow, 2002). Phosphorylation of the RB protein, which is critical for regulation of its function, is mediated by cyclin/cyclin dependent kinase (CDK) complexes (Hakem and Mak, 2001). *Rb* null mice die between days 13 and 15 of gestation, with pronounced defects in erythroid, neuronal, lens and placental development, as well as skeletal muscle defects (Chau and Wang, 2003). Although no retinoblastomas develop in mice with targeted disruption of one copy of *Rb*, mice that are heterozygous for *Rb* show an increased predisposition to multiple neuroendocrine neoplasms (Nikitin et al., 1999; Nikitin and Lee, 1996). Deletions of *RB* and its loss-of-function mutations have been extensively documented in familial and sporadic retinoblastomas and sporadic osteosarcomas. Loss of *RB* or alterations in RB pathway proteins is frequently observed in various sarcomas (Cohen and Geradts, 1997; Sabah et al., 2006; Scambia et al., 2006), including MFH/UPS (Chibon et al., 2000).

P53 is the most commonly mutated gene in human cancers (Hakem and Mak, 2001). Inherited *P53* mutations are associated with Li-Fraumeni syndrome, which is characterized by an increased risk for breast and lung carcinomas, soft tissue sarcomas, brain tumors, oesteosarcomas, and leukemia. Binding of MDM2 to P53 leads to P53 degradation and loss of activity. Once P53 is activated by mitogenic signals mediated through deregulated Myc, Ras, or E2F1, or DNA damages that involves the regulatory kinase ATM, CHK2, and ATR, P53 regulates multiple important cellular pathways such as cell cycle, apoptosis, and differentiation (Hakem and Mak, 2001). Additionally, P53 controls the G1 checkpoint of the cell cycle by inducing transcription of the cyclin/CDK inhibitor P21, and indirectly the G2 checkpoint by regulating expression of P21 and the protein 14-3-3σ. Mice bearing null mutations of *p53* appear normal, but are prone to the spontaneous development of a variety of neoplasms, particularly lymphomas, by 6 months of age (Donehower et al., 1992). Likewise, $p53^{+/-}$ mice are predisposed to carcinogenesis. These animals remain cancer-free for the first 9 months but about half go on to develop osteosarcomas, soft tissue sarcomas, and lymphomas by 18 months of age. Patients with Li-Faumeni syndrome have a 50% increase in the incidence of tumors by the age of 30, which is comparable to the tumor incidence in middle-aged (18 month) $p53^{+/-}$ mice. Mutations of *p53* has been observed in 30% to 60% of soft tissue sarcomas (Cormier and Pollock, 2004; Latres et al., 1994). Additionally, *MDM2* amplification has been observed as alternative to p53 alteration in many sarcomas (Leach et al., 1993). Since mutant p53 protein is expressed in some grade I STS, it has been suggested that its expression could have significant translational value as a selection criteria for the optimal treatment of sarcoma patients (Hieken and Das Gupta, 1996).

A cooperative effect on transformation between *P53* and *RB* mutations has been reported in several human cancers including sarcomas. Alterations in both *P53*

and *RB* have been shown in leiomyosarcomas, UPS, and rhabdomyosarcomas (Stratton MR, 1990). It is likely that patients with sarcomas carrying both *P53* and *RB* alterations have poorer prognosis as compared to those with STS with an alteration in one of those genes (Scambia et al., 2006). Based on the fact that human osteosarcomas contain mutations in both *P53* and *RB*, an osteosarcoma mouse model was developed which is based on inactivation of *p53* and *Rb* (Berman et al., 2008; Walkley et al., 2008). Recently, similar cooperation between *p53* and *Rb* inactivation in acceleration of osteosarcomas and some STS was observed after expression of *Prx1-Cre* in the early mesenchymal tissues of embryonic limb bud (Lin et al., 2009). However, given that the majority of human STS, including UPS develop in late adulthood, this model does not represent adequate approach for studies of pathogenesis of adult STS.

1.2 Role of CXCR4 expression in sarcomas

Recently, it has been reported that the expression of chemokine receptor CXCR4 in human STS is associated with poor prognosis and metastasis (Oda et al., 2009), particularly in malignant non-round cell tumors such as UPS and leiomyosarcoma. Importance of CXCR4-SDF1α signaling for cancer progression and metastasis has been reported for a number of human cancers. Human breast cancer cells produce high level of functionally active CXCR4, and their distinct *in vivo* distribution was observed in organs representing the main sites of breast cancer metastasis (Muller et al., 2001). Furthermore, carcinoma-associated fibroblasts (CAFs) located in between breast cancer cells, which have CXCR4, play an central role in promoting the growth of tumor cells through secretion of CXCR4 lignad SDF1α. CAFs producing SDF1α directly stimulates CXCR4-expressing tumor growth or promotes angiogenesis by recruiting endothelial progenitor cells into carcinomas (Orimo et al., 2005). Prostate cancer cells expressing CXCR4 were observed

migrating across bone marrow endothelial cell monolayers in response to SDF1α (Taichman et al., 2002). These observations indicate that CXCR4-SDF1α signaling is involved in prostate cancer bone metastasis. Additionally, high expression of CXCR4 is correlated with poor prognosis in several types of cancer, including pancreatic adenocarinoma (Marechal et al., 2009).

There are very few studies of CXCR4-SDF1α signaling in sarcomas. These studies focused on role of CXCR4 in metastasis of rhabdomyosarcomas. It has been demonstrated that rhabdomyosarcoma cells have increased metastasis-associated properties, such as locomotion, chemotaxis, and adhesion after stimulation by SDF1α in cell culture (Libura et al., 2002; Strahm et al., 2008).

Importantly, p53 has been shown to repress CXCR4 expression (Mehta et al., 2007). While p53 mutants have failed to repress CXCR4 promoter activity, rescuing of p53 deficient breast cancer cells with wild type p53 has reduced CXCR4 expression. Given frequent occurrence of p53 mutations in STS, these results may begin to provide a mechanistic link between p53 and CXCR4 overexpression in human STS.

1.3 Cellular origin of soft tissue sarcomas and a mesenchymal stem cell

The relative rarity of STS and diversity of their histology have hindered the identification of the cellular origin of STS and complicated development of rational therapeutic approaches. However, because of resemblances to tissues of mesenchymal origin, it has been postulated that STSs are derived from mesenchymal stem cells (MSC) or mesenchymal progenitor cells committed to specific cell lineages (Mackall et al., 2002). The lineage of committed cells belongs to the spectrum of specialized mesenchymal tissues including bone, cartilage, muscle, bone marrow, tendon, ligament, fat and other connective tissues like dermis (Caplana and Bruder, 2001).

MSC were isolated from various human adult tissues, including lung, skin, umbilical cord, and amniotic membrane, as a distinct population of primary fibroblast-like cells. These fibroblast-like cells can be cultured and are able to differentiate into at least one mesenchymal lineage, such as osteoblasts, chondrocytes, and adipocytes *ex vivo* (Sudo et al., 2007). Recently, it has been additionally reported that pericytes located in multiple human organs including skeletal muscle, pancreas, adipose tissue, and placenta may be a source of MSC (Crisan et al., 2008).

There is an increasing number of studies that support sarcoma derivation from MSC. For example, *ex vivo*-expanded MSC formed sarcomas in the tail, limb, and lung after intravenous injection into irradiated mice (Tolar et al., 2007). In addition, long cultured MSC spontaneously transformed and formed complex STS when injected subcutaneously into mice (Li et al., 2007). Similarly, sarcomas have arisen after MSC/bioscaffold constructs were planted into syngenic or immunodeficient recipients (Tasso et al., 2009). In this model, the bioscaffold provided a three-dimensional support for MSC to aggregate, thus producing the stimulus for triggering the process eventually leading to the transformation of surrounding cells and creating a surrogate tumor stroma.

Additional study has shown that MSC of adipose tissue deficient for *p21* and *p53* form fibrosarcomas with partial adipose differentiation when injected in immunodeficient mice either subcutaneously or intrafemorally (Rodriguez et al., 2009). The development of myxoid liposarcomas and Ewing sarcomas, characterized by the unique chromosomal translocation involving fusion proteins, FUS-CHOP and EWS-FLI1, respectively, were able to be induced by expression of those fusion proteins in MSC (Riggi et al., 2005; Riggi et al., 2006). Like these tumors, alveolar rhabdomyosarcoms develop in mice after xenografts of MSC carrying the PAX3-FKHR fusion proteins, although *p53* inactivation often occurs as a cooperative genetic

event (Charytonowicz et al., 2009; Ren et al., 2008). Loss of *p53* significantly impairs the differentiation of muscle progenitor cells and promotes rhabdomyosarcoma development in several oncogene-driven mouse tumor model (Stiewe, 2007). Furthermore, p53 family members have essential functions in the activation of RB during physiological myogenesis. These functions are commonly disabled in rhabdomyosarcoma patients, indicating that differentiation control is a critical tumor suppressor activity of the p53 family (Cam et al., 2006).

With poor characteristics and the lack of expression of phenotypic markers in undifferentiated pleomorphic sarcoma (UPS), also known as malignant fibrous histiocytoma (MFH), the origin of this sarcoma is still obscure. UPS is described as a heterogeneous sarcoma with pleomorphic histiocyte-like and fibroblast-like cells frequently arranged in a storiform pattern. These features led to debates about histiocyte, fibroblast, and MSC as potential cells of UPS/MFH origin. The derivation of histiocyte-like cells in UPS has been a matter of debate. Some initial studies based on observations after using human cells and tissues, as well as transplantation models have indicated that MFH could arise from the cells of the mononuclear phagocyte system, such as histocytes/macrophages (Binder et al., 1992; Hagari and Yumoto, 1987; Shirasuna et al., 1985; Strauchen and Dimitriu-Bona, 1986; Yamate et al., 1991; Yumoto and Morimoto, 1980). However, more recent studied have found no evidence of true histiocyte differentiation according to a number of experimental techniques, such as cell cultures, immunohistochemistry, and an electron microscopy and stage by stage studies of chemical carcinogenesis (Fu et al., 1975; Hoffman and Dickersin, 1983; Nikitin, 1993; Roholl et al., 1985; Takeya et al., 1995). These studies suggested that UPS is a sarcoma of either fibroblastic or primitive mesenchymal origin, which manifests both fibroblastic and histiocytic differentiation. For example, human UPS cells transplanted into mice developed a sarcoma including fibroblast-like cells from

human origin and histiocyte-like cells with positive expressions of mouse specific genes (Hatano et al., 1999). Recently, MSC has been favored as a cell of origin of UPS/MFH (Gazziola et al., 2003). Some researchers have suggested that UPS may have an origin from the perivascular mesenchymal cells that are supposed to have a potential for multidirectional differentiation. Monoclonal antibodies against whole cell antigens prepared from the established lines of human UPS recognized both perivascular MSC and UPS cells. At the same time, macrophages, monocytes and other blood cells showed negative immunostaining (Iwasaki et al., 1987). An approach using three-pair comparative mRNA profiling of bone marrow derived MSC and primary UPS cells showed the striking similarity in the gene expression patterns observed between MSC and MFH cells (Gazziola et al., 2003). Furthermore, comparative gene expression studies demonstrated similarities between UPS and hMSCs in such of stem-cell related properties as expression of DKK, a Wnt inhibitor, and absence of Wnt/β-catenin activity. hMSC immortalized with SV40 large T antigen were treated with recombinant DKK and injected subcutaneously into nude mice. These cells led to UPS development after subcutaneous injection into nude mice (Matushansky et al., 2007).

These results suggest that bone marrow MSC may be the cell of origin of some sarcomas, and that aberrant differentiation of MSC by molecular alteration may lead to the development of histologically diversified sarcomas. However, these studies were based on using MSC isolated from bone marrow cells. Recently, it has been shown that, according to cell lineage tracing experiments in irradiation chimeras, STS may arise from bone marrow-derived cells (Li et al., 2007). At the same time, no studies have yet demonstrated that STS, including UPS, develop from dermal MSC.

Recently, it has been postulated that cancers, whether solid or hematopoietic, contain cancer stem cells (CSC) or tumor-initiating cells that represent a

subpopulation of neoplastic cells that may be responsible for cancer initiation and/or progression (Cheng et al., 2009). CSC possess stem cell-like properties that include the active expression of telomerase and common stem cell genes, the activation of antiapoptotic pathways, and an increased ability to migrate and metastasize. Furthermore, CSC may remain relatively quiescent and have mechanisms enhancing their survival and multi-drug resistance, enabling them to evade traditional cancer therapies that target rapidly dividing cells (Cheng et al., 2009; Matoso and Nikitin, 2008).

The origin of CSC is still unknown. CSC may originate from mutated stem, transit-amplifying, or differentiated cells (Figure 1.1). It is also possible that the potential de-differentiation of mutated cells such that these cells acquire stem cell like characteristics. This possibility is often used as a potential alternative to any specific cell of origin, as it suggests that any cell might become CSC.

The histological diversity of sarcomas and lack of reliable markers have hindered identification of their CSC. Although recently CSC have been identified in Ewing's sarcoma (Suva et al., 2009) and embryonal rhabdomyosarcoma (Langenau et al., 2007), further studies to better identify them and understand the molecular basis of their activity are needed to develop novel therapies targeted against this critical subset of cancer cells. Connection between MSC and CSC in various sarcomas remains to be determined. Autochthonous mouse models of soft tissue sarcomas that permit the study of CSC are relatively underdeveloped. However, imitation of sarcomas by conditional gene inactivation, such as a model based on Cre-*loxP* mediated deletion of *p53* and activation of *K-ras (Kirsch et al., 2007),* is a welcome development. The generation of mouse models allowing selective targeting of either MSC or more differentiated transit-amplifying cells will eventually allow determining the role of mesenchymal stem cell compartment in sarcoma pathogenesis.

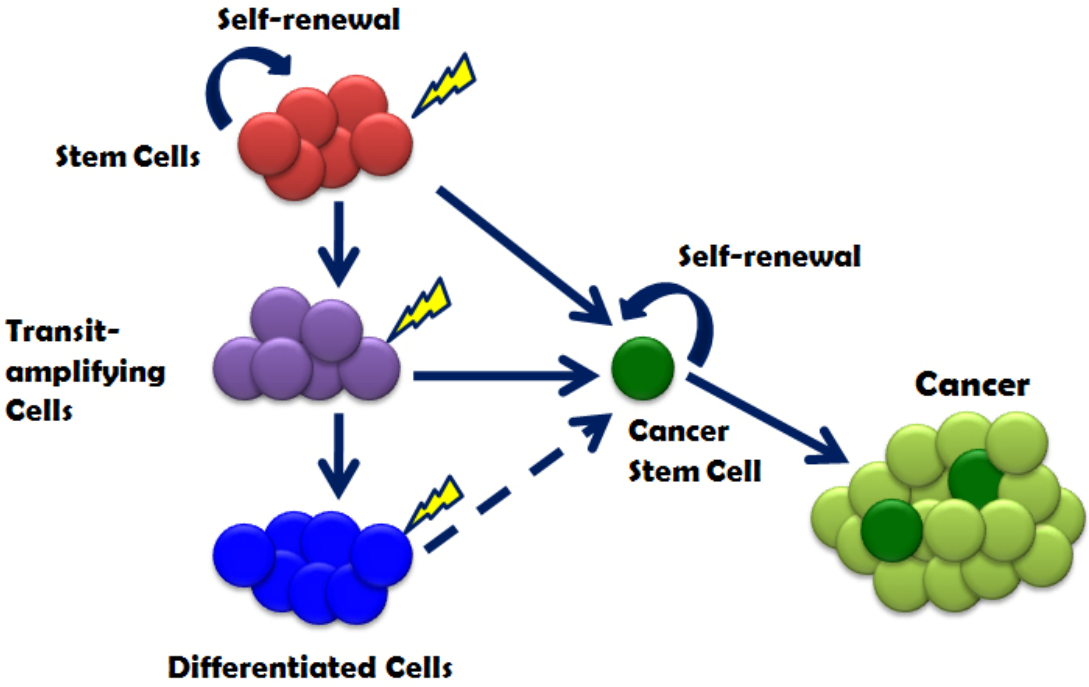

Figure 1.1. Cancer stem cell hypothesis. Cancer stem cells (CSC, dark green) have been defined as a very rare population of cells within tumors that are the only tumor cells with the capacity for limitless self-renewal. CSC may derive from mutations in stem cells (red), transit-amplifying cells (purple), and possibly even their differentiated cells (blue).

1.4 The status of animal sarcoma modeling

Animal models have been essential for determining mechanisms of human diseases, such as cancer, and for the design, characterization and evaluation of new therapeutic approaches (de Dios, 2002; Frese and Tuveson, 2007).

The earlier studies of STS histogenesis and pathogenesis were based on xenograft sarcoma models or models of sarcomagenesis induced by irradiation or chemical compounds. For example, xenografts of human cell lines were commonly used for studies of sarcoma progression in immunodeficient mice or nude rats (Maeda et al., 2008; Takeya et al., 1995; Tinkey et al., 1999; Zhang et al., 2000). Implantation of a 7, 12-dimethylbenz[α]anthracene (DMBA) into the subcutaneous tissue of rats or intramuscular injection of benzo[α]pyrene-oil mixture into rats have induced a development MFH (Nikitin, 1993; Richter KK, 1999). Furthermore, biomaterials, including polyvinyl alcohol (PVA) hydrogel, polyethylene, alphatic polyurethane, silicon, titanium, nickel chromium, cobalt-chromium alloy or aluminum oxide, been shown to induce MFH after subcutaneous implantation in rats (Kirkpatrick et al., 2000; Nakamura et al., 2001).

The manipulation of mouse genome with development of a broad variety of genetic tools has enhanced useful features of the mouse models with their original benefits, such as the small size and propensity to breed in captivity, relatively short lifespan of 3 years, physiological and genetic similarities with humans (Frese and Tuveson, 2007; Kile and Hilton, 2005; Rosenthal and Brown, 2007). Genetically modified mice provide the most sophisticated tools for modeling of cancer, and allow mimicking many pathophysiological and molecular features of human malignancies to a far greater extent than other experimental approaches, such as human xenografts and chemical and viral carcinogenesis. Importantly, methods for conditional control of gene functions, such as the Cre-*loxP* system, has offered an opportunity for

introduction of specific genetic alterations into living mice in temporal and spatial manner (Frese and Tuveson, 2007). Cre recombinase was originally isolated from bacteriophage P1. Cre recognizes the *loxP* site consisting of two inverted repeats of 13-bp flanking an asymmetric spacer region of 8-bp. The Cre enzyme efficiently catalyzes reciprocal conservative DNA recombination between pairs of loxP sites. Cre-mediated recombination between two directly repeated *loxP* sites results in excision of the DNA between them as a covalently closed circle (Pluck, 1996; Sauer, 1998).

About 20% of all sarcomas express recurrent or 'signature' genetic events, which include single chromosomal translocation (fusion gene) and specific point mutations (Riggi et al., 2007; Suva et al., 2007). There are several sarcoma mouse models generated transgenetically by expression of these fusion genes. For example, a mouse model of myxoid liposarcoma by expressing FUS-CHOP from the elongation factor 1α promoter in murine MSC has been developed (Perez-Losada et al., 2000). Using a conditional *PAX3-FOXO1A* knock-in allele targeted to terminally differentiating Myf6-expressing skeletal muscle, alveolar rhabdomyosarcoma developed at low frequency. Upon crossing these mice with p16INK4A/p19ARF deficient or *p53* conditional knock-out mice, the frequency of alveolar rhabdomyosarco formation was significantly enhanced (Keller et al., 2004; Keller and Capecchi, 2005). Similarly, the same sarcoma type was developed using conditional knock-in and knock-out techniques that were driven by the chromosomal translocation product, *Pax3:Fkhr* (Keller and Capecchi, 2005). Additionally, a synovial sarcoma model has been established recently using conditional expression of SS18-SSX2 in myoblast precursors. Beside fusion of genes, introduction of the *KIT* gene bearing the K641E point mutation into the germline has led to the development of both sporadic and familial gastrointestinal stromal tumors. Mice in this model show a phenotype that

reflects loss of KIT function, including loss of pigmentation, reduced numbers of dermal mast cells and sterility. The other GIST model, recently developed by expressing KIT bearing a mutation in exon 11 at V558, leads constitutive KIT activation in tumors resembled with human GIST (Riggi et al., 2007; Suva et al., 2007).

Modeling of sarcomas with complex genotypes, to which the majority of pleomorphic STS belong, has been far more challenging. Using Cre-*loxP* approach, high-grade sarcomas with myofibroblastic differentiation were initiated by intramuscular delivery of an adenovirus carrying Cre recombinase in mice with conditional mutations in *K-ras* and *p53* (Kirsch et al., 2007). However, since *Kras* mutations are not a common genetic alteration in STS (Yoo and Robinson, 1999), this model is not well suitable for elucidation of pathogenesis of common types of STS, including UPS. Thus development of a mouse model of adult STS associated with inactivation of common alterations, such as *p53* and *Rb* inactivation is of great importance.

Recently, mice carrying conditional *p53* alleles or *Rb* alleles were generated (Figure 1.2). Mice carrying *p53* alleles were generated by inserting *loxP* sites in intron 1 and intron 10 of the *p53* gene using a homologous recombination approach (Jonkers et al., 2001, Marino et al., 2000). $P53^{\Delta 2\text{-}10}$ mice, obtained after crossing with mice expressing *Cre* in the germ-line were showing the same tumor spectrum with conventional *p53* knockout mice (Jonkers et al., 2001; Marino, 2000; Schwenk et al., 1995). Mice carrying *Rb* alleles were generated using targeting vector in which two *loxP* sequences were inserted into the introns surrounding 19 of *Rb*. Excision of the region flanked by the *loxP* sites results in truncated Rb protein that is functionally equivalent to a null allele (Marino, 2000; Vooijs and Berns, 1999; Vooijs et al., 1998).

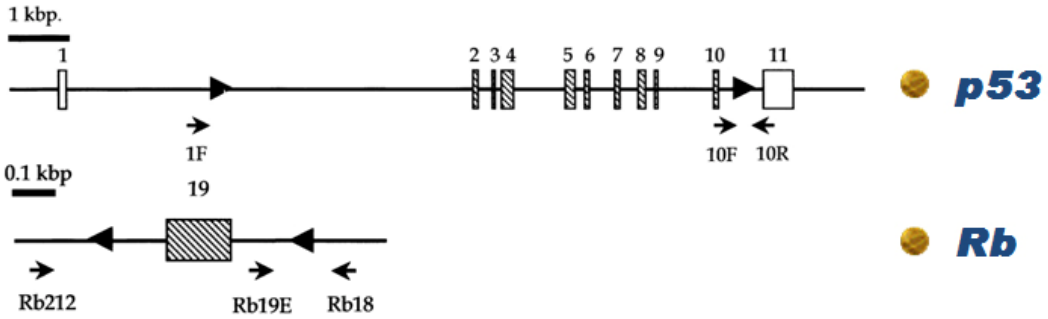

Figure 1.2. Structure of floxed alleles of *p53* and *Rb* genes. In the *p53* floxed allele, *loxP* sites are inserted into intron 1 and intron 10 of the *p53* gene. The *Rb* floxed allele contains *loxP* sites in the introns surrounding exon 19.

These mice represent a valuable tool to develop a mouse model of adult STS associated with *p53* and *Rb* inactivation.

1.5 Fluorescent nanoparticles as tools for biomedical imaging

Applications of nanotechnology in biology and biochemistry are a most rapidly developing area of research. In particular, the merging of cancer research and nanotechnology, has promised to provide extraordinary opportunities for delivering of cancer therapeutic, imaging and sensing system (Ferrari, 2005; Portney and Ozkan, 2006). For example, several types of nanoparticles have been used as tools for targeted delivery of therapeutic agents and cancer imaging. Liposomes have been used for drug-delivery, such as doxorubicin, modalities to treat cancers. Polyethyleneglycol (PEG) coated liposomes have showed the longest circulation time and greatest tumor accumulation in mice (Ishida et al., 1999). Silica and silicon are emerging as interesting candidate materials for injectable nanovectors. These particles have been demonstrated to label human leukemia, HepG liver cancer cell, human oral carcinoma, and lung carcinoma cells. Advanced forms of silica particles attached to folic acid molecules, which bind to folate receptors on the cancer cell surface, have been applied for targeted cancer imaging. Metal-based Quantum dots (QDs) or gold nanoparticles were recently widely used in cancer imaging (Tan and Zhang, 2005). QDs are the most well-known nanoparticles and have been tried in many biological applications including labeling cells *in vivo* or *in vitro*, mapping lymph nodes or blood vessels, visualizing cancers *in vivo,* and tracking metastatic tumors (Gao et al., 2004; Michalet et al., 2005; Voura et al., 2004). Beyond nanoparticles, nanotubes and nanowires are promising materials for development of biomolecular nanosensors (Portney and Ozkan, 2006). These nanomaterials have been applied as nanoscale field-effect transistors, scanning probe microscopy tips, and sensing array elements.

QDs are synthesized via colloidal synthesis. Monodisperse CdSe nanocrystallites prepared via a high-temperature colloidal growth followed by size selective precipitation are overcoated by adding the Zn and S precursors at intermediate temperatures (Dabbousi et al., 1997). Since QDs have been introduced as new nano-sized fluorophores, they have been widely used in the field of biochemistry and biomedical application including cellular labeling and *in vivo* imaging. QDs have overcome handicaps of conventional organic fluorphores with high luminescence, stability against photobleaching, and a wide range of fluorescence wavelengths from blue to infrared depending on the size. In spite of their strong advantages in imaging, a cellular toxicity of QDs has been suggested since they are mainly composed of toxic materials like Cd^{2+}, which is a part of a component of CdSe and CdSe/ZnS QDs. The toxicity of QDs is well established. For example, the release of Cd^{2+} ions from the surface of CdSe or CdSe/ZnS nanoparticles directly correlates with cytotoxic effects. In addition to their cadmium content, the interaction of the nanoparticles surface with the cells could influence cell damages (Kirchner et al., 2005). QDs are insoluble in biological solvents because non-polar groups of organic molecules are exposed on the surface of QDs. In order to overcome this disadvantage, QDs have been modified with water-soluble material like mercaptopropionic acid, silanization, and polymer coating. However, it has been reported that cells treated with the water-soluble QDs covered with mercapto-undecanoic acid showed decreased cell viability and cell death over a certain range of concentration of QDs (Shiohara et al., 2004). Despite of the surface modification of QDs, cells get damaged with high concentration of nanoparticles (Hoshino et al., 2004; Shiohara et al., 2004).

Recently Dr. Wiesner at Cornell University has developed highly fluorescent monodisperse silica nanoparticles, referred to as C dots, with core-shell architecture consisting of organic fluorophores–rich center protected within a siliceous shell (Ow

et al., 2005). Covalent incorporation of dye species such as tetramethylrhodamine isothiocyanate (TRITC) into the pseudo-solid state environment within the silica particle enhances both the brightness and photostability of the dyes, while providing a robust, water-soluble vehicle, compared to free TRITC. Although the brightness per C dot is two to three orders of magnitude less than similar hydrodynamic size and emission wavelength of QDs, the C dot silica architecture leads to the easy modification of surface properties to facilitate targeting or uptake in biological systems.

Application of these new nanoparticles may facilitate our understanding of STS formation and monitoring of STS responses to treatment. For example, such studies may lead to intravital identification of cells involved in initiation or progression of sarcomagenesis.

1.5 Project overview

Due to relative rarity, heterogeneity, and variety of subtypes, studies of histogenesis and pathogenesis of STS have been challenging thereby leading to insufficient development of advanced diagnostic and treatment approaches. This situation has been further complicated by the paucity of accurate genetic mouse models for the most common type of STS, UPS/MFH.

STS contain several main characteristics. Mutations and deletions in *P53* and *RB* are the most common genetic alterations in human STS. Because of their resemblances with tissues of mesenchymal origin, STS may derive from mesenchymal stem cells (MSC) or mesenchymal progenitor cells committed to specific cell lineages. Several studies has shown that MSC isolated from human or rodent skin or dermal tissue differentiated into adipocytes, osteocytes, chondrocytes, neurons, glial cells or/and smooth muscle cells (Bartsch et al., 2005; Shi and Cheng, 2003; Toma et al.,

2001; Toma et al., 2005). Based on these observations, I hypothesized that *p53* and *Rb* play critical roles in the STS development and adult dermal mesenchymal stem cells represent the preferential target of malignant transformation associated with *p53* and *Rb* deficiency.

Here, I generated a mouse model of STS initiated by Cre-*loxP* mediated conditional inactivation of *p53* and *Rb* tumor suppressors in connective tissue cells of the dermis. In chapter 2, the generation of a mouse STS model and identification of STS histogenesis will be described in detail. My study demonstrates that according to morpho-functional features neoplasms in this model are similar to human STS. Similar to their human counterparts, mouse sarcomas overexpress Cxcr4, and its knockdown results in reduction of invasive properties of sarcoma cells. By using bone marrow transplantation chimeras, I determined that sarcomas did not originate from bone marrow cells. Furthermore, to test a possibility that sarcomas originate from resident MSC of the dermis I established an enhanced procedure for the isolation of dermal MSC by plastic adherence and Sca-1 low expression. I further demonstrated that isolated dermal MSC have increased neoplastic potential after inactivation of p53 and Rb.

In order to apply advanced imaging approaches for monitoring mutant connective tissue cells in living mouse, I evaluated potential use of core-shell silica nanoparticles (C dots). As described in chapter 3, I tested *in vivo* toxicity and biodistribution of C dots after intravenous and subcutaneous administration. After the absence of C dot toxicity was established, I was able to demonstrate successful labeling of dermal cells including macrophages and blood vessels with C dots and to trace cells labeled with different colors into living mice. These approaches will be used for future studies of STS pathogenesis.

Finally, I will summarize the studies and outline future directions in chapter 4.

REFERENCES

Adrien, D., Ludger, K. H., Ingo, S., Oliver, M., Cornelius, K., Michael, C. A., Lars, S., Ole, G., Hans-Ulrich, S., and Marcus, L. (2009). Malignant fibrous histiocytoma-pleomorphic sarcoma, NOS gene expression, histology, and clinical course. A pilot study. Langenbecks Arch Surg.

Bartsch, G., Yoo, J. J., De Coppi, P., Siddiqui, M. M., Schuch, G., Pohl, H. G., Fuhr, J., Perin, L., Soker, S., and Atala, A. (2005). Propagation, expansion, and multilineage differentiation of human somatic stem cells from dermal progenitors. Stem Cells Dev *14*, 337-348.

Berman, S. D., Calo, E., Landman, A. S., Danielian, P. S., Miller, E. S., West, J. C., Fonhoue, B. D., Caron, A., Bronson, R., Bouxsein, M. L.*, et al.* (2008). Metastatic osteosarcoma induced by inactivation of Rb and p53 in the osteoblast lineage. Proc Natl Acad Sci U S A *105*, 11851-11856.

Binder, S. W., Said, J. W., Shintaku, I. P., and Pinkus, G. S. (1992). A histiocyte-specific marker in the diagnosis of malignant fibrous histiocytoma. Use of monoclonal antibody KP-1 (CD68). Am J Clin Pathol *97*, 759-763.

Cam, H., Griesmann, H., Beitzinger, M., Hofmann, L., Beinoraviciute-Kellner, R., Sauer, M., Huttinger-Kirchhof, N., Oswald, C., Friedl, P., Gattenlohner, S.*, et al.* (2006). p53 family members in myogenic differentiation and rhabdomyosarcoma development. Cancer Cell *10*, 281-293.

Caplana, A. I., and Bruder, S. P. (2001). Mesenchymal stem cells: building blocks for molecular medicine in the 21st century. Trends in Molecular Medicine *7*, 259-264.

Charytonowicz, E., Cordon-Cardo, C., Matushansky, I., and Ziman, M. (2009). Alveolar rhabdomyosarcoma: is the cell of origin a mesenchymal stem cell? Cancer Lett *279*, 126-136.

Chau, B. N., and Wang, J. Y. (2003). Coordinated regulation of life and death by RB. Nat Rev Cancer *3*, 130-138.

Cheng, L., Ramesh, A. V., Flesken-Nikitin, A., Choi, J., and Nikitin, A. Y. (2009). Mouse models for cancer stem cell research. Toxicol Pathol *38*, 62-71.

Chibon, F., Mairal, A., Fréneaux, P., Terrier, P., Coindre, J., Sastre, X., and Aurias, A. (2000). The RB1 Gene Is the Target of Chromosome 13 Deletions in Malignant Fibrous Histiocytoma1. Cancer Research *60*, 6339-6345.

Classon, M., and Harlow, E. (2002). The retinoblastoma tumor suppressor in development and cancer. Nature reviews cancer *2*, 910-917.

Cohen, J. A., and Geradts, J. (1997). Loss of RB and MTS1/CDKN2 (p16) expression in human sarcomas. Hum Pathol *28*, 893-898.

Cormier, J. N., and Pollock, R. E. (2004). Soft Tissue Sarcomas. CA Cancer J Clin *54*, 94-109.

Crisan, M., Yap, S., Casteilla, L., Chen, C. W., Corselli, M., Park, T. S., Andriolo, G., Sun, B., Zheng, B., Zhang, L.*, et al.* (2008). A perivascular origin for mesenchymal stem cells in multiple human organs. Cell Stem Cell *3*, 301-313.

Dabbousi, B. O., Rodriguez-Viejo, J., Mikulec, F. V., Heine, J. R., Mattoussi, H., Ober, R., Jensen, K. F., and Bawendi, M. G. (1997). (CdSe)ZnS Core-Shell Quantum Dots: Synthesis and Characterization of a Size Series of
Highly Luminescent Nanocrystallites. J Phys Chem B *101* 9463–9475.

Daugaard, S. (2004). Current soft-tissue sarcoma classifications. European Journal of Cancer *40*, 543-548.

de Dios, E. S. (2002). The use of animal models in cancer research Clin Transl Oncol *4*, 55-58.

Donehower, L. A., Harvey, M., Slagle, B. L., McArthur, M. J., Montgomery, C. A., Jr., Butel, J. S., and Bradley, A. (1992). Mice deficient for p53 are developmentally normal but susceptible to spontaneous tumours. Nature *356*, 215-221.

Enzinger, F., and Weiss, S. (2001). Enzinger's soft tissue sarcoma (Moscoby, St. Louis).

Ferrari, M. (2005). Cancer nanotechnology: opportunities and challenges. Nat Rev Cancer *5*, 161-171.

Frese, K. K., and Tuveson, D. A. (2007). Maximizing mouse cancer models. Nat Rev Cancer *7*, 645-658.

Fu, Y. S., Gabbiani, G., Kaye, G. I., and Lattes, R. (1975). Malignant soft tissue tumors of probable histiocytic origin (malignant fibrous histiocytomas): general considerations and electron microscopic and tissue culture studies. Cancer *35*, 176-198.

Gao, X., Cui, Y., Levenson, R. M., Chung, L. W., and Nie, S. (2004). In vivo cancer targeting and imaging with semiconductor quantum dots. Nat Biotechnol *22*, 969-976.

Gazziola, C., Cordani, N., Wasserman, B., Carta, S., Colombatti, A., and Perris, R. (2003). Malignant fibrous histiocytoma: a proposed cellular origin and identification of its characterizing gene transcripts. Int J Oncol *23*, 343-351.

Hagari, Y., and Yumoto, T. (1987). Experimental tumors of myxoid malignant fibrous histiocytoma and hyaluronic acid production. Acta Pathol Jpn *37*, 975-988.

Hakem, R., and Mak, T. W. (2001). Animal models of tumor-suppressor genes. Annu Rev Genet *35*, 209-241.

Hatano, H., Tokunaga, K., Ogose, A., Imaizumi, S., Hayami, T., Yamagiwa, H., Hotta, T., Endo, N., Takahashi, H. E., and Naito, M. (1999). Origin of histiocyte-like cells

and multinucleated giant cells in malignant fibrous histiocytoma: neoplastic or reactive? Pathol Int *49*, 14-22.

Helman, L. J., and Meltzer, P. (2003). Mechanisms of sarcoma development. Nat Rev Cancer *3*, 685-694.

Hieken, T. J., and Das Gupta, T. K. (1996). Mutant p53 expression: a marker of diminished survival in well-differentiated soft tissue sarcoma. Clin Cancer Res *2*, 1391-1395.

Hoffman, M. A., and Dickersin, G. R. (1983). Malignant fibrous histiocytoma: an ultrastructural study of eleven cases. Hum Pathol *14*, 913-922.

Hoshino, A., Fujioka, K., T., O., Suga, M., Sasaki, Y. F., Ohta, T., Yasuhara, M., Suzuki, K., and Yamamoto, K. (2004). Physicochemical Properties and Cellular Toxicity of Nanocrystal Quantum Dots Depend on Their Surface Modification. Nano Lett *4*, 2163 - 2169.

Ishida, O., Maruyama, K., Sasaki, K., and Iwatsuru, M. (1999). Size-dependent extravasation and interstitial localization of polyethyleneglycol liposomes in solid tumor-bearing mice. Int J Pharm *190*, 49-56.

Iwasaki, H., Isayama, T., Johzaki, H., and Kikuchi, M. (1987). Malignant fibrous histiocytoma. Evidence of perivascular mesenchymal cell origin immunocytochemical studies with monoclonal anti-MFH antibodies. Am J Pathol *128*, 528-537.

Jemal, A., Siegel, R., Ward, E., Hao, Y., Xu, J., and Thun, M. J. (2009). Cancer statistics, 2009. CA Cancer J Clin *59*, 225-249.

Jonkers, J., Meuwissen, R., van der Gulden, H., Peterse, H., van der Valk, M., and Berns, A. (2001). Synergistic tumor suppressor activity of BRCA2 and p53 in a conditional mouse model for breast cancer. Nat Genet *29*, 418-425.

Kauffman, S. L., and Stout, A. P. (1961). Histiocytic tumors (fibrous xanthoma and histiocytoma) in children. Cancer *14*, 469-482.

Keller, C., Arenkiel, B. R., Coffin, C. M., El-Bardeesy, N., DePinho, R. A., and Capecchi, M. R. (2004). Alveolar rhabdomyosarcomas in conditional Pax3:Fkhr mice: cooperativity of Ink4a/ARF and Trp53 loss of function. Genes Dev *18*, 2614-2626.

Keller, C., and Capecchi, M. R. (2005). New genetic tactics to model alveolar rhabdomyosarcoma in the mouse. Cancer Res *65*, 7530-7532.

Kile, B. T., and Hilton, D. J. (2005). The art and design of genetic screens: mouse. Nat Rev Genet *6*, 557-567.

Kirchner, C., Liedl, T., Kudera, S., Pellegrino, T., Munoz Javier, A., Gaub, H. E., Stolzle, S., Fertig, N., and Parak, W. J. (2005). Cytotoxicity of colloidal CdSe and CdSe/ZnS nanoparticles. Nano Lett *5*, 331-338.

Kirkpatrick, C. J., Alves, A., Kohler, H., Kriegsmann, J., Bittinger, F., Otto, M., Williams, D. F., and Eloy, R. (2000). Biomaterial-induced sarcoma: A novel model to study preneoplastic change. Am J Pathol *156*, 1455-1467.

Kirsch, D. G., Dinulescu, D. M., Miller, J. B., Grimm, J., Santiago, P. M., Young, N. P., Nielsen, G. P., Quade, B. J., Chaber, C. J., Schultz, C. P., *et al.* (2007). A spatially and temporally restricted mouse model of soft tissue sarcoma. Nat Med *13*, 992-997.

Langenau, D. M., Keefe, M. D., Storer, N. Y., Guyon, J. R., Kutok, J. L., Le, X., Goessling, W., Neuberg, D. S., Kunkel, L. M., and Zon, L. I. (2007). Effects of RAS on the genesis of embryonal rhabdomyosarcoma. Genes Dev *21*, 1382-1395.

Latres, E., Drobnjak, M., Pollack, D., Oliva, M. R., Ramos, M., Karpeh, M., Woodruff, J. M., and Cordon-Cardo, C. (1994). Chromosome 17 abnormalities and TP53 mutations in adult soft tissue sarcomas. Am J Pathol *145*, 345-355.

Leach, F. S., Tokino, T., Meltzer, P., Burrell, M., Oliner, J. D., Smith, S., Hill, D. E., Sidransky, D., Kinzler, K. W., and Vogelstein, B. (1993). p53 Mutation and MDM2 amplification in human soft tissue sarcomas. Cancer Res *53*, 2231-2234.

Li, H., Fan, X., Kovi, R. C., Jo, Y., Moquin, B., Konz, R., Stoicov, C., Kurt-Jones, E., Grossman, S. R., Lyle, S., *et al.* (2007). Spontaneous expression of embryonic factors and p53 point mutations in aged mesenchymal stem cells: a model of age-related tumorigenesis in mice. Cancer Res *67*, 10889-10898.

Libura, J., Drukala, J., Majka, M., Tomescu, O., Navenot, J. M., Kucia, M., Marquez, L., Peiper, S. C., Barr, F. G., Janowska-Wieczorek, A., and Ratajczak, M. Z. (2002). CXCR4-SDF-1 signaling is active in rhabdomyosarcoma cells and regulates locomotion, chemotaxis, and adhesion. Blood *100*, 2597-2606.

Lin, P. P., Pandey, M. K., Jin, F., Raymond, A. K., Akiyama, H., and Lozano, G. (2009). Targeted mutation of p53 and Rb in mesenchymal cells of the limb bud produces sarcomas in mice. Carcinogenesis *30*, 1789-1795.

Mackall, C. L., Meltzer, P. S., and Helman, L. J. (2002). Focus on sarcomas. Cancer Cell *2*, 175-178.

Maeda, T., Hashitani, S., Zushi, Y., Segawa, E., Tanaka, N., Sakurai, K., and Urade, M. (2008). Establishment of a nude mouse transplantable model of a human malignant fibrous histiocytoma of the mandible with high metastatic potential to the lung. J Cancer Res Clin Oncol *134*, 1005-1011.

Marechal, R., Demetter, P., Nagy, N., Berton, A., Decaestecker, C., Polus, M., Closset, J., Deviere, J., Salmon, I., and Van Laethem, J. L. (2009). High expression of CXCR4 may predict poor survival in resected pancreatic adenocarcinoma. Br J Cancer *100*, 1444-1451.

Marino, S., Vooijs, M., van Der Gulden, H., Jonkers, J., Berns, A. (2000). Induction of medulloblastomas in *p53*-null mutant mice by somatic inactivation of *Rb* in the external granular layer cells of the cerebellum. GENES & DEVELOPMENT *14*, 994-1004.

Matoso, A., and Nikitin, A. Y. (2008). Cancer stem cells in solid tumors. In Stem Cells and Cancer Nova Science).

Matushansky, I., Hernando, E., Socci, N. D., Mills, J. E., Matos, T. A., Edgar, M. A., Singer, S., Maki, R. G., and Cordon-Cardo, C. (2007). Derivation of sarcomas from mesenchymal stem cells via inactivation of the Wnt pathway. J Clin Invest *117*, 3248-3257.

Mehta, S. A., Christopherson, K. W., Bhat-Nakshatri, P., Goulet, R. J., Jr., Broxmeyer, H. E., Kopelovich, L., and Nakshatri, H. (2007). Negative regulation of chemokine receptor CXCR4 by tumor suppressor p53 in breast cancer cells: implications of p53 mutation or isoform expression on breast cancer cell invasion. Oncogene *26*, 3329-3337.

Michalet, X., Pinaud, F. F., Bentolila, L. A., Tsay, J. M., Doose, S., Li, J. J., Sundaresan, G., Wu, A. M., Gambhir, S. S., and Weiss, S. (2005). Quantum dots for live cells, in vivo imaging, and diagnostics. Science *307*, 538-544.

Muller, A., Homey, B., Soto, H., Ge, N., Catron, D., Buchanan, M. E., McClanahan, T., Murphy, E., Yuan, W., Wagner, S. N., *et al.* (2001). Involvement of chemokine receptors in breast cancer metastasis. Nature *410*, 50-56.

Nakamura, T., Ueda, H., Tsuda, T., Li, Y. H., Kiyotani, T., Inoue, M., Matsumoto, K., Sekine, T., Yu, L., Hyon, S. H., and Shimizu, Y. (2001). Long-term implantation test and tumorigenicity of polyvinyl alcohol hydrogel plates. J Biomed Mater Res *56*, 289-296.

Nikitin, A. Y., Juarez-Perez, M. I., Li, S., Huang, L., and Lee, W. H. (1999). RB-mediated suppression of spontaneous multiple neuroendocrine neoplasia and lung metastases in Rb+/- mice. Proc Natl Acad Sci U S A *96*, 3916-3921.

Nikitin, A. Y., and Lee, W. H. (1996). Early loss of the retinoblastoma gene is associated with impaired growth inhibitory innervation during melanotroph carcinogenesis in Rb+/- mice. Genes Dev *10*, 1870-1879.

Nikitin, A. Y., Rajewsky, M. F., Pozharisski, K. M. (1993). Development of malignant fibrous histiocytoma induced by 7,12-dimethylbenz[a]anthracene in the rat: characterization of early atypical cells. Virchows Arch B Cell Pathol Incl Mol Pathol *64*, 151-159.

O'Brien, J. E., and Stout, A. P. (1964). Malignant fibrous xanthomas. Cancer *17*, 1445-1455.

Oda, Y., Tateishi, N., Matono, H., Matsuura, S., Yamamaoto, H., Tamiya, S., Yokoyama, R., Matsuda, S., Iwamoto, Y., and Tsuneyoshi, M. (2009). Chemokine receptor CXCR4 expression is correlated with VEGF expression and poor survival in soft-tissue sarcoma. Int J Cancer *124*, 1852-1859.

Orimo, A., Gupta, P. B., Sgroi, D. C., Arenzana-Seisdedos, F., Delaunay, T., Naeem, R., Carey, V. J., Richardson, A. L., and Weinberg, R. A. (2005). Stromal fibroblasts present in invasive human breast carcinomas promote tumor growth and angiogenesis through elevated SDF-1/CXCL12 secretion. Cell *121*, 335-348.

Ow, H., Larson, D. R., Srivastava, M., Baird, B. A., Webb, W. W., and Wiesner, U. (2005). Bright and stable core-shell fluorescent silica nanoparticles. Nano Lett *5*, 113-117.

Ozzello, L., Stout, A. P., and Murray, M. R. (1963). Cultural characteristics of malignant histiocytomas and fibrous xanthomas. Cancer *16*, 331-344.

Perez-Losada, J., Sanchez-Martin, M., Rodriguez-Garcia, M. A., Perez-Mancera, P. A., Pintado, B., Flores, T., Battaner, E., and Sanchez-Garcia, I. (2000). Liposarcoma initiated by FUS/TLS-CHOP: the FUS/TLS domain plays a critical role in the pathogenesis of liposarcoma. Oncogene *19*, 6015-6022.

Pluck, A. (1996). Conditional mutagenesis in mice: the Cre/loxP recombination system. International journal of experimental pathology *77*, 269-278.

Portney, N. G., and Ozkan, M. (2006). Nano-oncology: drug delivery, imaging, and sensing. Anal Bioanal Chem *384*, 620-630.

Ren, Y. X., Finckenstein, F. G., Abdueva, D. A., Shahbazian, V., Chung, B., Weinberg, K. I., Triche, T. J., Shimada, H., and Anderson, M. J. (2008). Mouse mesenchymal stem cells expressing PAX-FKHR form alveolar rhabdomyosarcomas by cooperating with secondary mutations. Cancer Res *68*, 6587-6597.

Richter KK, P. D., Scheele J, Hinze R, Rath FW (1999). Presarcomatous lesions of experimentally induced sarcomas in rats: morphologic, histochemical, and immunohistochemical features. In Vivo *13*, 349-356.

Riggi, N., Cironi, L., Provero, P., Suva, M. L., Kaloulis, K., Garcia-Echeverria, C., Hoffmann, F., Trumpp, A., and Stamenkovic, I. (2005). Development of Ewing's sarcoma from primary bone marrow-derived mesenchymal progenitor cells. Cancer Res *65*, 11459-11468.

Riggi, N., Cironi, L., Provero, P., Suva, M. L., Stehle, J. C., Baumer, K., Guillou, L., and Stamenkovic, I. (2006). Expression of the FUS-CHOP fusion protein in primary mesenchymal progenitor cells gives rise to a model of myxoid liposarcoma. Cancer Res *66*, 7016-7023.

Riggi, N., Cironi, L., Suva, M. L., and Stamenkovic, I. (2007). Sarcomas: genetics, signalling, and cellular origins. Part 1: The fellowship of TET. J Pathol *213*, 4-20.

Rodriguez, R., Rubio, R., Masip, M., Catalina, P., Nieto, A., de la Cueva, T., Arriero, M., San Martin, N., de la Cueva, E., Balomenos, D.*, et al.* (2009). Loss of p53 induces tumorigenesis in p21-deficient mesenchymal stem cells. Neoplasia *11*, 397-407.

Roholl, P. J., Kleijne, J., van Basten, C. D., van der Putte, S. C., and van Unnik, J. A. (1985). A study to analyze the origin of tumor cells in malignant fibrous histiocytomas. A multiparametric characterization. Cancer *56*, 2809-2815.

Rosenthal, N., and Brown, S. (2007). The mouse ascending: perspectives for human-disease models. Nat Cell Biol *9*, 993-999.

Sabah, M., Cummins, R., Leader, M., and Kay, E. (2006). Aberrant expression of the Rb pathway proteins in soft tissue sarcomas. Appl Immunohistochem Mol Morphol *14*, 397-403.

Sauer, B. (1998). Inducible Gene Targeting in Mice Using the Cre/loxSystem. Methods *14*, 381-392.

Scambia, G., Lovergine, S., and Masciullo, V. (2006). RB family members as predictive and prognostic factors in human cancer. Oncogene *25*, 5302-5308.

Schwenk, F., Baron, U., and Rajewsky, K. (1995). A cre-transgenic mouse strain for the ubiquitous deletion of loxP-flanked gene segments including deletion in germ cells. Nucleic Acids Res *23*, 5080-5081.

Shi, C., and Cheng, T. (2003). Effects of acute wound environment on neonatal rat dermal multipotent cells. Cells Tissues Organs *175*, 177-185.

Shiohara, A., Hoshino, A., Hanaki, K., Suzuki, K., and Yamamoto, K. (2004). On the cyto-toxicity caused by quantum dots. Microbiol Immunol *48*, 669-675.

Shirasuna, K., Sugiyama, M., and Miyazaki, T. (1985). Establishment and characterization of neoplastic cells from a malignant fibrous histiocytoma. A possible stem cell line. Cancer *55*, 2521-2532.

Steen, S., and Stephenson, G. (2008). Current treatment of soft tissue sarcoma. Proc (Bayl Univ Med Cent) *21*, 392-396.

Stiewe, T. (2007). The p53 family in differentiation and tumorigenesis. Nat Rev Cancer *7*, 165-168.

Strahm, B., Durbin, A. D., Sexsmith, E., and Malkin, D. (2008). The CXCR4-SDF1alpha axis is a critical mediator of rhabdomyosarcoma metastatic signaling induced by bone marrow stroma. Clin Exp Metastasis *25*, 1-10.

Stratton MR, M. S., Warren W, Patterson H, Clark J, Fisher C, Fletcher CD, Ball A, Thomas M, Gusterson BA, and Cooper CS (1990). Mutation of the p53 gene in human soft tissue sarcomas: association with abnormalities of the RB1 gene. Oncogene *5*, 1297-1301.

Strauchen, J. A., and Dimitriu-Bona, A. (1986). Malignant fibrous histiocytoma. Expression of monocyte/macrophage differentiation antigens detected with monoclonal antibodies. Am J Pathol *124*, 303-309.

Sudo, K., Kanno, M., Miharada, K., Ogawa, S., Hiroyama, T., Saijo, K., and Nakamura, Y. (2007). Mesenchymal progenitors able to differentiate into osteogenic, chondrogenic, and/or adipogenic cells in vitro are present in most primary fibroblast-like cell populations. Stem Cells *25*, 1610-1617.

Suva, M. L., Cironi, L., Riggi, N., and Stamenkovic, I. (2007). Sarcomas: genetics, signalling, and cellular origins. Part 2: TET-independent fusion proteins and receptor tyrosine kinase mutations. J Pathol *213*, 117-130.

Suva, M. L., Riggi, N., Stehle, J. C., Baumer, K., Tercier, S., Joseph, J. M., Suva, D., Clement, V., Provero, P., Cironi, L., *et al.* (2009). Identification of cancer stem cells in Ewing's sarcoma. Cancer Res *69*, 1776-1781.

Taichman, R. S., Cooper, C., Keller, E. T., Pienta, K. J., Taichman, N. S., and McCauley, L. K. (2002). Use of the stromal cell-derived factor-1/CXCR4 pathway in prostate cancer metastasis to bone. Cancer Res *62*, 1832-1837.

Takeya, M., Yamashiro, S., Yoshimura, T., and Takahashi, K. (1995). Immunophenotypic and immunoelectron microscopic characterization of major

constituent cells in malignant fibrous histiocytoma using human cell lines and their transplanted tumors in immunodeficient mice. Lab Invest *72*, 679-688.

Tan, W. B., and Zhang, Y. (2005). Surface modification of gold and quantum dot nanoparticles with chitosan for bioapplications. J Biomed Mater Res A *75*, 56-62.

Tasso, R., Augello, A., Carida, M., Postiglione, F., Tibiletti, M. G., Bernasconi, B., Astigiano, S., Fais, F., Truini, M., Cancedda, R., and Pennesi, G. (2009). Development of sarcomas in mice implanted with mesenchymal stem cells seeded onto bioscaffolds. Carcinogenesis *30*, 150-157.

Tinkey, P. T., Milas, M., and Pollock, R. E. (1999). Reliable establishment of human sarcoma xenografts in the nude rat. Sarcoma *3*, 129-133.

Tolar, J., Nauta, A. J., Osborn, M. J., Panoskaltsis Mortari, A., McElmurry, R. T., Bell, S., Xia, L., Zhou, N., Riddle, M., Schroeder, T. M.*, et al.* (2007). Sarcoma derived from cultured mesenchymal stem cells. Stem Cells *25*, 371-379.

Toma, J. G., Akhavan, M., Fernandes, K. J., Barnabe-Heider, F., Sadikot, A., Kaplan, D. R., and Miller, F. D. (2001). Isolation of multipotent adult stem cells from the dermis of mammalian skin. Nat Cell Biol *3*, 778-784.

Toma, J. G., McKenzie, I. A., Bagli, D., and Miller, F. D. (2005). Isolation and characterization of multipotent skin-derived precursors from human skin. Stem Cells *23*, 727-737.

Vooijs, M., and Berns, A. (1999). Developmental defects and tumor predisposition in Rb mutant mice. Oncogene *18*, 5293-5303.

Vooijs, M., van der Valk, M., te Riele, H., and Berns, A. (1998). Flp-mediated tissue-specific inactivation of the retinoblastoma tumor suppressor gene in the mouse. Oncogene *17*, 1-12.

Voura, E. B., Jaiswal, J. K., Mattoussi, H., and Simon, S. M. (2004). Tracking metastatic tumor cell extravasation with quantum dot nanocrystals and fluorescence emission-scanning microscopy. Nat Med *10*, 993-998.

Walkley, C. R., Qudsi, R., Sankaran, V. G., Perry, J. A., Gostissa, M., Roth, S. I., Rodda, S. J., Snay, E., Dunning, P., Fahey, F. H., *et al.* (2008). Conditional mouse osteosarcoma, dependent on p53 loss and potentiated by loss of Rb, mimics the human disease. Genes Dev *22*, 1662-1676.

Wrede, D., Tidy, J. A., Crook, T., Lane, D., and Vousden, K. H. (1991). Expression of RB and p53 proteins in HPV-positive and HPV-negative cervical carcinoma cell lines. Mol Carcinog *4*, 171-175.

Yamate, J., Tajima, M., Togo, M., Shibuya, K., Ihara, M., and Kudow, S. (1991). Heterogeneity of cloned cell lines established from a transplantable rat malignant fibrous histiocytoma. Jpn J Cancer Res *82*, 298-307.

Yoo, J., and Robinson, R. A. (1999). H-ras and K-ras mutations in soft tissue sarcoma: comparative studies of sarcomas from Korean and American patients. Cancer *86*, 58-63.

Yumoto, T., and Morimoto, K. (1980). Experimental approach to fibrous histiocytoma. Acta Pathol Jpn *30*, 767-778.

Zhang, L., Yu, D., Hu, M., Xiong, S., Lang, A., Ellis, L. M., and Pollock, R. E. (2000). Wild-type p53 suppresses angiogenesis in human leiomyosarcoma and synovial sarcoma by transcriptional suppression of vascular endothelial growth factor expression. Cancer Res *60*, 3655-3661.

CHAPTER 2

Local mesenchymal stem/progenitor cells are a preferential target for initiation of adult soft tissue sarcomas associated with p53 and Rb deficiency

2.1 Abstract

The cell of origin and pathogenesis of the majority of adult soft tissue sarcomas (STS) remains poorly understood. Since mutations in *P53* and *RB* tumor suppressor genes are frequent in STS in humans, these genes have been inactivated by Cre-*loxP* mediated recombination in mice with floxed *p53* and *Rb*. Ninety three per cent of mice developed spindle cell/pleomorphic sarcomas after a single subcutaneous injection of adenovirus carrying Cre-recombinase. Similar to human STS, these sarcomas overexpress Cxcr4, which contributes to their invasive properties. By using irradiation chimeras generated by transplanting bone marrow cells from mice carrying the *Rosa26Stop*^{loxP}*LacZ* or the *Z/EG* reporter, as well as floxed *p53* and *Rb* genes, to irradiated *p53*$^{loxP/loxP}$*Rb*$^{loxP/loxP}$ mice, it has been determined that sarcomas do not originate from bone marrow derived cells, such as macrophages, but arise from the local resident cells. At the same time, dermal mesenchymal stem cells isolated by strict plastic adherence and low levels of Sca-1 expression (Sca-1^{low}, CD31^{neg}CD45^{neg}) have shown enhanced potential for malignant transformation according to soft agar, invasion, and tumorigenicity assays, following conditional inactivation of *p53* and *Rb*. Sarcomas formed after transplantation of these cells have features typical for undifferentiated high grade pleomorphic sarcomas. Taken together, our studies indicate that local Sca-1^{low} dermal mesenchymal stem/progenitor cells are a preferential target for malignant transformation associated with *p53* and *Rb* deficiency.

2.2 Introduction

Soft tissues sarcomas (STS) are malignant neoplasms arising from nonepithelial and extraskeletal tissues, such as connective tissue, muscles, vessels and peripheral nerves. While some sarcomas resemble a specific differentiated tissue (e.g. muscle, fat, etc.), many are poorly differentiated and their cell of origin remains a topic of debate. Not surprisingly, diagnosis of STS is a difficult task and few reliable prognostic criteria, mainly based on sarcoma grade and stage, have been identified (Collini et al., 2009; Guillou and Aurias, 2009; Mackall et al., 2002; Weiss and Goldblum, 2008).

During recent years, a concept has been developed that many STS, particularly those without significant presentation of cell lineage-specific markers, may arise from mesenchymal stem cells (MSC). The majority of those studies have been based on MSC derived from the bone marrow (Li et al., 2009; Matushansky et al., 2007; Tasso et al., 2009). The possibility that STS may develop from bone marrow MSC has been raised by a report that, according to cell lineage tracing experiments in irradiation chimeras, STS arise from bone marrow-derived cells (Li et al., 2007).

Genetically, STS can be divided into two groups. One group has a consistent set of recurrent genetic alterations, such as translocations (e.g., PAX3-FOXO1A in alveolar rhabdomyosarcoma) and specific mutations (e.g. KIT activating mutation in gastrointestinal stromal tumors). Another group, which comprises the majority of STS, is characterized by complex genomic profiles and frequent presence of mutations in tumor suppressor genes *P53* and *Retinoblastoma 1* (*RB*) (Collini et al., 2009; Guillou and Aurias, 2009; Mackall et al., 2002; Weiss and Goldblum, 2008). Further supporting importance of these genes for sarcomagenesis, patients with Li-Fraumeni syndrome, which is associated with germline *P53* mutations, as well as patients with germline *RB* mutation have a higher frequency of STS (Mackall et al., 2002; Weiss

and Goldblum, 2008). In agreement with known cooperation between P53 and RB pathways, mutations in both genes are frequent in STS (Stratton et al., 1990). It has been recently reported that conditional Cre-*loxP* mediated inactivation of *p53* by expression of *Osterix-Cre* transgene in committed osteoblast progenitors results in formation of osteosarcomas, and loss of *Rb* potentiates osteosarcomagenesis (Berman et al., 2008; Walkley et al., 2008). Similar cooperation between *p53* and *Rb* inactivation in acceleration of sarcomagenesis was also observed after expression of *Prx1-Cre* transgene in mesenchymal cells of mouse embryonic limbs (Lin et al., 2009). In addition to predominant osteosarcoma formation, development of poorly differentiated STS was also reported in that model. However, given that the majority of human STS affect adults (Weiss and Goldblum, 2008), interpretation of this model has been somewhat complicated due to expression of *Prx1-Cre* transgene in the early mesenchymal tissues.

By using conditional activation of *K-ras* and inactivation of *p53* by intramuscular injection of adenovirus expressing Cre recombinase (Ad*CMVCre*) into adult mice Kirsch et al. (Kirsch et al., 2007) have established a mouse model of adult high-grade sarcomas with myofibroblastic differentiation. We have used a similar approach for initiation of STS associated with p53 and Rb deficiency by subcutaneous Ad*CMVCre* administration and demonstrate that the majority of these neoplasms are undifferentiated high grade pleomorphic sarcomas (UPS), also known as malignant fibrous histiocytomas (MFH). Notably, similar to their human counterparts, mouse sarcomas overexpress Cxcr4, and its knockdown results in reduction of invasive properties of sarcoma cells. Based on bone marrow reconstitution experiments we have determined that STS have local as opposed to bone marrow origin. Finally, by using enhanced purification of dermal MSC we have demonstrated that these cells have superior transformation potential and form UPS after *p53* and *Rb* inactivation.

2.3 Materials and methods

Experimental animals

Mice with floxed copies of *p53* and *Rb* genes were prepared as described previously (Jonkers et al., 2001; Marino, 2000). FVB/N mice were used for controls. Reporter mice *Z/EG* (Tg(*ACTB-Bgeo/GFP*)21Lbe/J; (Novak et al., 2000)), *Rosa26Stop*^{loxP}*LacZ* (B6;129-*Gt(ROSA)26Sor*^{tm1Sor}/J; (Chai et al., 2000; Jiang et al., 2000)), *B5/EGFP* (FVB.Cg-Tg(*ACTB-EGPF*)B5Nagy/J (Hadjantonakis et al., 1998)) and *Rosa26LacZ* (B6; 129S-Gt*(ROSA)26Sor/J*; (Soriano, 1999)) were obtained from the Jackson Laboratory (Bar Harbor, ME). All experiments were conducted under identical conditions, following recommendations of the Institutional Laboratory Animal Use and Care Committee of Cornell University.

Genotyping

p53$^{loxP/loxP}$ and *Rb*$^{loxP/loxP}$ mice were identified by PCR genotyping essentially as previously described (Flesken-Nikitin et al., 2003). Mice carrying *LacZ* were detected with PCR primers LACZ5' (5' GCG TTG GCA ATT TAA CCG CCA GTC A 3') and LACZ3' (5' TCA GCA CCG CAT CAG CAA GTG TAT C 3') yielding 240-bp DNA fragment. Mice carrying *EGFP* were identified with PCR primers ZEGneo1 (5' AGA GGC TAT TCG GCT ATG ACT G 3') and ZEGneo2 (5' TTC GTC CAG ATC ATC CTG ATC 3') yielding 430-bp DNA fragment.

Adenovirus administration

Recombinant adenoviruses Ad*CMVLacZ*, Ad*CMVCre,* Ad*CMVeGFP*, and Ad*CMVCre-EGFP* are modifications of the adenovirus-5 genome, from which the *ela* and *elb* regions required for viral replication have been deleted and replaced with *Escherichia coli*-derived *LacZ, Cre,* or enhanced green fluorescent protein (*EGFP*)

adjacent to the CMV immediate early regulatory sequence ((Anderson et al., 2000), Gene Transfer Vector Core; University of Iowa, Iowa City, IA). After deep anesthesia with intraperitoneal (IP) Avertin (2.5% v/v in 0.85% NaCl; 0.02 ml/g body weight), mice were shaved and adenovirus (5×10^8 pfu/µl in saline) was injected into the subcutaneous (SC) tissue of the dorsal area with 21 gauge needle under the control of a dissection microscope. The needle was slowly withdrawn to avoid any accidental leak of adenovirus. According to experiments with Ad*CMVEGFP*, Ad*CMVCre* and C-dots (Choi et al., 2007) labeled cells were located in the reticular layer of the dermis and in the adjacent loose connective tissue of the hypodermis. Given the continuum of both areas, cells of both regions were used in all experiments and indicated as "dermal" cells.

Generation of irradiation chimeras

Six to seven weeks old wild-type FVB/N or $p53^{loxP/loxP}Rb^{loxP/loxP}$ mice were irradiated at 11 Gy, 2 Gy/min) by using PRIMUS Linear Accelerator (SIEMENS, Malvern, PA) or a sealed cesium^{137} source irradiator Mark 1- 68 (JL Shepherd and Associates, San Fernando, CA). According to the preliminary test experiments, irradiation in both devices resulted in comparable depletion of bone marrow cells. Within 4 hours after irradiation, mice were rescued by tail vein injection of 10^6 bone marrow cells derived from the *Z/EG* or the $Rosa26Stop^{loxP}LacZ\ p53^{loxP/loxP}RB^{loxP/loxP}$ mice as described in (Cui et al., 2002; McDonald et al., 1970). To generate positive control mice, bone marrow cells from *B5/EGFP* or *Rosa26LacZ* reporter mice were administrated into irradiated mice. Fourteen days after bone marrow reconstitution, Ad*CMVCre* was administrated subcutaneously into chimeras to induce a sarcoma as described above. In addition to tumor collection, blood for PCR genotyping was collected from the orbital sinus after anesthesia.

In order to evaluate a proportion of donor bone marrow cells in chimeras, bone marrow cells were collected from the femur and the dermis of chimeras rescued by bone marrow cells from *B5/EGFP* reporter mice. Bone marrow cells were stained with PerCP-Cy5.5 anti-mouse Gr-1 (eBioscience, Inc., San Diego, CA) for 30 minutes on ice and then analyzed by a BD LSRII analyzer (BD Biosciences, Franklin Lakes, NJ). All collected data was analyzed by FlowJo software (Tree Star, Inc. Ashland, OR). The skin tissues were fixed in 4% paraformaldehyde overnight and embedded in paraffin.

Pathological evaluation

For long-term survival experiments mice were monitored daily for 600 days, until becoming moribund or until tumor reached 1 cm in diameter. For short-term experiments, mice were killed at 1, 3, 7, and 14 days post-administration of adenovirus. Mice were anesthetized with Avertin and subjected to cardiac perfusion at 90 mm of Hg with phosphate-buffered 4% paraformaldehyde. Tumor, skin, lung, liver, and spleen, as well as organs with pathological changes, were examined during necropsy and placed into 4% paraformaldehyde for postfixation overnight. For short-term experiments with *EGFP* adenoviruses, the entire dorsal skin from the shoulder to hip was collected and visualized using fluorescence microscopy. Representative specimens were further characterized by microscopic analysis of paraffin sections, cut 4 μm thick, and stained with hematoxylin and eosin. All neoplasms were classified according to current histological classification of mouse (Mohr, 2001) and human (Weiss and Goldblum, 2008) STS.

Immunohistochemical analyses.

For avidin-biotin-peroxidase-based (ABC) detection, deparaffinized and rehydrated sections were subjected to antigen retrieval by either boiling in 10 mM sodium citrate buffer (pH 6.0, 10 min) for antibodies to desmin, procollagen type I, EGFP and CXCR4 or trypsin pre-treatment for antibodies to CD31 and F4/80. The antibodies to F4/80 (1:200; Serotec, Raleigh, NC), procollagen type I (Y-18; 1:50; Santa Cruz Biotechnology, Santa Cruz, CA), CD31 (PECAM-1; 1:100; BD Biosciences), smooth muscle actin (1:300; Spring bioscience, Fremont, CA), desmin (1:200; Accurate Chemical & Scientific Corporation, Wesbury, NY), CXCR4 antibody (1:200; Santa Cruz Biotechnology, Inc., Santa Cruz, CA, β-galactosidase (1:500; abcam, Cambridge, MA) or EGFP (1:500; NOVUS biologicals, Littleton, CO) were incubated for 1 hour at room temperature (RT) with exception of except CD31 used for overnight at 4°C. The antibody to α-sarcomeric actin (1:1500; Sigma, St. Louis, MO) was incubated using MOM Kit (Vector, Burlingame, CA) for 20 min at RT. Following treatment with 0.3% H_2O_2 in methanol, sections were incubated with biotinylated secondary antibodies and ABC complex and visualized using 3,3'-diaminobenzidine tetrahydrochloride (DAB) and counterstaining with hematoxylin essentially as described previously (Zhou et al., 2006). As a control, primary antibodies were replaced with non-immune sera of the same species.

For immunostaining of STS array (US Biomax, Inc., Rockville, MD) slides were incubated at 60°C for 2 hours according to the manufacturer's instructions and then processed for staining with antibody to CXCR4 as described above. The semiquantitative assessment of staining level was performed as follows: -, no detectable staining; +, <30% of cells are positive, ++ 30-60% of cells are positive, +++, > 60% of cells are positive.

For double immunofluorescence analysis the deparaffinized sections of 4% paraformaldehyde-fixed tissue were incubated with rabbit antibodies to EGFP (1:300) for 1 hour at 37°C or rabbit antibodies to CXCR4 (1:100) or rat antibodies to F4/80 (1:100) for 1 hour, RT, followed by Alexa Fluor 488 conjugated donkey anti-rabbit or anti-rat secondary antibody (Invitrogen, Carlsbad, CA) for 30 min, RT. Subsequently, goat antibodies to procollagen type I (1:50), Iba-1 (1:200; abcam) or rabbit antibodies to CXCR4 (1:100) were applied for 1 hour, RT, followed by Alexa Fluor 594 conjugated donkey anti-goat or anti-rabbit secondary antibody (Invitrogen) was incubated with sections.

For immunostaining on frozen sections, tissues were frozen in liquid nitrogen with Tissue-Tek® (SAKURA®, McGaw Park, IL). Seven µm thick tissue sections were placed onto Superfrost plus-coated slides (Fisher Scientific, Pittsburgh, PA) and fixed in cold acetone (-20°C) for 10 min. Sections were incubated with primary antibody to F4/80 (1:100), Iba-1 (1:200), CD31 (1:100), smooth muscle actin (1:200), and procollagen type I (1:50) at RT for 1 hour or to CD31 (1:100) at 4°C for overnight followed by secondary antibodies conjugated with Alexa Fluor 594. Counterstaining was performed by incubation for 1 minute with DAPI (1 mg/ml of an aqueous solution diluted 1:100 in TBS). Slides were mounted with GEL/MOUNT™ (Biomeda corp, Foster City, CA) and viewed with a Zeiss LSM 510-META confocal microscope.

Cell culture

Tissue cultures were maintained using Dulbecco's modification of Eagle's medium (DMEM; Cellgro®**,** Mediatech, Inc., Manassas, VA**),** containing 10% heat inactivated Fetal Bovine Serum (FBS; Sigma), 100 U/ml penicillin, 100 µg/ml streptomycin, 2 mM L-glutamine, and 1 mM sodium pyruvate (Cellgro®). Primary fibroblast culture was prepared from tail dermis of adult $p53^{loxP/loxP}Rb^{loxP/loxP}$ mice. The collected tissue

was washed 3 times in 70% EtOH and 3 times in PBS, minced finely, and disaggregated with 0.05% trypsin/0.53 mM EDTA (Cellgro®) for 1 hr, 37°C. The trypsin was removed by centrifugation and the cells were resuspended in medium. The cells were plated in two 6 cm diameter tissue culture dishes.

For adenovirus infection adherent or suspension cells were plated at a concentration of 10^5 cells in 3 ml of complete growth medium per well in 6-well plates. When cells reached 70% confluence, they were washed twice with PBS and Ad*CMVCre* or Ad*CMVEGFP* was added at a concentration of $5x10^8$ pfu/ml in 1 ml of serum free growth medium. After incubation for 2 hours at 37°C with 5% CO_2, the virus containing medium was removed and the cells were washed two times with PBS. The cells were given at least 3 days to recover in complete growth medium before use in further assays.

Cell lines STN1 and STN2 were established from angiosarcoma and UPS, respectively, developed in $p53^{loxP/loxP}Rb^{loxP/loxP}$ mice after SC AdCMVCre injection. FBN1 cell line was established 40 passages after Cre-*loxP*-mediated deletion of *p53* and *Rb* in plastic adherent dermal cells. Cultures were maintained at 37ºC and 5% CO_2, and medium replaced every 3-4 days.

Western blotting

Cells were lysed in RIPA (25mM Tris, pH8.2, 50 mM NaCl, 0.1% SDS, 0.5% Nonidet P-40 and 0.5% deoxycholate) buffer with protease inhibitors as described previously (Matoso et al., 2008). Proteins were resolved on SDS-PAGE gels and transferred to nitrocellulose via semi-dry transfer (BioRad, Hercules, CA). Immunoblots were blocked with 5% milk in TBST for 1 hour and washed three times with fresh TBST. CXCR4 antibody (1:200; Santa Cruz Biotechnology, Inc.) was incubated with immunoblots for overnight at 4°C followed by HRP-conjugated anti-rabbit antibody (1

hour at RT) and detection with SuperSignal West Pico Chemiluminescent Substrate (Pierce Biotechnology, Inc., Rockland, IL).

Cxcr4-siRNA transfection

One day before transfection, cells were plated with 2 ml of growth medium without antibiotics in a 6-well plate. Five nmol Cxcr4-siRNA (Accell SMART pool siRNA A-060184-13~16, CXCR4; Target sequence CGAUCAGUGUGAGUAUAUA, GUGGUAAAUUGAAUAAAGC, GCAUCGUGCACAAGUGGAU, or GGUUUGACUUAAUUUAUAU) or control-siRNA oligomer (Thermo Scientific, Waltham, MA) was diluted in siRNA buffer (Thermo Scientific) to make a 100 μM siRNA solution. 7.5 μL of the 100 μM siRNA was combined with 750 μL Accell delivery media (Thermo Scientific) and 100 μL of the appropriate delivery mix was added to each well containing cells with ~50% of confluence. Cells were incubated at 37°C in a 5% CO_2 incubator for 72 hours until using for an invasion assay.

Isolation of mesenchymal stem cells

Plastic adherent dermal (PAD) cells were prepared from six to seven weeks old $p53^{loxP/loxP}Rb^{loxP/loxP}$ male transgenic mice according to a protocol by Wilson et al. (Wilson et al., 2002) with modifications. Briefly, euthanized mice were shaved and treated with Nair® (Church & Dwight Co., Inc., Princeton, NJ) prior to skin removal. Harvested skin was cut into 1 cm^2 pieces and incubated for 1 hour at 37ºC in enzyme mix A, consisting of 5 U/ml dispase (Sigma) and 3% FBS in PBS. Following this, the epidermis was discarded by mechanical dissociation and the remaining tissue was incubated overnight at 4ºC in enzyme mix A. Tissue was then incubated for 2 hours at 37ºC in enzyme mix B, consisting of 1.0 U/ml dispase, 0.13 U/ml collagenase (Sigma), 700 U/ml hyaluronidase (Sigma), and 20 U/ml DNAse I (Sigma) in 1xPBS.

Both enzyme mix A and B were combined and forced through a 70 μm strainer for a single cell suspension. Cells were subsequently plated in complete medium at $5x10^6$ cells/10 cm plate. PAD cells in passage 1 were detached and suspended in antibody staining buffer, consisting of 0.1% bovine serum albumin (BSA; Sigma) in PBS. Negative selection was carried out using magnetic Dynabeads® (Invitrogen) with CD31 (Platelet Endothelial Cell Adhesion Molecule-1, PECAM-1) and CD45 (Leukocyte Common Antigen, Ly-5) biotinylated antibodies (BD Biosciences). Cells were incubated at 4°C for 30 minutes at a concentration 1 μg of antibodies per 10^6 cells, according to the manufacturer's instructions. Supernatant containing $CD31^-$ /$CD45^-$ cells was used for Fluorescence-Activated Cell Sorting (FACS) after incubation with fluorescein-conjugated antibodies to Ly-6A/E (Sca-1; BD Biosciences) at a concentration of 1 μg of antibodies per 10^6 cells at 4ºC, in the dark, for 30 minutes. Appropriate isotype controls were utilized for accurate gating parameters. FACS was conducted using a FACSAria™ cell sorter (BD Biosciences).

Differentiation assay

Sorted cells in passage 3 were re-plated onto 6-well plates at a concentration of $5x10^5$ cells per well in 3 ml of a complete growth medium. When cells were confluent, medium was removed and replaced with appropriate differentiation or control medium. Control medium consisted of DMEM with 1% FBS in order to reduce non-specific differentiation. Cells were cultured from 6 to 21 days, depending on the assay type, and had medium replaced every 2 days. Adipocyte differentiation medium contains 5 μg/ml insulin (Sigma), 1 μM dexamethasone (Sigma), 0.5 mM IBMX (Sigma), and 10% FBS in DMEM:F12 (Cellgro®). The cells were maintained for 7 days, then fixed with 4% paraformaldehyde, stained with 0.21% (w/v) Oil Red O (Sigma) in 60% isopropanol for 10 minutes, and washed with tap water. Chondrocytes

were maintained in medium consisting of 200 μM L-ascorbic acid 2-phosphate, 100 nM dexamethasone, 10 ng/ml TGF- β1 (R&D Systems, Minneapolis, MN), 40 μg/ml L-proline (Sigma), 1:100 ITS + Premix (BD Biosciences) and 10% FBS in DMEM for 14 days. Then, cells were fixed in 2.5% glutaraldehyde, 25 mM sodium acetate, and 0.4 M $MgCl_2$ containing 0.05% (w/v) Alcian Blue (Sigma) for 48 hours and washed in steps with 3% acetic acid, 3% acetic acid/25% ethanol, and 3% acetic acid/50% ethanol. For the osteocyte differentiation assay, cells were cultured in 300 μM L-ascorbic acid 2-phosphate (Sigma), 10 nM dexamethasone, 10 mM β-glycerophosphate (Sigma), and 10% FBS in DMEM:F12 for 21 days. Then, cells were fixed in 70% ice-cold ethanol for 1 hour, stained with 2% (w/v) Alizarin Red (Sigma) pH 4.2, for 10 minutes, and rinsed with 1xPBS. Ten random images of each well were taken at 20x magnification for quantification.

Soft agar colony formation, invasion and tumorigenicity assays

All assays were performed as previously described (Corney et al., 2007; Corney et al., 2010; Zhou et al., 2007). Briefly, for soft agar colony formation, PAD cells in passage 3 were suspended in an agar mix at $5x10^5$ cells/6 cm plate and incubated at 37ºC and 5% CO_2. Analysis was conducted by comparing the number of colonies present in each group after 3 weeks of growth in soft agar. For uniformity, a colony was considered to be a group of 4 or more cells. For invasion assay, PAD cells in passage 3 or tumor cells were placed into Matrigel™ Invasion Chambers (BD Biosciences, Franklin Lakes, NJ) at concentration $2.5x10^4$ cells/well. For PAD cells, complete medium was added in each chamber. For tumor cells treated with either Cxcr4-siRNA or scrambled siRNA, 400 ng of Sdf-1 (R&D Systems, Inc.) in serum-free medium was added in lower chamber. The plates were then incubated for 22 hours at 37ºC and 5% CO_2 and invasion ability was determined by comparing cell number on the bottom of

control and invasion wells, respectively, to the original plated density. For tumorigenicity assay, 10^6 PAD cells in passage 3 were injected subcutaneously into 7-week-old male SCID/NCr mice (Animal production program, NCI-Frederick, Frederick, MD) and monitoring of tumor growth and tumor collection were performed as described in section Pathological evaluation.

Statistical analyses

All statistical analyses were performed with the programs InStat 3.05 and Prism 4.03 (GraphPad, Inc. San Diego, CA). Survival fractions were calculated using the Kaplan-Meier method. Survival curves were compared by log rank Mantel-Haenszel tests. Means were compared by estimation of the two-tailed *P* with Mann-Whitney test.

2.4 Results

2.4.1 Conditional inactivation of p53 and Rb in dermal connective tissue cells results in formation of soft tissue tumors

In order to test if inactivation of *p53* and/or *Rb* induces soft tissue sarcomas, Ad*CMVCre* was subcutaneously injected into the right lower dorsal quadrant of wild-type or $p53^{loxP/loxP}$ and/or $Rb^{loxP/loxP}$ adult male mice. By 600 days of age, three of 30 $p53^{loxP/loxP}$ mice (10%) and 2 of 26 $Rb^{loxP/loxP}$ mice (8%) developed subcutaneous tumors (Figure 2.1 and Table 2.1). At the same time, tumors were formed in 27 of 29 (93%) $p53^{loxP/loxP}Rb^{loxP/loxP}$ mice starting at 116 days post-injection. Following initial detection of a small, hard mass on the site of injection, tumors developed rapidly and aggressively over a period of 1 to 2 weeks and frequently showed ulceration, necrosis and hemorrhage. No tumors were found in the place of Ad*CMVLacZ* injection,

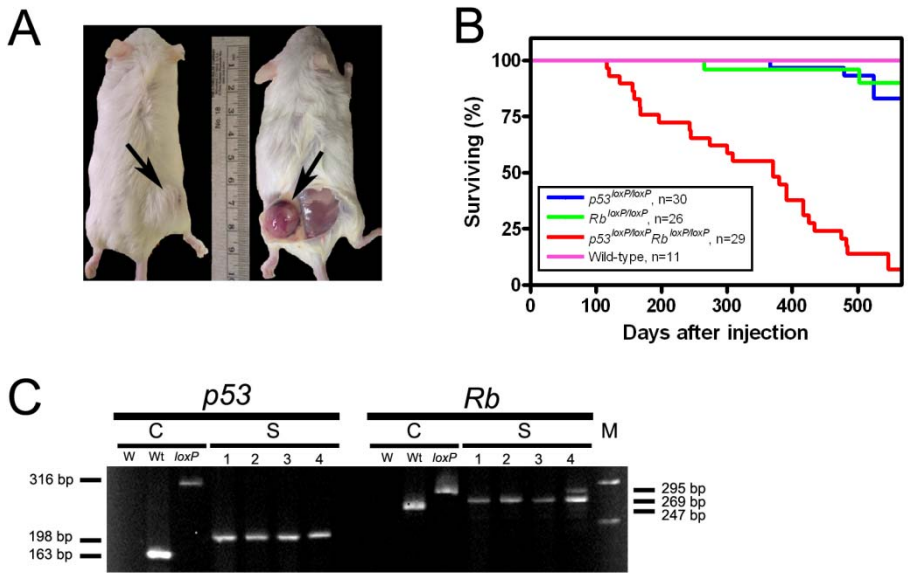

Figure 2.1. Induction of soft tissue sarcomas by conditional inactivation of *p53* and/or *Rb*. (A) Sarcomas are detected as a hard mass under the skin (left, before opening the skin, right, after opening the skin) at the site of Ad*CMVCre* (dorsal right lower quadrant, arrow) but not Ad*CMVLacZ* injection (dorsal left lower quadrant) of $p53^{loxp/loxP}Rb^{loxP/loxP}$ mice. (B) Survival of wild-type, $p53^{loxP/loxP}$, $Rb^{loxP/loxP}$, and $p53^{loxP/loxP}Rb^{loxP/loxP}$ male mice after a single subcutaneous injection of Ad*CMVCre*. Mice were sacrificed when sarcoma diameter reached 10 mm in diameter. All remaining mice were euthanized at the day 600 end point. Median survival for $p53^{loxP/loxP}Rb^{loxP/loxP}$ mice was 370 days. n, number of mice in the experimental group. (C) Loss of the *p53* and *Rb* genes in soft tissue tumors according to PCR analysis. Lanes 1 and 2: STN1 and STN2 cell lines, respectively. Lanes 3 and 4: cells from primary tumors negatively sorted for F4/80 and CD11b and analyzed 1 passage (lane 3) and directly after sorting (lane 4). 295-, 269-, and 247-bp fragments are diagnostic for floxed, excised, and wild-type alleles of the *Rb* gene, respectively. 316-, 198-, and 163-bp fragments are diagnostic for floxed, excised, and wild-type alleles of the *p53* gene, respectively. C, controls, S, samples, W, blank control, Wt, wild type DNA, *loxP*, DNA with floxed gene, M, DNA marker.

Table 2.1. Soft tissue sarcomas induced by a single subcutaneous administration of Ad*CMVCre* into mice carrying floxed *p53* and/or *Rb*.

Genotype	$p53^{loxP/loxP}$	$Rb^{loxP/loxP}$	$p53^{loxP/loxP}Rb^{loxP/loxP}$	Wild type
Mice with neoplasms, total, %*	9.1(3/33)	7.7(2/31)	93(27/29)	0(0/19)
UPS, %[&]	33.3(1/3)	0(0/2)	70(19/27)	0(0/0)
Leiomyosarcoma, %	33.3(1/3)	0(0/2)	11(3/27)	0(0/0)
Rhabdomyosarcoma, %	33.3(1/3)	0(0/2)	7(2/27)	0(0/0)
Angiosarcoma, %	0(0/3)	50(1/2)	4(1/27)	0(0/0)
Histocytic sarcoma, %	0(0/3)	0(0/2)	4(1/27)	0(0/0)
Fibrosarcoma, %	0(0/3)	0(0/2)	4(1/27)	0(0/0)
Dermatofibroma, %	0(0/3)	50(1/2)	0(0/27)	0(0/0)

*Numbers in parentheses indicate number of mice with neoplasm out of total number of mice.

[&]Numbers in parentheses indicate number of particular neoplasm out of total number of neoplasms.

the right lower dorsal quadrant of the same mice. Similarly, no tumors were found in wild-type mice injected with Ad*CMVCre*. PCR genotyping of primary cells, as well as established cell lines from tumors of $p53^{loxP/loxP}Rb^{loxP/loxP}$ mice showed deletion of both *p53* and *Rb.*

2.4.2 Characterization of soft tissue sarcomas

The majority of tumors were high grade pleomorphic sarcomas and contained highly variable areas consisting of plump spindle cells intermixed with more polygonal or round, frequently giant cells with hyperchromatic irregular nuclei (Figure 2.2A). Multiple mitotic figures and some apoptotic cells were observed and the stroma consisted of delicate collagen fibrils encircling individual cells. Invasion of surrounding tissues was commonly observed and pulmonary metastasis were detected in 1 of 3 (33%) and 7 of 29 (24%) sarcomas of $p53^{loxP/loxP}$ and $p53^{loxP/loxP}Rb^{loxP/loxP}$ mice respectively. Few neoplasms had distinct histological features consistent with angiosarcoma, histiocytic sarcoma, fibrosarcoma and dermatofibroma (Table 2.1). Angiosarcoma, and histiocytic sarcoma, respectively expressed markers of endothelial (CD31) and histiocytic (F4/80) differentiation.

According to immunohistochemical analysis significant areas of desmin and either smooth muscle actin or α-sarcomeric actin were detected in several pleomorphic sarcomas which were respectively classified as leiomyosarcoma and rhabdomyosarcoma. However, seventy per cent of sarcomas (19 of 27) and 33% (1 of 30) of $p53^{loxP/loxP}Rb^{loxP/loxP}$ and $p53^{loxP/loxP}$ mice, respectively, did not demonstrate any significant (over 5 %) differentiation with an exception of procollagen type I, a marker of collagen producing cells, such as fibroblasts. Additionally, sarcomas frequently contained a significant number of cells expressing macrophage marker F4/80 (Figure 2.2 A). However, these cells did not have neoplastic morphology. Consistently,

Figure 2.2. Characterization of soft tissue sarcomas. (A) Pathology of soft tissue sarcomas induced by *p53* and/or *Rb* inactivation. Expression (arrows, brown color) of F4/80 and procollagen type I (PrC), desmin, smooth muscle actin (SMA), α-sarcomeric actin (α-SA) and CD31 in undifferentiated high grade pleomorphic sarcoma (UPS), leiomyosarcoma (LS), rhabdomyosarcoma (RS) and angiosarcoma (AS). Hematoxylin and eosin (left column images), and ABC Elite method with hematoxylin counterstaining (right column images). Calibration bar: 50 μm (All large images), 20 μm (All insets). (B) Gating of STS cells positive (double pos, 17%) or negative (double neg, 6%) for F4/80 (PE) and CD11b (FITC) during FACS based isolation. (C) Detection of Cre-*loxP* mediated deletion of the *Rb* gene by PCR in $F4/80^{+}CD11b^{+}$ (+) and F4/80-CD11b-(-) cell subpopulations isolated by FACS from primary STS. *loxP*, DNA with floxed gene, S1 and S2 indicate representative individual tumor samples. See Figure 1 for description of PCR fragments.

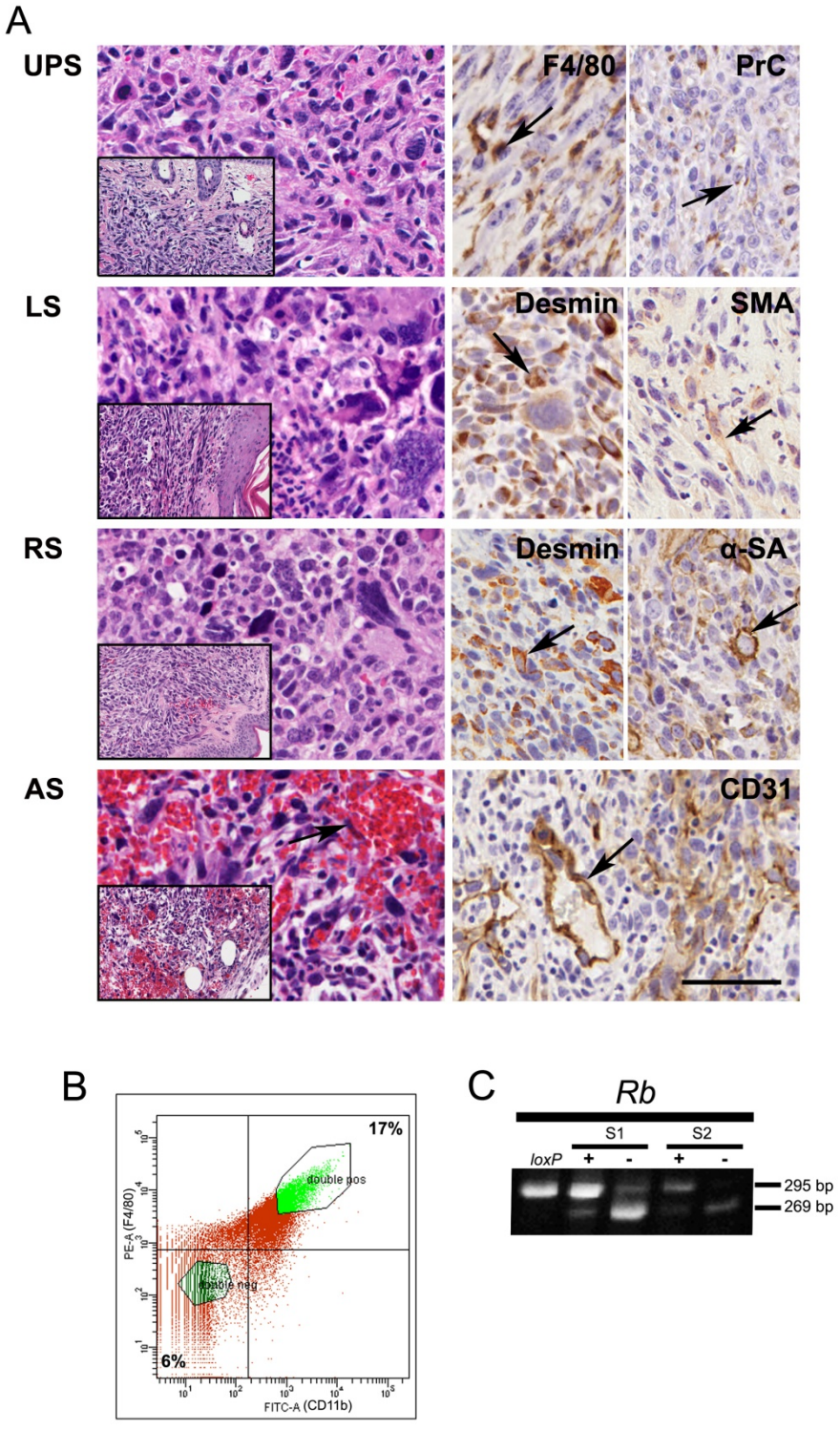
A
UPS
F4/80
PrC
LS
Desmin
SMA
RS
Desmin
α-SA
AS
CD31
B
17%
double pos
double neg
6%
PE-A (F4/80)
FITC-A (CD11b)
C
Rb
S1
S2
loxP
+
-
+
-
295 bp
269 bp

macrophage population selected by fluorescence-activated cell sorting with antibodies to F4/80 and CD11b, contained only traces of Cre-*loxP* mediated deletion of the *Rb* gene (Figure 2.2B and C), likely due to phagocytosis of neoplastic cells and/or presence of contaminating neoplastic cells.

2.4.3 CXCR4 overexpression contributes to invasive properties of STS

It has been reported that the expression of CXCR4 in human STSs is associated with poor prognosis and metastasis (Oda et al., 2009), particularly in malignant non-round cell tumors such as UPS and leiomyosarcoma. In agreement with these observations, we determined high expression of CXCR4 in human UPS (MFH) and leiomyosarcoma (Table 2.2). Notably, we observed that expression of CXCR4 was high in UPS, moderate in fibrosarcoma, and negligible in dermatofibrosarcoma protuberans (Figure 2.3A).

Consistent with observations in human STS, mouse sarcomas expressed Cxcr4 according to immunostaining and western blot analyses (Figure 2.3B and C). The majority of Cxcr4 expressing cells also expressed procollagen type I but not macrophage marker F4/80. Levels of CXCR4 were negligible in primary fibroblast cell cultures but increased after inactivation of *p53* and *Rb*. To test if Cxcr4 plays role in sarcoma progression, Matrigel invasion assays were performed with STS cell lines STN1 and STN2 as well as p53 and Rb deficient fibroblastic cell line FBN1. Cells of all lines showed increased invasion after addition of Cxcr4 ligand Sdf-1 (Figure 2.3D). At the same time, siRNA-mediated knockdown of Cxcr4 significantly reduced invasion activity of these cells (Figure 2.3D).

Figure 2.3. CXCR4 overexpression contributes to invasive properties of STS. (A) CXCR4 expression (brown color) in human undifferentiated high grade sarcoma (UPS), fibrosarcoma (FS), dermatofibrosarcoma protuberans (DFSP). Note preferential expression of CXCR4 in UPS. ABC *Elite* method with hematoxylin counterstaining. (B) Co-localization (yellow color) of Cxcr4 expression in cells containing procollagen type I (PrC) but not F4/80. Double immunofluorescence with DAPI counterstaining. (A and B) Calibration bar: 50 μm. (C) Cxcr4 expression in wild type (Wt) and $p53^{loxP/loxP}Rb^{loxP/loxP}$ fibroblasts 2 (p4/2) and 4 (p6/4) passages after exposure to Ad*CMVCre*, and in established cell lines FBN1, STN1 and STN2. (D) Effects of Sdf1 (left panel) and siRNA-mediated knockdown of Cxcr4 (right panel) on cell invasion in Matrigel assay. Control siRNA, scrambled siRNA.

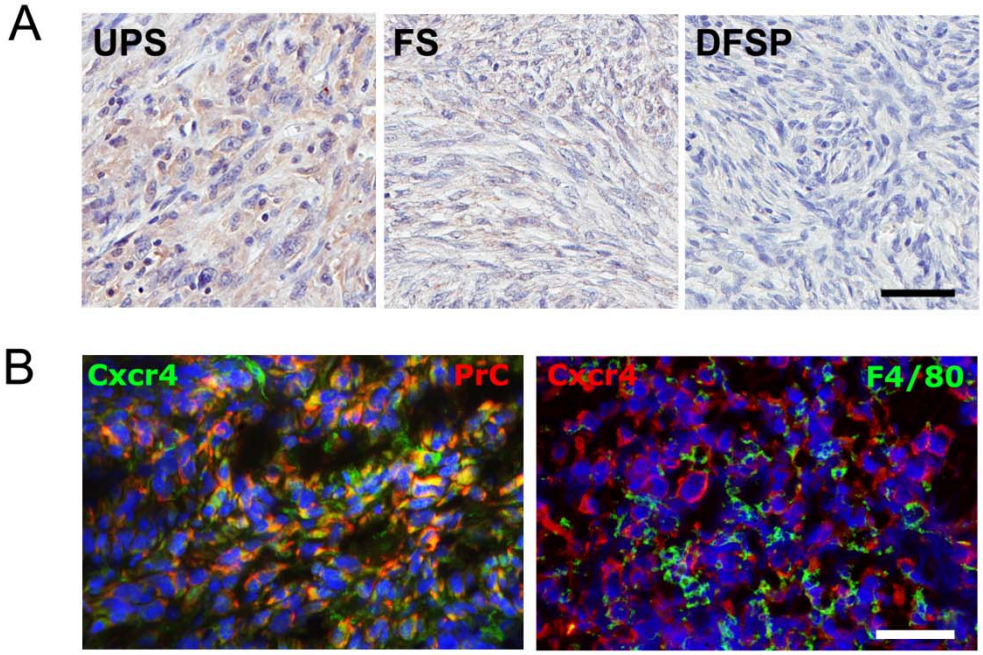
A
UPS
FS
DFSP
B
Cxcr4
PrC
Cxcr4
F4/80
C
Wt
p4/2
p6/4
FBN1
STN1
STN2
Cxcr4
Gapdh
D
Cells/Well
1500
1000
500
0
P=0.0387
P=0.0379
P=0.0056
Sdf1
FBN1
STN1
STN2
Cells/Well
200
150
100
50
0
P=0.0071
P=0.0125
P=0.037
Control siRNA
Cxcr4 siRNA
FBN1
STN1
STN2

Table 2.2. Expression of CXCR4 in human soft tissue tumors

Tumor type	Frequency of tumors with specific level of staining, %*			
	-	+	++	+++
UPS,*	26.7(4/15)	20(3/15)	46.7(7/15)	6.7(1/15)
Fibrosarcoma	28.6(2/7)	42.9(3/7)	28.6(2/7)	0(0/7)
DFSP[&]	100(5/5)	0(0/5)	0(0/5)	0(0/5)
Neurofibrosarcoma	50(2/4)	25(1/4)	25(1/4)	0(0/4)
Liposarcoma	18.8(3/16)	50(8/16)	31.3(5/16)	0(0/16)
Leiomyosarcoma	18.2(2/11)	18.2(2/11)	45.5(5/11)	18.2(2/11)
Rhabdomyosarcoma	0(0/1)	100(1/1)	0(0/1)	0(0/1)
Hemangiosarcoma	0(0/1)	0(0/1)	0(0/1)	100(1/1)
M. Schwannoma	100(1/1)	0(0/1)	0(0/1)	0(0/1)

* Numbers in parentheses indicate number of particular tumors with specific level of CXCR4 expression out of total number of neoplasm's of the same type.

[&] Expression CXCR4 is significantly lower in dermatofibrosarcoma protuberance (DFSP) as compared to UPS (Fisher's exact test P=0.0081) and to leiomyosarcoma (Fisher's exact test P=0.0048).

2.4.4 Connective tissue cells targeted with adenovirus

To establish which dermal cells were targeted by adenovirus, expression of EGFP was detected within 1 to 14 days after subcutaneous injection of adenovirus expressing Cre-EGFP (Ad*CMVCre-EGFP).* EGFP expression in subcutaneous tissues was strongest at 1 and 3 days post infection. According to cell phenotyping, 39% of fibroblasts (procollagen type I+), 44% (F4/80+) or 42% (Iba-1+) of macrophages, 33% of smooth muscle cells (smooth muscle actin+) and 16% of endothelial cells (CD31+) were labeled with Ad*CMVCre-EGFP* (Table 2.3 and Figure 2.4A).

To test if adenovirus also infected MSC, this population was isolated from dissociated dermal cells by strict plastic adhesion followed by negative selection for CD45, a marker for cells of hematopoietic origin, including hematopoietic stem cells, and for endothelial cell marker CD31 and positive selection for Sca-1 expression (Figure 2.4B). Although all plastic adherent cells had a potential for differentiation towards adipogenic and osteogenic differentiation (Rodriguez et al., 2009), our studies demonstrated that further selection for Sca-1^{low} fraction results in additional enrichment for cells with enhanced ability to form adipocytes, chondrocytes and osteocytes (Figure 2.4C). All cell subpopulations of plastic adherent cells were equally well infected with Ad*CMVEGFP* (Figure 2.9A).

2.4.5 Local origin of STS

In order to discriminate between bone marrow and local dermal cell of origin of STS, irradiation chimeras reconstituted with donor-derived bone marrow cells isolated from mice with reporter transgenes were generated (Figure 2.5).

In order to evaluate a proportion of donor bone marrow cells, bone marrow cells and the dermal cells were evaluated for EGFP expression at 1, 3, 7, and 14 days

Table 2.3. Percentage of EGFP-expressing cells in dermal cell populations 3 days after Ad*CMVCre-EGFP* infection

Cell marker	Pro-collagen Type I	F4/80	Iba-1	Smooth Muscle Actin	CD31
Mean ±SD (%)*	38.88±18.77	44.33±14.38	42.28±6.53	32.8±33.37	15.66±26.46

*At least 50 DAPI stained cells per field were counted in 10 fields at magnification 400X.

Figure 2.4. Identification of connective tissue cells infected with Ad*CMVCre-EGFP* adenovirus. (A) Co-localization (yellow color) of EGFP and fibroblastic (procollagen type I, PrC), macrophage (F4/80), smooth muscle (smooth muscle actin, SMA) or endothelial (CD31) markers. Calibration bar: 50 μm. (B) Expression of CD45, CD31 and Sca 1 in plastic adherent dermal cells (left panel). Sorting gates for isolation of Sca-1^{high}, Sca-1^{low}, and Sca-1^{neg}. cell populations after negative selection for CD45 and CD31 (right panel). (C) Sca-1^{low} cells have a greater potential for differentiation into adipocytes, chondrocytes and osteocytes as compared to Sca-1^{high} population ($p<0.005$). Additionally, Sca-1^{low} cells have greater adipocyte and chondrocyte potential as compared to Sca-1^{neg} cells ($p<0.005$). Values (mean ± SD, n=3) represent percent of controls without differentiation medium. All experiments were repeated at least twice.

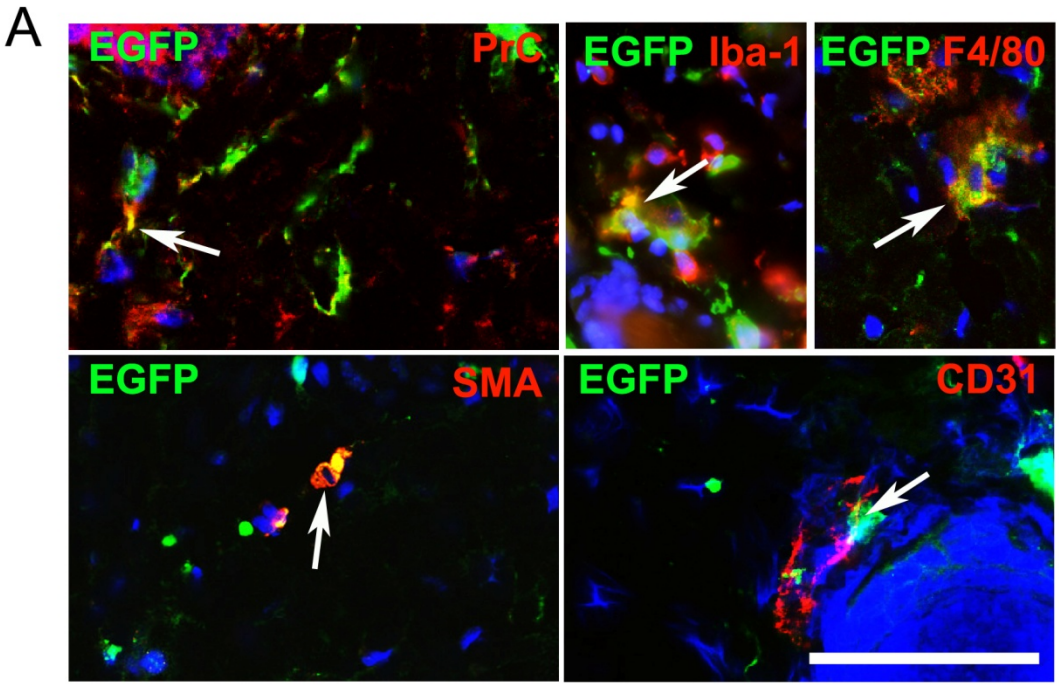
A
EGFP
PrC
EGFP Iba-1
EGFP F4/80
EGFP
SMA
EGFP
CD31

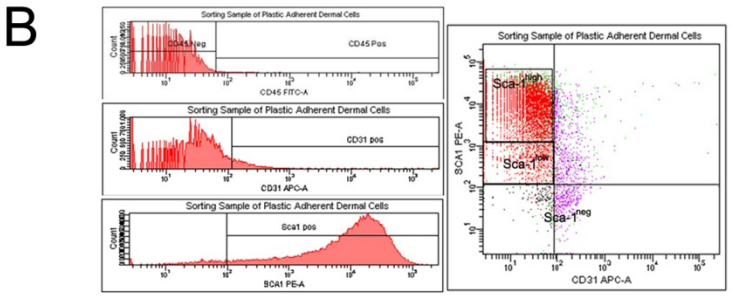
B
Sorting Sample of Plastic Adherent Dermal Cells
CD45 Neg
CD45 Pos
CD45 FITC-A
Sorting Sample of Plastic Adherent Dermal Cells
CD31 pos
CD31 APC-A
Sorting Sample of Plastic Adherent Dermal Cells
Sca1 pos
SCA1 PE-A
Sorting Sample of Plastic Adherent Dermal Cells
Sca-1high
Sca-1low
Sca-1neg
SCA1 PE-A
CD31 APC-A

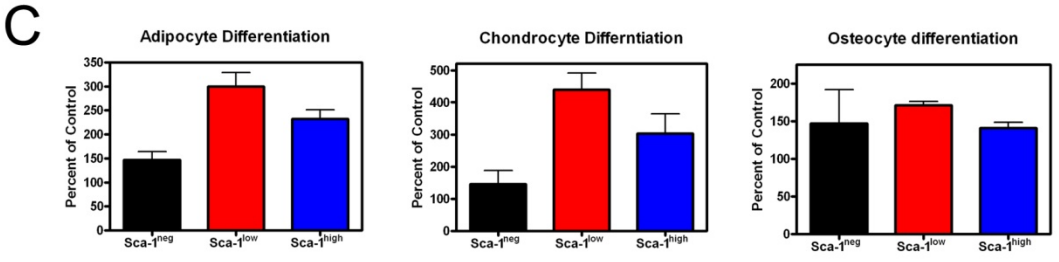
C
Adipocyte Differentiation
Chondrocyte Differntiation
Osteocyte differentiation
Percent of Control
Sca-1neg
Sca-1low
Sca-1high

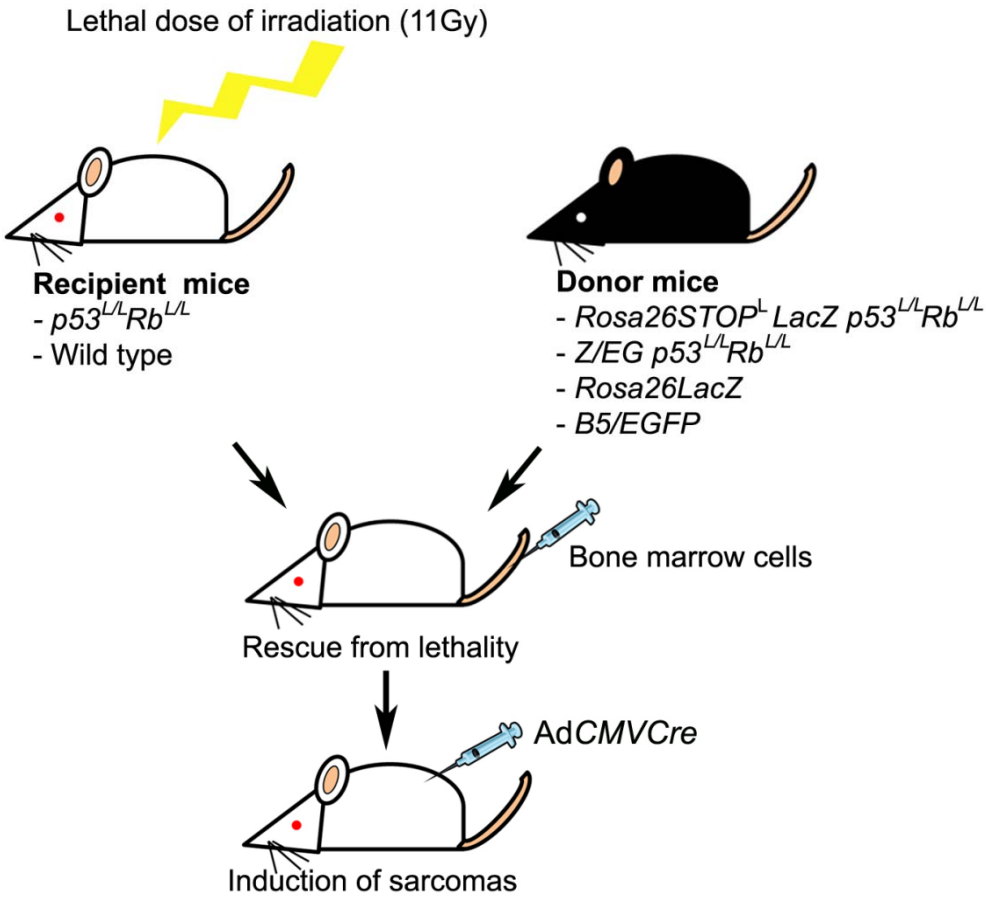

Figure 2.5. Identification of soft tissue sarcoma cellular origin in irradiation chimeras. *p53*$^{loxP/loxP}$*Rb*$^{loxP/loxP}$ (*p53*$^{L/L}$*Rb*$^{L/L}$) or wild-type mice were exposed to lethal dose (11 Gy) of irradiation, followed by rescue with bone marrow cells derived from the *Rosa26Stop*^{loxP}*LacZ* (*Rosa26Stop*^{L}*LacZ*) or the Z/EG reporter mice containing either wild type or floxed *p53* and *Rb*. Soft tissue sarcomas were induced by the subcutaneous Ad*CMVCre* injection 14 days after bone marrow reconstitution.

Figure 2.6. Assessment of bone marrow rescue in irradiation chimeras. (A) Efficiency of reconstitution of bone marrow cells according to co-expression of donor-derived EGFP and granulocyte/monocyte marker Gr-1 between 1 and 14 days after irradiation and transplantation of bone marrow from *B5/EGFP* mice (lower row). Wt and *B5/EGFP*, Gr-1/EGFP profiles of bone marrow cells from wild- type and *B5/EGFP* mice respectively. (B) Detection of *ACTBStop*^{loxP}*EGFP* transgene (430 bp) by PCR analysis of blood from chimeras that were transplanted with bone marrow cells from the Z/EG reporter mice. 316 bp DNA fragment diagnostic of floxed p53 was used as internal reference control. (W; water control, C; DNA from a mouse carrying the *Z/EG* reporter, as well as floxed *p53* and *Rb* genes, M; marker). Silver staining of acrylamide gels. (C) Co-expression of EGFP and macrophage marker Iba-1 (arrow) in dermal cells 14 days after irradiation and transplantation of bone marrow cells derived *B5/EGFP* donor mice. Calibration bar: 50 μm.

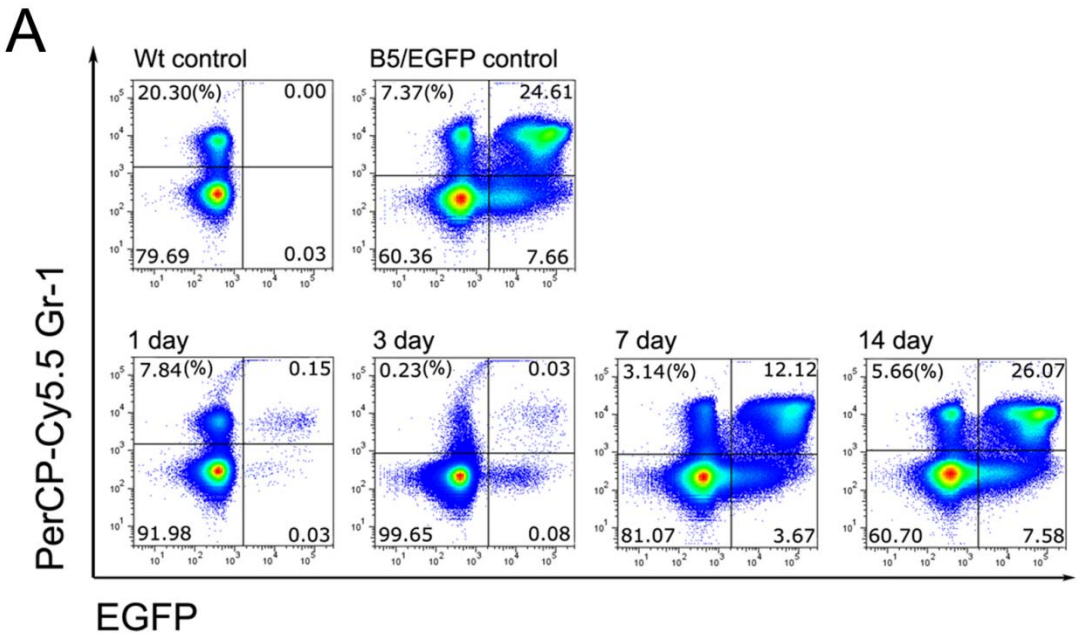
A
Wt control
B5/EGFP control
20.30(%)
0.00
79.69
0.03
7.37(%)
24.61
60.36
7.66
1 day
7.84(%)
0.15
91.98
0.03
3 day
0.23(%)
0.03
99.65
0.08
7 day
3.14(%)
12.12
81.07
3.67
14 day
5.66(%)
26.07
60.70
7.58
PerCP-Cy5.5 Gr-1
EGFP

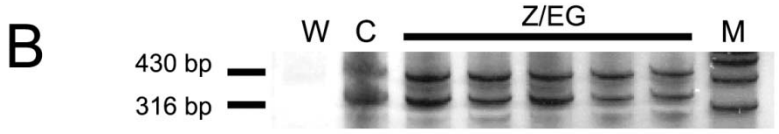
B
W
C
Z/EG
M
430 bp
316 bp

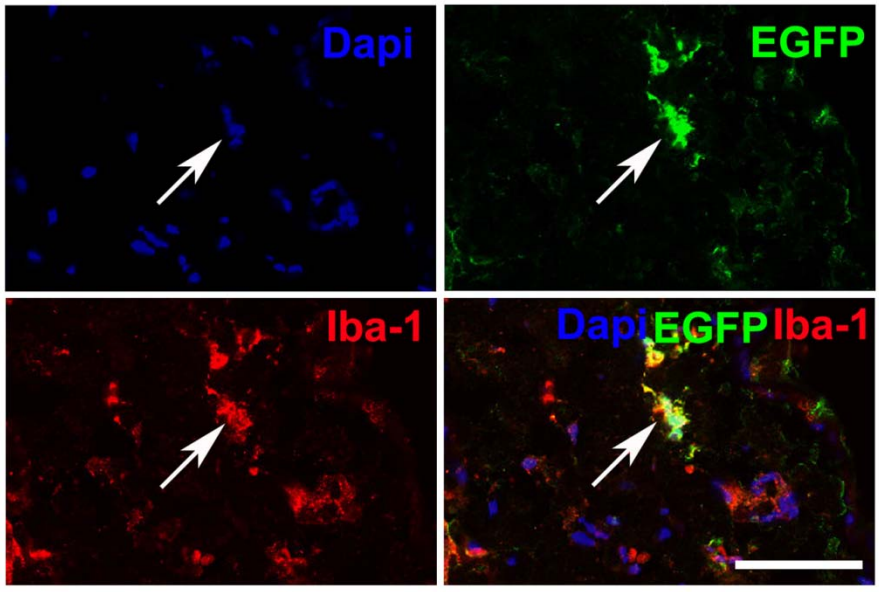
C
Dapi
EGFP
Iba-1
Dapi EGFP Iba-1

following irradiation and transplantation of bone marrow cells from *B5/EGFP* reporter mouse. Reduced number of cells expressing Gr-1, a marker for granulocytes and monocytes, and limited EGFP expression was detected at 1 and 3 days after irradiation followed by immediate bone marrow transplantation (Figure 2. 6 A). Both cell populations increased by day 7 and were within range normal for *B5/EGFP* reporter mouse. These results were consistent with detection of with *EGFP* transgene copy numbers similar to those in *B5/EGFP* mouse by multiplex PCR (Figure 2.6B). At the same time, 24% of Iba-1+ macrophages (98.5 ± 29, Mean ± SD, out of 410 ± 86.3 counted) expressed EGFP 14 days post-irradiation (Figure 2.6C).

In order to determine if any STS developed from bone marrow, sarcomas were initiated by a single subcutaneous injection of Ad*CMVCre* into irradiated $p53^{loxP/loxP}Rb^{loxP/loxP}$ (n=29) and wild-type mice (n=9) reconstituted with bone marrow from mice carrying floxed *p53* and *Rb* as well as $Rosa26Stop^{loxP}LacZ$ or *Z/EG* reporter constructs. In these reporter constructs, expression of β-galactosidase or EGFP, respectively, is possible only after deletion of a STOP codon flanked by *loxP* sites. Additionally, another group of $p53^{loxP/loxP}Rb^{loxP/loxP}$ mice (n=4) was reconstituted with bone marrow of mice carrying constitutively expressed *EGFP* (*B5/EGFP*) or *LacZ* (*Rosa26LacZ*) transgene. In parallel with collecting tumors, blood from each chimera was collected and genotyped by PCR analysis to confirm the reconstitution with donor cells.

All chimeric mice with host $p53^{loxP/loxP}Rb^{loxP/loxP}$ genotype (n=33) but none of wild type (n=9) developed sarcomas independently of the type of donor mouse strain. The sarcomas were diagnosed as UPS similar to the majority of sarcomas associated with p53 and Rb deficiency. The immunohistochemistry results showed that tumors from control chimeras rescued with bone marrow of mice carrying constitutively expressed *EGFP* (*B5/EGFP*) or *LacZ* (*Rosa26LacZ*) transgene contained numerous

Figure 2.7. Detection of bone-marrow derived cells in soft tissue sarcomas. (A) Expression of β-galactosidase (β-gal, arrow) and EGFP (arrow) in sarcomas initiated by a single sSC Ad*CMVCre* injection into lethally irradiated $p53^{loxP/loxP}Rb^{loxP/loxP}$ mice transplanted with bone marrow cells from *Rosa26LacZ* (upper left panel) and *B5/EGFP* reporter mice (lower left panel), but not in those with $Rosa26Stop^{loxP}LacZ$ (upper right panel), or a *Z/EG* (lower right panel) bone marrow cells. ABC Elite method with hematoxylin counterstaining. (B) Expression of EGFP, procollagen type I (PrC) and F4/80 markers in sarcomas of $p53^{loxP/loxP}Rb^{loxP/loxP}$ irradiation chimeras reconstituted with bone marrow cells from a *B5/EGFP* (left panels) and *Z/EG* reporter mice (right panels). Note co-expression (yellow color) of EGFP and F4/80 in sarcoma of mouse reconstituted with *B5/EGFP* bone marrow. Double immunofluorescence with DAPI counterstaining. Calibration bar: 50 μm.

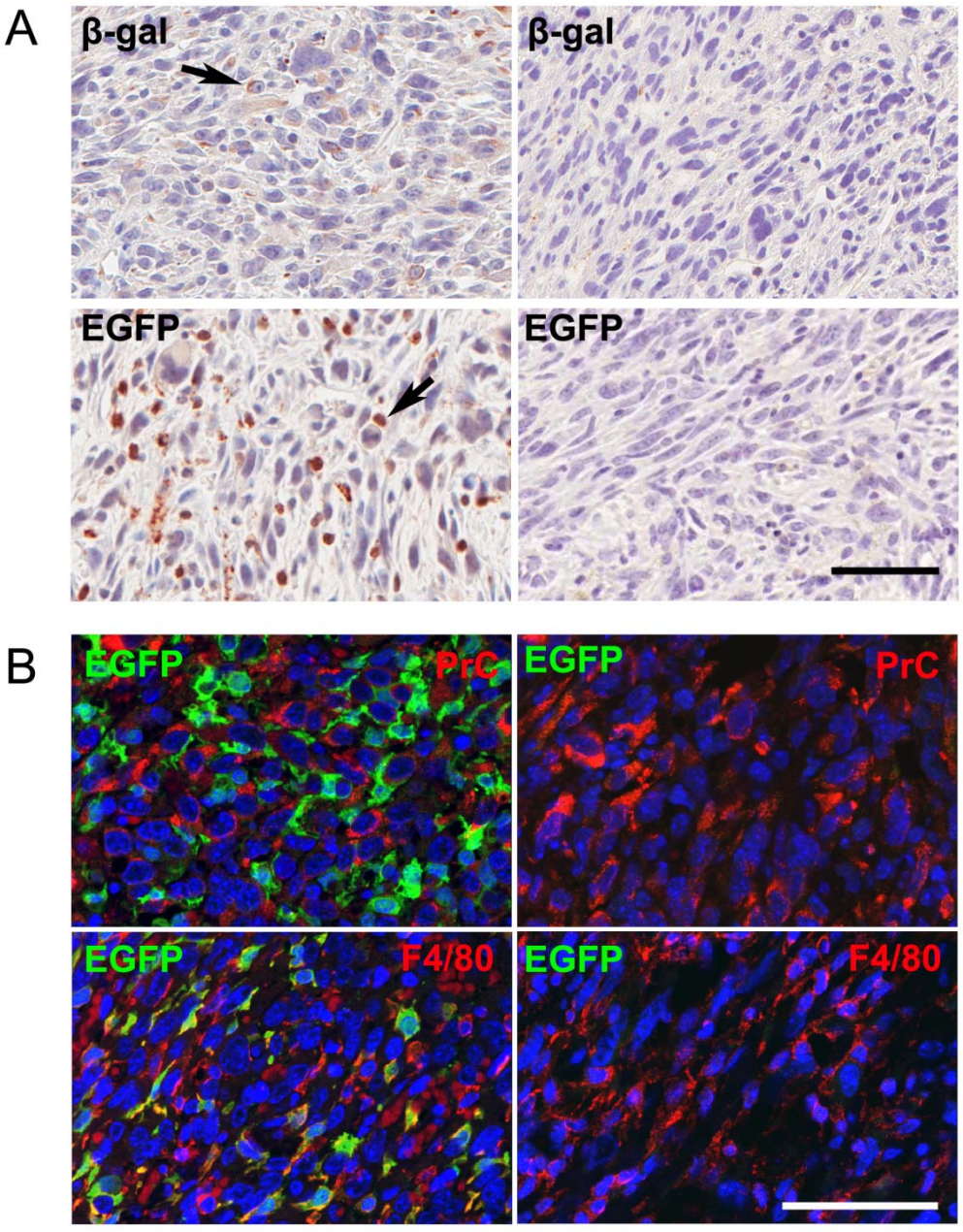
A
β-gal
β-gal
EGFP
EGFP
B
EGFP
PrC
EGFP
PrC
EGFP
F4/80
EGFP
F4/80

cells expressing EGFP or β-galactosidase (Figure 2.7). These cells did not have atypical cytological features and expressed macrophage marker F4/80 but no procollagen type I (Figure 2.7). At the same time, sarcomas developed from chimeras that contain bone marrow cells from the *Z/EG* (n=19) or the *Rosa26STOP^{loxP}LacZ* (n=10) reporter mice did not show any GFP or β-galactosidase expression (Figure 2.7). Thus none of 38 mice developed STS from bone marrow with floxed *p53* and *Rb*. Taken together with complete reconstitution of bone marrow cells and 24% reconstitution of dermal macrophage population, these results indicate that STS associated with *p53* and *Rb* inactivation are most likely originate from the local resident as opposed to bone marrow derived cells, such as macrophages.

2.4.6 MSC have enhanced potential for malignant transformation

To investigate whether dermal MSC could be a target for malignant transformation in our model, these cells were subjected to a series of transformation-related assays after Ad*CMVCre*-mediated inactivation of *p53* and *Rb.* First, the ability of the three plastic adherent dermal cell populations to form colonies in soft agar was compared. Interestingly, Sca-1^{low} cells showed an increase in the number of colonies when compared to the other 2 plastic adherent dermal cell populations (Figure 2.8A). Secondly, invasion ability of transformed plastic adherent dermal cells among Sca-1^{neg}, Sca-1^{low}, and Sca-1^{high} populations was tested using a Matrigel invasion chamber. Sca-1^{low} cells once again exhibited the greatest potential for malignant transformation compared to the other 2 plastic adherent dermal cell populations (Figure 2.8A). Finally, tumorigenicity of MSC was tested after their subcutaneous transplantation into scid mice. Sca-1^{low} cells formed tumors faster (Figure 2.8B). Importantly, tumors were UPS histologically similar to conditionally induced sarcomas in

Figure 2.8. Neoplastic potential of dermal mesenchymal stem cells (MSC) after conditional inactivation of p53 and Rb. (A) Compared to Sca-1^{neg} and Sca-1^{high} subpopulations, the Sca-1^{low} MSC cells have significantly higher propensity for forming colonies in soft agar (A, left panel, mean ± SD, n=3, $p<0.0001$) and invasion in Matrigel chamber (right panel, mean ± SD, n=3, Sca-1^{low} versus Sca-1^{neg}, $p=0.002$; Sca-1^{low} versus Sca-1^{high}, $p<0.0001$) (B) Accelerated formation of tumors after SC transplantation of MSC (the Sca-1^{low} MSC cells, median survival 44 days, n=3) as compared to mesenchymal non-stem cells (MnSC, Sca-1^{neg} and Sca-1^{high} cells, median survival 74 days, n=6; $P=0.0376$). (C) Undifferentiated high grade pleomorphic sarcoma with mitotic figures (H&E, arrow) and expression of procollagen type I (PrC, arrow) formed after MSC implantation. Desmin is detected only in smooth muscle cells of blood vessels (arrow). Left panel, Hematoxylin and eosin, right panels, ABC Elite method with hematoxylin counterstaining. Calibration bar: 50 μm.

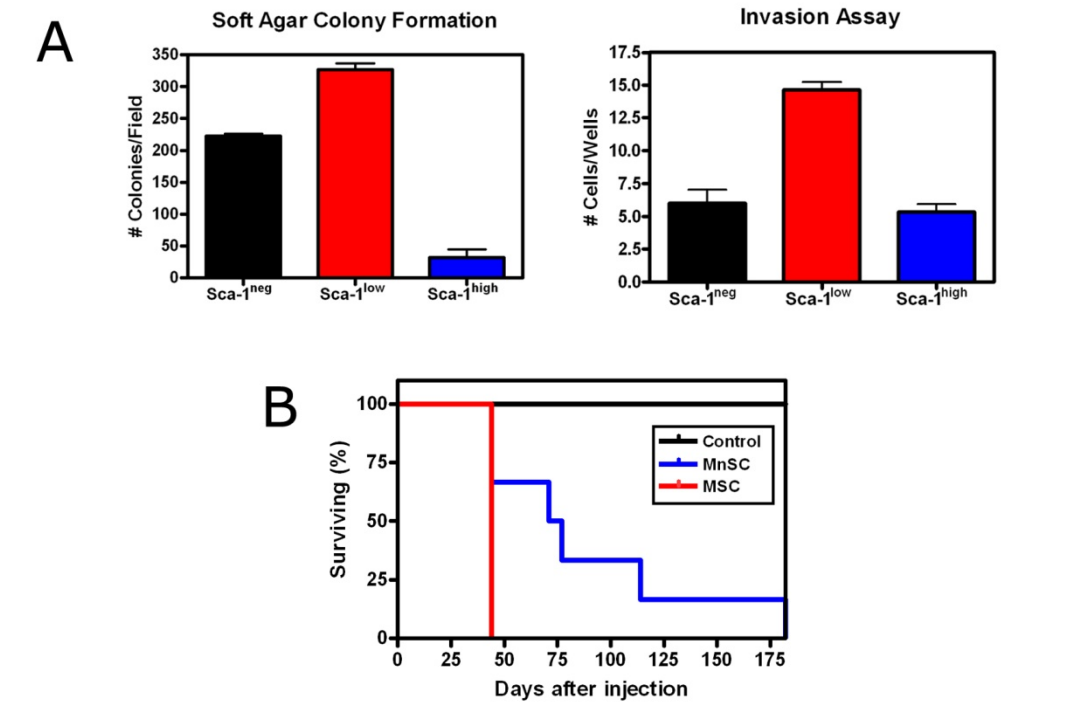
A
Soft Agar Colony Formation
Colonies/Field
350
300
250
200
150
100
50
0
Sca-1neg
Sca-1low
Sca-1high
Invasion Assay
Cells/Wells
17.5
15.0
12.5
10.0
7.5
5.0
2.5
0.0
Sca-1neg
Sca-1low
Sca-1high
B
Surviving (%)
100
75
50
25
0
0
25
50
75
100
125
150
175
Days after injection
Control
MnSC
MSC
C
H&E
PrC
Desmin

p53$^{loxP/loxP}$*Rb*$^{loxP/loxP}$ mice (Figure 2.8D). These tumors expressed procollagen type I but no other diagnostic markers in neoplastic cells, including desmin (Figure 2.8C).

These results indicate that Sca-1^{low} multipotent dermal stem/progenitor cells are a preferential target for malignant transformation associated with *p53* and *Rb* deficiency.

2.5 Discussion

STS are relatively uncommon neoplasms and constitute less than 1% of all cancers, with an estimated 10,660 new STSs diagnoses and 3,820 related deaths in 2009 (Jemal et al., 2009). However, lack of identifiable precursor lesions and high heterogeneity of these neoplasms, as well as incomplete understanding of ontogenesis and phenotypical plasticity of normal connective tissue cells represent a continuous challenge for diagnosis, which is reflected in continuous shift in STS classifications. Therefore, development of mouse models which accurately recapitulate both morphological features and frequent genetic alterations of human STS is of critical importance. The mouse model of STS reported here addresses this need because histology of induced sarcomas is similar to those of human STS. Furthermore, mutations in *p53* and *Rb* are the most common genetic alterations occurring in sarcomas with complex genotype, such as UPS, fibrosarcoma and leiomyosarcoma.

Similarity between human STS and sarcomas in our mouse model was further confirmed by observation of expression of CXCR4 which is a receptor of chemokine CXCL12 (SDF-1α). It has been previously reported that signaling through CXCR4 plays an important role in progression of a broad variety of malignancies, including breast cancers (Muller et al., 2001), prostate cancers (Taichman et al., 2002), malignant melanomas (Muller et al., 2001; Scala et al., 2005), gastric cancer (Yasumoto et al., 2006), osteosarcomas (Oda et al., 2006) and rhabdomyosarcomas

(Strahm et al., 2008). In agreement with a previous report that expression of CXCR4 is associated with poor prognosis of STS (Oda et al., 2009) we observed that expression of CXCR4 is significantly higher in high grade sarcomas, such as UPS and leiomyosarcomas as compared to low grade dermatofibrosarcoma and fibrosarcoma. Furthermore, according to our Matrigel invasion assays, stimulation of Cxcr4 by addition of Sdf-1 increased invasion of sarcoma cells, while siRNA-mediated knockdown of Cxcr4 significantly reduced their invasion. Taken together, these results demonstrate that the CXCR4/SDF-1 axis is an important mediator in sarcoma progression. It has been reported that CXCR4 expression is repressed by p53 (Mehta et al., 2007). Our observations of increased Cxcr4 expression in fibroblasts after *p53* and *Rb* inactivation is consistent with that report and indicate that inactivation of *p53* during sarcoma initiation may predetermine some of the advanced metastatic traits.

Diagnosis of UPS, also known as malignant fibrous histiocytoma (MFH), is a matter of a particular controversy. Given the lack of specific immunohistochemical markers and firm diagnostic criteria of this neoplasm, it is not surprising that the frequency of UPS/MFH diagnosis ranges from 5% to 70 % (Engellau et al., 2004; Guillou and Aurias, 2009; Weiss and Goldblum, 2008). MFH was originally described by A. P. Stout and colleagues (Kauffman and Stout, 1961; O'Brien and Stout, 1964; Ozzello et al., 1963) as a neoplasm consisting of histiocyte-like and fibroblast-like cells. Some initial studies performed on human cells and tissues, as well as in transplantation experiments, have supported origin of these sarcomas from bone marrow derived cells of the mononuclear phagocyte system, that is histiocytes/macrophages (Binder et al., 1992; Hagari and Yumoto, 1987; Ozzello et al., 1963; Shirasuna et al., 1985; Strauchen and Dimitriu-Bona, 1986; Yamate et al., 1991; Yumoto and Morimoto, 1980). However, later observations based on advanced ultrastructural and immunohistochemical characterization of neoplastic cells, as well

as studies of sequential evaluation of sarcoma formation in rats and mice, favor a view that UPS/malignant fibrous histiocytomas originate from fibroblastic or mesenchymal precursor/stem cells (Fu et al., 1975; Hoffman and Dickersin, 1983; Mackall et al., 2002; Nikitin, 1993; Takeya et al., 1995). These studies have also demonstrated that UPS/MFH frequently contain a large number of non neoplastic infiltrating macrophages (Kato et al., 1990; Roessner et al., 1987; Takeya et al., 1995; Takeya et al., 1991). Consistent with those reports we observed that cells expressing macrophage markers F4/80 and/or Iba1 do not have neoplastic morphology and lack Cre-*loxP* mediated recombination,

Some UPS may represent other STS that exhibit high degree of phenotypical plasticity during tumor progression (Brooks, 1986; Dehner, 1988; Fletcher, 1992; Hollowood and Fletcher, 1995; Katenkamp, 1988). However, findings of MFH-specific genomic alterations (Mairal et al., 1999; Mandahl et al., 1989; Meltzer et al., 1991) and gene expression profiles (Nielsen et al., 2002; Segal et al., 2003) indicate that diagnosis of UPS/MFH corresponds to a distinct nosologic entity and may reflect development of these neoplasms from MSC.

Recent progress in isolation of MSC and their potential use in therapeutic approaches (Mata et al., 2002; Toma et al., 2001) have renewed interest in assessment of transformation potential of these cells. By using human bone marrow MSC Matushansky et al. (Matushansky et al., 2007) demonstrated that expression pattern of these cells correlates with that of UPS/MFH. Furthermore, they demonstrated that MSC immortalized with SV-40 large T antigen recapitulated UPS/MFH morphology after subcutaneous transplantation into nude mice. Consistently, formation of UPS was reported after transplantation of bone marrow derived mouse MSC treated with 2-methylcholanthrene (Li et al., 2009). Intriguingly, it has been reported that according

to cell lineage tracing experiments in irradiation chimeras, spontaneous fibrosarcomas arise from bone marrow-derived cells in the mouse (Li et al., 2007).

To evaluate a possibility of bone marrow origin of STS in our model, we have performed irradiation chimera experiments in which donor and recipient cells carried floxed copies of *p53* and *Rb*. Given 24% reconstitution of dermal macrophage population in irradiation chimeras, 70% frequency of UPS in our model and near equal infectivity of macrophages and fibroblasts by adenovirus, one would expect that sarcomas in 6 to 7 mice could arise from macrophages. However, none of 38 mice developed STS from bone marrow with floxed *p53* and *Rb*. These results provide the direct experimental evidence that UPS/MFH do not arise from macrophages and indicate that initiation of sarcomas from bone marrow derived cells is unlikely.

To test if STS may preferentially arise from local resident MSC following *p53* and *Rb* inactivation we have isolated dermal mesenchymal stem/progenitors cells based on their adherence to plastic and expression of Sca-1 marker. Current methods for dissociating and isolating cell populations from the dermal are quite variable (Fernandes et al., 2004; Gawronska-Kozak, 2004; Rim et al., 2005; Shi and Cheng, 2003; Toma et al., 2001; Wilson et al., 2002) and different isolation techniques lead to enrichment of prospective stem cells with markedly differing characteristics. For example, skin-derived precursor cells which form spherical aggregates are capable of differentiating into multiple lineages, including cells of the nervous system and mesoderm (Fernandes et al., 2004; Toma et al., 2001). At the same time, plastic adherent cells of the dermis have proven to be capable of differentiating along classic mesenchymal lineages (Gawronska-Kozak, 2004; Rim et al., 2005; Shi and Cheng, 2003).

We concentrated on the plastic adherent dermal (PAD) cells for several reasons. First of all, PAD cells expressed adenovirus delivered vectors at much high levels than

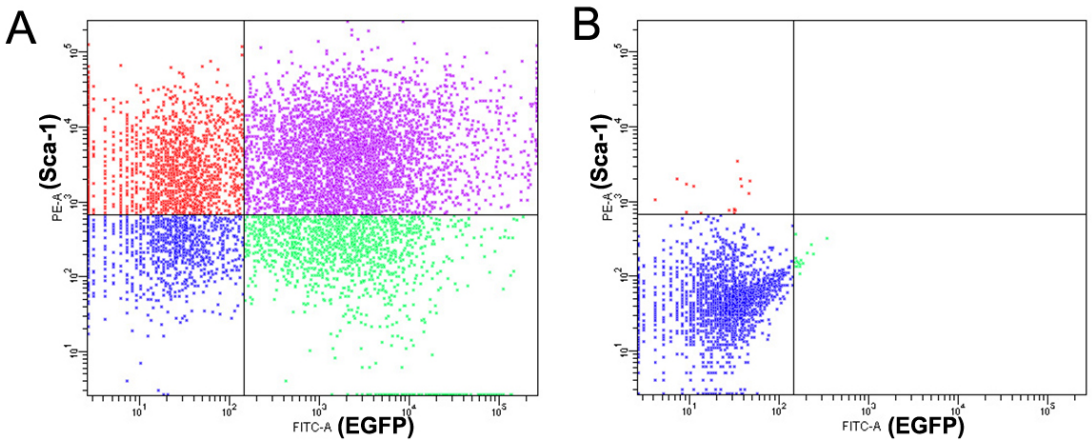

Figure 2.9. EGFP and Sca-1 expression in one week cultured murine dermal cells after adenovirus-induced EGFP expression. Sca-1 expression (Y-axis) and EGFP expression (X-axis) was measured by flow cytometry for both plastic adherent (A) and suspension cells (B).

their suspension counterparts (Figure 2.9). Since our model is based on adenovirus delivery of Cre-recombinase, we can assume that PAD cells in $p53^{loxP/loxP}Rb^{loxP/loxP}$ mice are more readily infected by Ad*CMVCre* and, therefore, are preferentially transformed by Cre-*loxP*-mediated gene inactivation. Additionally, our soft tissue sarcoma model does not display any tumors of neuronal origin, but does result in the formation of many tumors of mesenchymal origin. Shi, et al. (Shi and Cheng, 2003) has shown that strict selection for plastic adherence, within the population of cells isolated from the rodent dermis, will enrich for multipotent dermal cells. Similar observations have been reported for MSC derived from adipose tissue (Rodriguez et al., 2009).

We decided to further purify MSC population by using Sca-1 (Ly-6A/E) expression in combination with negative selection for CD45 and CD31. Sca-1 has been shown to be an effective marker for stem cells in many different tissues, including MSC (Meirelles Lda and Nardi, 2003; Oh et al., 2004; Sun et al., 2003; Welm et al., 2002; Xin et al., 2005). Interestingly, in our experiments the Sca-1^{low} population was enriched for multipotent cells. It was reported that Sca-1^{low} population was more enriched for stem cells than the expected Sca-1^{high} population in the mammary epithelial cells (Stingl et al., 2006) and low levels of positive staining for Sca-1 were detected in spermatogonial stem cells (Guan et al., 2006). Similar to these observations we also found that prolonged culturing of cells, prior to staining and FACS, induced expression of Sca-1 (Curtis and Nikitin, unpublished observations). Therefore, it is quite possible that the culture step necessary to select for plastic adherence upregulated Sca-1 expression in the PAD cells, throwing off the Sca-1 expression levels that would be expected based on the majority of studies that sort cells prior to any culturing (Kim et al., 2005; Xin et al., 2005).

By using isolated dermal MSC enriched for Sca-1^{low} fraction we were able to demonstrate their increased transformation potential, as comported to more differentiated connective tissue cells of the dermis, after inactivation of *p53* and *Rb*. Interestingly, transformation of dermal MSC resulted in formation of UPS, consistent with previous reports which used bone marrow MSC (Li et al., 2009; Matushansky et al., 2007). At the same time, Rodriguez et al. (Rodriguez et al., 2009) reported formation of fibrosarcomas with areas of adipose tissue differentiation after subcutaneous injection of MSC derived from adipose tissue of $p21^{-/-}$ $p53^{-/-}$ mice into immunodeficient mice. These variations in tumor type may reflect either different differentiation potential of MSC derived from different locations, or gene-dependent differentiation potential.

Recent observations indicate that *p53* and *Rb* tumor suppressors have important functions in stem cells. *p53* has been shown to mediate the onset of senescence of endothelial progenitor cells, to negatively regulate proliferation and survival of neural stem cells, to induce differentiation of embryonic stem cells and to control efficiency of induced pluripotent stem cell generation (Feng et al., 2009; Stingl and Caldas, 2007; Zhao et al., 2008). *Rb* and its pathway are involved in control of stem cell cycle progression, senescence and tissue homeostasis (Galderisi et al., 2006). It has been reported that fibroblasts lacking Rb form spheres and become cancer stem cells (Liu et al., 2009). Notably, p16/Rb and ARF/p53 pathways are extensively connected and may be coordinately regulated by Bmi-1, which is required for maintenance and self-renewal of hematopoietic and neural stem and progenitor cells (Valk-Lingbeek et al., 2004). Consistently it has been demonstrated that combined p53 and Rb deficiency results in prostate cancer arising from the prostate stem cell compartment (Zhou et al., 2007). Further studies of established STS model will address the specific molecular and cellular mechanisms responsible for cooperation of

p53 and Rb in control of MSC and their malignant transformation. It also remains to be addressed if sarcomas with distinct differentiation features, such as leiomyosarcoma and angiosarcoma, originate from MSC or more committed progenitor cells which are less prone to transformation following p53 and Rb inactivation. It is of interest that according to comparative genomic hybridization studies, UPS/MFH share similarities with leiomyosarcomas (Derre et al., 2001; Segal et al., 2003), consistent with frequent observations of areas of smooth muscle differentiation in UPS, including our model.

In conclusion, we have established a genetically engineered mouse model of the STS by temporally and spatially controlled *p53* and *Rb* inactivation in connective tissue cells of the dermis. We have also demonstrated that STS develop locally, most likely from MSC. This mouse model of STS will serve as a valuable basis for future studies of STS pathogenesis, particularly of those for sarcomas with complex genotypes. This model also provides new opportunities for exploration of targeted therapies and screening for novel therapeutic agent to treat the disease.

REFERENCES

Anderson, R. D., Haskell, R. E., Xia, H., Roessler, B. J., and Davidson, B. L. (2000). A simple method for the rapid generation of recombinant adenovirus vectors. Gene Ther *7*, 1034-1038.

Berman, S. D., Calo, E., Landman, A. S., Danielian, P. S., Miller, E. S., West, J. C., Fonhoue, B. D., Caron, A., Bronson, R., Bouxsein, M. L.*, et al.* (2008). Metastatic osteosarcoma induced by inactivation of Rb and p53 in the osteoblast lineage. Proc Natl Acad Sci U S A *105*, 11851-11856.

Binder, S. W., Said, J. W., Shintaku, I. P., and Pinkus, G. S. (1992). A histiocyte-specific marker in the diagnosis of malignant fibrous histiocytoma. Use of monoclonal antibody KP-1 (CD68). Am J Clin Pathol *97*, 759-763.

Brooks, J. J. (1986). The significance of double phenotypic patterns and markers in human sarcomas. A new model of mesenchymal differentiation. Am J Pathol *125*, 113-123.

Chai, Y., Jiang, X., Ito, Y., Bringas, P., Jr., Han, J., Rowitch, D. H., Soriano, P., McMahon, A. P., and Sucov, H. M. (2000). Fate of the mammalian cranial neural crest during tooth and mandibular morphogenesis. Development *127*, 1671-1679.

Choi, J., Burns, A. A., Williams, R. M., Zhou, Z., Flesken-Nikitin, A., Zipfel, W. R., Wiesner, U., and Nikitin, A. Y. (2007). Core-shell silica nanoparticles as fluorescent labels for nanomedicine. J Biomed Opt *12*, 064007.

Collini, P., Sorensen, P. H., Patel, S., Blay, J. Y., Issels, R. D., Maki, R. G., Eriksson, M., and del Muro, X. G. (2009). Sarcomas with spindle cell morphology. Semin Oncol *36*, 324-337.

Corney, D. C., Flesken-Nikitin, A., Godwin, A. K., Wang, W., and Nikitin, A. Y. (2007). MicroRNA-34b and MicroRNA-34c are targets of p53 and cooperate in

control of cell proliferation and adhesion-independent growth. Cancer Res *67*, 8433-8438.

Corney, D. C., Hwang, C. I., Matoso, A., Vogt, M., Flesken-Nikitin, A., Godwin, A. K., Kamat, A. A., Sood, A. K., Ellenson, L. H., Hermeking, H., and Nikitin, A. Y. (2010). Frequent downregulation of miR-34 family in human ovarian cancers. Clin Cancer Res *16*, 1119-1128.

Cui, Y. Z., Hisha, H., Yang, G. X., Fan, T. X., Jin, T., Li, Q., Lian, Z., and Ikehara, S. (2002). Optimal protocol for total body irradiation for allogeneic bone marrow transplantation in mice. Bone Marrow Transplant *30*, 843-849.

Dehner, L. P. (1988). Regressing atypical histiocytosis: the controversy continues. Arch Dermatol *124*, 319-321.

Derre, J., Lagace, R., Nicolas, A., Mairal, A., Chibon, F., Coindre, J. M., Terrier, P., Sastre, X., and Aurias, A. (2001). Leiomyosarcomas and most malignant fibrous histiocytomas share very similar comparative genomic hybridization imbalances: an analysis of a series of 27 leiomyosarcomas. Lab Invest *81*, 211-215.

Engellau, J., Anderson, H., Rydholm, A., Bauer, H. C., Hall, K. S., Gustafson, P., Akerman, M., Meis-Kindblom, J., Alvegard, T. A., and Nilbert, M. (2004). Time dependence of prognostic factors for patients with soft tissue sarcoma: a Scandinavian Sarcoma Group Study of 338 malignant fibrous histiocytomas. Cancer *100*, 2233-2239.

Feng, B., Ng, J. H., Heng, J. C., and Ng, H. H. (2009). Molecules that promote or enhance reprogramming of somatic cells to induced pluripotent stem cells. Cell Stem Cell *4*, 301-312.

Fernandes, K. J., McKenzie, I. A., Mill, P., Smith, K. M., Akhavan, M., Barnabe-Heider, F., Biernaskie, J., Junek, A., Kobayashi, N. R., Toma, J. G., *et al.* (2004). A

dermal niche for multipotent adult skin-derived precursor cells. Nat Cell Biol *6*, 1082-1093.

Flesken-Nikitin, A., Choi, K. C., Eng, J. P., Shmidt, E. N., and Nikitin, A. Y. (2003). Induction of carcinogenesis by concurrent inactivation of p53 and Rb1 in the mouse ovarian surface epithelium. Cancer Res *63*, 3459-3463.

Fletcher, C. D. (1992). Pleomorphic malignant fibrous histiocytoma: fact or fiction? A critical reappraisal based on 159 tumors diagnosed as pleomorphic sarcoma. Am J Surg Pathol *16*, 213-228.

Fu, Y. S., Gabbiani, G., Kaye, G. I., and Lattes, R. (1975). Malignant soft tissue tumors of probable histiocytic origin (malignant fibrous histiocytomas): general considerations and electron microscopic and tissue culture studies. Cancer *35*, 176-198.

Galderisi, U., Cipollaro, M., and Giordano, A. (2006). The retinoblastoma gene is involved in multiple aspects of stem cell biology. Oncogene *25*, 5250-5256.

Gawronska-Kozak, B. (2004). Regeneration in the ears of immunodeficient mice: identification and lineage analysis of mesenchymal stem cells. Tissue Eng *10*, 1251-1265.

Guan, K., Nayernia, K., Maier, L. S., Wagner, S., Dressel, R., Lee, J. H., Nolte, J., Wolf, F., Li, M., Engel, W., and Hasenfuss, G. (2006). Pluripotency of spermatogonial stem cells from adult mouse testis. Nature *440*, 1199-1203.

Guillou, L., and Aurias, A. (2009). Soft tissue sarcomas with complex genomic profiles. Virchows Arch.

Hadjantonakis, A. K., Gertsenstein, M., Ikawa, M., Okabe, M., and Nagy, A. (1998). Generating green fluorescent mice by germline transmission of green fluorescent ES cells. Mech Dev *76*, 79-90.

Hagari, Y., and Yumoto, T. (1987). Experimental tumors of myxoid malignant fibrous histiocytoma and hyaluronic acid production. Acta Pathol Jpn *37*, 975-988.

Hoffman, M. A., and Dickersin, G. R. (1983). Malignant fibrous histiocytoma: an ultrastructural study of eleven cases. Hum Pathol *14*, 913-922.

Hollowood, K., and Fletcher, C. D. (1995). Malignant fibrous histiocytoma: morphologic pattern or pathologic entity? Semin Diagn Pathol *12*, 210-220.

Jemal, A., Siegel, R., Ward, E., Hao, Y., Xu, J., and Thun, M. J. (2009). Cancer statistics, 2009. CA Cancer J Clin *59*, 225-249.

Jiang, X., Rowitch, D. H., Soriano, P., McMahon, A. P., and Sucov, H. M. (2000). Fate of the mammalian cardiac neural crest. Development *127*, 1607-1616.

Jonkers, J., Meuwissen, R., van der Gulden, H., Peterse, H., van der Valk, M., and Berns, A. (2001). Synergistic tumor suppressor activity of BRCA2 and p53 in a conditional mouse model for breast cancer. Nat Genet *29*, 418-425.

Katenkamp, D. (1988). Cellular heterogeneity. Explanation for changing of tumor phenotype and biologic behavior in soft tissue sarcomas. Pathol Res Pract *183*, 698-705.

Kato, T., Takeya, M., Takagi, K., and Takahashi, K. (1990). Chemically induced transplantable malignant fibrous histiocytoma of the rat. Analyses with immunohistochemistry, immunoelectron microscopy and [3H]thymidine autoradiography. Lab Invest *62*, 635-645.

Kauffman, S. L., and Stout, A. P. (1961). Histiocytic tumors (fibrous xanthoma and histiocytoma) in children. Cancer *14*, 469-482.

Kim, C. F., Jackson, E. L., Woolfenden, A. E., Lawrence, S., Babar, I., Vogel, S., Crowley, D., Bronson, R. T., and Jacks, T. (2005). Identification of bronchioalveolar stem cells in normal lung and lung cancer. Cell *121*, 823-835.

Kirsch, D. G., Dinulescu, D. M., Miller, J. B., Grimm, J., Santiago, P. M., Young, N. P., Nielsen, G. P., Quade, B. J., Chaber, C. J., Schultz, C. P., *et al.* (2007). A spatially and temporally restricted mouse model of soft tissue sarcoma. Nat Med *13*, 992-997.

Li, H., Fan, X., Kovi, R. C., Jo, Y., Moquin, B., Konz, R., Stoicov, C., Kurt-Jones, E., Grossman, S. R., Lyle, S., *et al.* (2007). Spontaneous expression of embryonic factors and p53 point mutations in aged mesenchymal stem cells: a model of age-related tumorigenesis in mice. Cancer Res *67*, 10889-10898.

Li, Q., Hisha, H., Takaki, T., Adachi, Y., Li, M., Song, C., Feng, W., Okazaki, S., Mizokami, T., Kato, J., *et al.* (2009). Transformation potential of bone marrow stromal cells into undifferentiated high-grade pleomorphic sarcoma. J Cancer Res Clin Oncol.

Lin, P. P., Pandey, M. K., Jin, F., Raymond, A. K., Akiyama, H., and Lozano, G. (2009). Targeted mutation of p53 and Rb in mesenchymal cells of the limb bud produces sarcomas in mice. Carcinogenesis *30*, 1789-1795.

Liu, Y., Clem, B., Zuba-Surma, E. K., El-Naggar, S., Telang, S., Jenson, A. B., Wang, Y., Shao, H., Ratajczak, M. Z., Chesney, J., and Dean, D. C. (2009). Mouse fibroblasts lacking RB1 function form spheres and undergo reprogramming to a cancer stem cell phenotype. Cell Stem Cell *4*, 336-347.

Mackall, C. L., Meltzer, P. S., and Helman, L. J. (2002). Focus on sarcomas. Cancer Cell *2*, 175-178.

Mairal, A., Terrier, P., Chibon, F., Sastre, X., Lecesne, A., and Aurias, A. (1999). Loss of chromosome 13 is the most frequent genomic imbalance in malignant fibrous histiocytomas. A comparative genomic hybridization analysis of a series of 30 cases. Cancer Genet Cytogenet *111*, 134-138.

Mandahl, N., Heim, S., Willen, H., Rydholm, A., Eneroth, M., Nilbert, M., Kreicbergs, A., and Mitelman, F. (1989). Characteristic karyotypic anomalies identify subtypes of malignant fibrous histiocytoma. Genes Chromosomes Cancer *1*, 9-14.

Marino, S., Vooijs, M., van Der Gulden, H., Jonkers, J., Berns, A. (2000). Induction of medulloblastomas in *p53*-null mutant mice by somatic inactivation of *Rb* in the external granular layer cells of the cerebellum. GENES & DEVELOPMENT *14*, 994-1004.

Mata, A., Boehm, C., Fleischman, A. J., Muschler, G., and Roy, S. (2002). Growth of connective tissue progenitor cells on microtextured polydimethylsiloxane surfaces. J Biomed Mater Res *62*, 499-506.

Matoso, A., Zhou, Z., Hayama, R., Flesken-Nikitin, A., and Nikitin, A. Y. (2008). Cell lineage-specific interactions between Men1 and Rb in neuroendocrine neoplasia. Carcinogenesis *29*, 620-628.

Matushansky, I., Hernando, E., Socci, N. D., Mills, J. E., Matos, T. A., Edgar, M. A., Singer, S., Maki, R. G., and Cordon-Cardo, C. (2007). Derivation of sarcomas from mesenchymal stem cells via inactivation of the Wnt pathway. J Clin Invest *117*, 3248-3257.

McDonald, T. P., Lange, R. D., Congdon, C. C., and Toya, R. E. (1970). Effect of hypoxia, irradiation, and bone marrow transplantation on erythropoietin levels in mice. Radiat Res *42*, 151-163.

Mehta, S. A., Christopherson, K. W., Bhat-Nakshatri, P., Goulet, R. J., Jr., Broxmeyer, H. E., Kopelovich, L., and Nakshatri, H. (2007). Negative regulation of chemokine receptor CXCR4 by tumor suppressor p53 in breast cancer cells: implications of p53 mutation or isoform expression on breast cancer cell invasion. Oncogene *26*, 3329-3337.

Meirelles Lda, S., and Nardi, N. B. (2003). Murine marrow-derived mesenchymal stem cell: isolation, in vitro expansion, and characterization. Br J Haematol *123*, 702-711.

Meltzer, P. S., Jankowski, S. A., Dal Cin, P., Sandberg, A. A., Paz, I. B., and Coccia, M. A. (1991). Identification and cloning of a novel amplified DNA sequence in human malignant fibrous histiocytoma derived from a region of chromosome 12 frequently rearranged in soft tissue tumors. Cell Growth Differ *2*, 495-501.

Mohr, U. (2001). International classification of rodent tumours. The mouse, 1st edition edn (Berlin, Heidelberg, Springer).

Muller, A., Homey, B., Soto, H., Ge, N., Catron, D., Buchanan, M. E., McClanahan, T., Murphy, E., Yuan, W., Wagner, S. N., *et al.* (2001). Involvement of chemokine receptors in breast cancer metastasis. Nature *410*, 50-56.

Nielsen, T. O., West, R. B., Linn, S. C., Alter, O., Knowling, M. A., O'Connell, J. X., Zhu, S., Fero, M., Sherlock, G., Pollack, J. R., *et al.* (2002). Molecular characterisation of soft tissue tumours: a gene expression study. Lancet *359*, 1301-1307.

Nikitin, A. Y., Rajewsky, M. F., Pozharisski, K. M. (1993). Development of malignant fibrous histiocytoma induced by 7,12-dimethylbenz[a]anthracene in the rat: characterization of early atypical cells. Virchows Arch B Cell Pathol Incl Mol Pathol *64*, 151-159.

Novak, A., Guo, C., Yang, W., Nagy, A., and Lobe, C. G. (2000). Z/EG, a double reporter mouse line that expresses enhanced green fluorescent protein upon Cre-mediated excision. Genesis *28*, 147-155.

O'Brien, J. E., and Stout, A. P. (1964). Malignant fibrous xanthomas. Cancer *17*, 1445-1455.

Oda, Y., Tateishi, N., Matono, H., Matsuura, S., Yamamaoto, H., Tamiya, S., Yokoyama, R., Matsuda, S., Iwamoto, Y., and Tsuneyoshi, M. (2009). Chemokine receptor CXCR4 expression is correlated with VEGF expression and poor survival in soft-tissue sarcoma. Int J Cancer *124*, 1852-1859.

Oda, Y., Yamamoto, H., Tamiya, S., Matsuda, S., Tanaka, K., Yokoyama, R., Iwamoto, Y., and Tsuneyoshi, M. (2006). CXCR4 and VEGF expression in the primary site and the metastatic site of human osteosarcoma: analysis within a group of patients, all of whom developed lung metastasis. Mod Pathol *19*, 738-745.

Oh, H., Chi, X., Bradfute, S. B., Mishina, Y., Pocius, J., Michael, L. H., Behringer, R. R., Schwartz, R. J., Entman, M. L., and Schneider, M. D. (2004). Cardiac muscle plasticity in adult and embryo by heart-derived progenitor cells. Ann N Y Acad Sci *1015*, 182-189.

Ozzello, L., Stout, A. P., and Murray, M. R. (1963). Cultural characteristics of malignant histiocytomas and fibrous xanthomas. Cancer *16*, 331-344.

Rim, J. S., Mynatt, R. L., and Gawronska-Kozak, B. (2005). Mesenchymal stem cells from the outer ear: a novel adult stem cell model system for the study of adipogenesis. Faseb J *19*, 1205-1207.

Rodriguez, R., Rubio, R., Masip, M., Catalina, P., Nieto, A., de la Cueva, T., Arriero, M., San Martin, N., de la Cueva, E., Balomenos, D.*, et al.* (2009). Loss of p53 induces tumorigenesis in p21-deficient mesenchymal stem cells. Neoplasia *11*, 397-407.

Roessner, A., Vassallo, J., Vollmer, E., Zwadlo, G., Sorg, C., and Grundmann, E. (1987). Biological characterization of human bone tumors. X. The proliferation behavior of macrophages as compared to fibroblastic cells in malignant fibrous histiocytoma and giant cell tumor of bone. J Cancer Res Clin Oncol *113*, 559-562.

Scala, S., Ottaiano, A., Ascierto, P. A., Cavalli, M., Simeone, E., Giuliano, P., Napolitano, M., Franco, R., Botti, G., and Castello, G. (2005). Expression of CXCR4

predicts poor prognosis in patients with malignant melanoma. Clin Cancer Res *11*, 1835-1841.

Segal, N. H., Pavlidis, P., Antonescu, C. R., Maki, R. G., Noble, W. S., DeSantis, D., Woodruff, J. M., Lewis, J. J., Brennan, M. F., Houghton, A. N., and Cordon-Cardo, C. (2003). Classification and subtype prediction of adult soft tissue sarcoma by functional genomics. Am J Pathol *163*, 691-700.

Shi, C., and Cheng, T. (2003). Effects of acute wound environment on neonatal rat dermal multipotent cells. Cells Tissues Organs *175*, 177-185.

Shirasuna, K., Sugiyama, M., and Miyazaki, T. (1985). Establishment and characterization of neoplastic cells from a malignant fibrous histiocytoma. A possible stem cell line. Cancer *55*, 2521-2532.

Soriano, P. (1999). Generalized lacZ expression with the ROSA26 Cre reporter strain. Nat Genet *21*, 70-71.

Stingl, J., and Caldas, C. (2007). Molecular heterogeneity of breast carcinomas and the cancer stem cell hypothesis. Nat Rev Cancer *7*, 791-799.

Stingl, J., Eirew, P., Ricketson, I., Shackleton, M., Vaillant, F., Choi, D., Li, H. I., and Eaves, C. J. (2006). Purification and unique properties of mammary epithelial stem cells. Nature *439*, 993-997.

Strahm, B., Durbin, A. D., Sexsmith, E., and Malkin, D. (2008). The CXCR4-SDF1alpha axis is a critical mediator of rhabdomyosarcoma metastatic signaling induced by bone marrow stroma. Clin Exp Metastasis *25*, 1-10.

Stratton, M. R., Moss, S., Warren, W., Patterson, H., Clark, J., Fisher, C., Fletcher, C. D., Ball, A., Thomas, M., Gusterson, B. A., and Cooper, C. S. (1990). Mutation of the p53 gene in human soft tissue sarcomas: association with abnormalities of the RB1 gene. Oncogene *5*, 1297-1301.

Strauchen, J. A., and Dimitriu-Bona, A. (1986). Malignant fibrous histiocytoma. Expression of monocyte/macrophage differentiation antigens detected with monoclonal antibodies. Am J Pathol *124*, 303-309.

Sun, S., Guo, Z., Xiao, X., Liu, B., Liu, X., Tang, P. H., and Mao, N. (2003). Isolation of mouse marrow mesenchymal progenitors by a novel and reliable method. Stem Cells *21*, 527-535.

Taichman, R. S., Cooper, C., Keller, E. T., Pienta, K. J., Taichman, N. S., and McCauley, L. K. (2002). Use of the stromal cell-derived factor-1/CXCR4 pathway in prostate cancer metastasis to bone. Cancer Res *62*, 1832-1837.

Takeya, M., Yamashiro, S., Yoshimura, T., and Takahashi, K. (1995). Immunophenotypic and immunoelectron microscopic characterization of major constituent cells in malignant fibrous histiocytoma using human cell lines and their transplanted tumors in immunodeficient mice. Lab Invest *72*, 679-688.

Takeya, M., Yoshimura, T., Leonard, E. J., Kato, T., Okabe, H., and Takahashi, K. (1991). Production of monocyte chemoattractant protein-1 by malignant fibrous histiocytoma: relation to the origin of histiocyte-like cells. Exp Mol Pathol *54*, 61-71.

Tasso, R., Augello, A., Carida, M., Postiglione, F., Tibiletti, M. G., Bernasconi, B., Astigiano, S., Fais, F., Truini, M., Cancedda, R., and Pennesi, G. (2009). Development of sarcomas in mice implanted with mesenchymal stem cells seeded onto bioscaffolds. Carcinogenesis *30*, 150-157.

Toma, J. G., Akhavan, M., Fernandes, K. J., Barnabe-Heider, F., Sadikot, A., Kaplan, D. R., and Miller, F. D. (2001). Isolation of multipotent adult stem cells from the dermis of mammalian skin. Nat Cell Biol *3*, 778-784.

Valk-Lingbeek, M. E., Bruggeman, S. W., and van Lohuizen, M. (2004). Stem cells and cancer; the polycomb connection. Cell *118*, 409-418.

Walkley, C. R., Qudsi, R., Sankaran, V. G., Perry, J. A., Gostissa, M., Roth, S. I., Rodda, S. J., Snay, E., Dunning, P., Fahey, F. H., *et al.* (2008). Conditional mouse osteosarcoma, dependent on p53 loss and potentiated by loss of Rb, mimics the human disease. Genes Dev *22*, 1662-1676.

Weiss, S. W., and Goldblum, J. R. (2008). Enzinger & Weiss's Soft tissue tumors Fifth Edition edn (Philadelphia, Mosby, Inc., affiliate of Elsevier, Inc.).

Welm, B. E., Tepera, S. B., Venezia, T., Graubert, T. A., Rosen, J. M., and Goodell, M. A. (2002). Sca-1(pos) cells in the mouse mammary gland represent an enriched progenitor cell population. Dev Biol *245*, 42-56.

Wilson, L., Fathke, C., and Isik, F. (2002). Tissue dispersion and flow cytometry for the cellular analysis of wound healing. Biotechniques *32*, 548-551.

Xin, L., Lawson, D. A., and Witte, O. N. (2005). The Sca-1 cell surface marker enriches for a prostate-regenerating cell subpopulation that can initiate prostate tumorigenesis. Proc Natl Acad Sci U S A *102*, 6942-6947.

Yamate, J., Tajima, M., Togo, M., Shibuya, K., Ihara, M., and Kudow, S. (1991). Heterogeneity of cloned cell lines established from a transplantable rat malignant fibrous histiocytoma. Jpn J Cancer Res *82*, 298-307.

Yasumoto, K., Koizumi, K., Kawashima, A., Saitoh, Y., Arita, Y., Shinohara, K., Minami, T., Nakayama, T., Sakurai, H., Takahashi, Y., *et al.* (2006). Role of the CXCL12/CXCR4 axis in peritoneal carcinomatosis of gastric cancer. Cancer Res *66*, 2181-2187.

Yumoto, T., and Morimoto, K. (1980). Experimental approach to fibrous histiocytoma. Acta Pathol Jpn *30*, 767-778.

Zhao, Y., Yin, X., Qin, H., Zhu, F., Liu, H., Yang, W., Zhang, Q., Xiang, C., Hou, P., Song, *Z., et al.* (2008). Two supporting factors greatly improve the efficiency of human iPSC generation. Cell Stem Cell *3*, 475-479.

Zhou, Z., Flesken-Nikitin, A., Corney, D. C., Wang, W., Goodrich, D. W., Roy-Burman, P., and Nikitin, A. Y. (2006). Synergy of p53 and Rb deficiency in a conditional mouse model for metastatic prostate cancer. Cancer Res *66*, 7889-7898.

Zhou, Z., Flesken-Nikitin, A., and Nikitin, A. Y. (2007). Prostate cancer associated with p53 and Rb deficiency arises from the stem/progenitor cell-enriched proximal region of prostatic ducts. Cancer Res *67*, 5683-5690.

*CHAPTER 3

Core-shell silica nanoparticles as fluorescent labels for nanomedicine

3.1 Abstract

Progress in biomedical imaging depends on the development of probes which combine low toxicity with high sensitivity, resolution and stability. Towards that end, a new class of highly fluorescent core-shell silica nanoparticles with narrow size distributions and enhanced photostability, known as C dots, provide an appealing alternative to quantum dots. Here C dots are evaluated with a particular emphasis on *in vivo* applications in cancer biology. It is established that C dots are non-toxic at biologically-relevant concentrations and can be used in a broad range of imaging applications including intravital visualization of capillaries and macrophages, sentinel lymph node mapping, and peptide-mediated multi-color cell labeling for real-time imaging of tumor metastasis and tracking of injected bone marrow cells in mice. These results demonstrate that fluorescent core-shell silica nanoparticles represent a powerful novel imaging tool within the emerging field of nanomedicine.

3.2 Introduction

Advances in biomedical imaging are expected to improve disease detection and staging, facilitate treatment selection and monitoring, accelerate our understanding of disease pathogenesis and, together with the development of more selective and higher-affinity targeted diagnostic and therapeutic agents, lead to the transformation of general clinical practice towards personalized medicine. Among current challenges for effective translation of newly developing biomedical imaging technologies into

* Published previously as Choi, J., Burns, A.A., Williams, R.M., Zhou, Z. Flesken-Nikitin, A., Zipfel, W.R., Wiesner, U., Nikitin, A.Y. (2007) Core-shell silica nanoparticles as fluorescent labels for nanomedicine. *J Biomed Opt*. 12(6):064007

clinical settings is identification of the most promising versatile, biocompatible, and non-toxic optical probes. In recent years, a variety of nanomaterials including quantum dots (QDs`; Alivisatos et al., 2005; Kim et al., 2004; Larson et al., 2003; Medintz et al., 2005; Michalet et al., 2005; Stroh et al., 2005), metal nanoshells (Hirsch et al., 2003), gold and functional silica nanoparticles (Burns et al., 2006a) have begun to show their utility in imaging applications promising to realize the tremendous scientific and technological potential of nanobiotechnology (Ferrari, 2005; Guan et al., 2006; Santra et al., 2005a).

Currently, the most prominent class of fluorescent nanoprobes in biological imaging is QDs. They are characterized by outstanding photostability and brightness and have been used for a variety of biomedical applications, such as circulatory system imaging, sentinel lymph node mapping, cellular imaging and *in vivo* cell tracking (Akerman et al., 2002; Albini, 1998; Ballou et al., 2004; Gao et al., 2005; Kim et al., 2004; Portney and Ozkan, 2006; Shiohara et al., 2004; Stroh et al., 2005; Voura et al., 2004).

Although QDs offer a number of potential benefits, several properties limit their widespread application. There are considerable concerns about QD disposal and the toxic heavy metals within the QD core (*i.e.*, cadmium, lead) which can leach into solution and cause harm to both cells in culture and animals (Derfus et al., 2004; Kirchner et al., 2005; Shiohara et al., 2004). Further, the lack of detailed toxicological information on the potential side effects of *in vivo* QD usage raises the question of whether or not these nanoparticles are appropriate for use in biological, and, particularly, clinical applications (Alivisatos et al., 2005; Oberdorster et al., 2005). Quantum dots are natively incompatible with water, and must be coated with a polymer to allow for use in aqueous and biological settings, thus introducing a second foreign material into cells, tissue or living organisms (Nagasaki, 2004). Furthermore,

single colloidal quantum dots emit intermittently due, in part, to uncontrolled surface states, decreasing their usefulness in single particle tracking within live cells or intracellular fluids (Neuhauser, 2000).

Organic and metallorganic dye molecules have long been used for labeling biological samples to increase contrast in both optical and fluorescent analyses (Lakowicz, 2006). For fluorescent analyses, emitters are available in colors spanning the spectrum from ultraviolet to near-infrared wavelengths (300-900 nm). Although there are a wide variety of organic fluorophores available, individual dye molecules may suffer from limited brightness (low absorption cross-section and/or low quantum yield), environment dependent quenching and photobleaching (Wang et al., 2006).

Recent work has shown that the properties of organic fluorophores can be improved by covalently integrating them into the core of a core-shell silica nanoparticle (Figure 3.1a), (Burns et al., 2006a; Ow et al., 2005). These particles, referred to as C dots, can be synthesized with hydrodynamic radii down to 10-15 nm as shown by Transmission Electron Microscopy (Figure 3.1b). Covalent incorporation of dye species such as tetramethylrhodamine isothiocyanate (TRITC, Figure 3.1a) into the pseudo-solid state environment within the silica particle enhances both the brightness and photostability of the dyes, while providing a robust, water-soluble vehicle. As previously reported (Ow et al., 2005), the brightness per C dot is more than an order of magnitude greater than that of the constituent dye, creating a probe with a per-particle brightness within a factor of two to three of QDs of similar hydrodynamic size and emission wavelength. As well, by integrating multiple independent emitters into a single particle, the particles are less prone to stochastic blinking, facilitating sustained imaging of the particles. Under excitation saturation conditions, a single C dot can emit 10 or more photons (depending on the number of

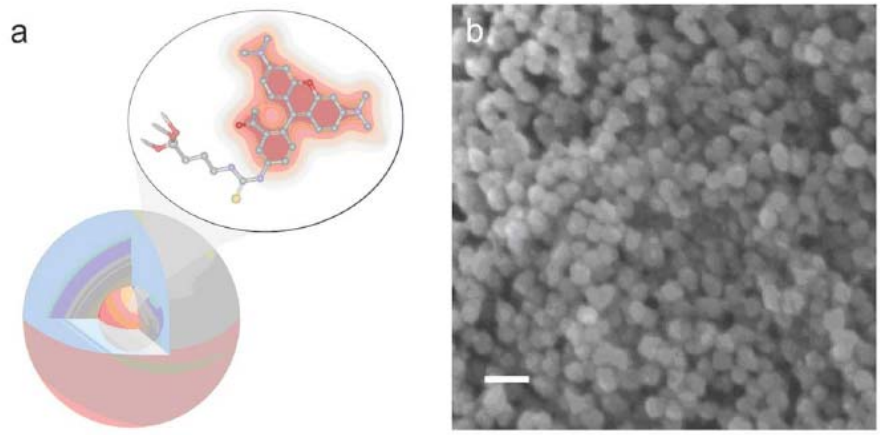

Figure 3.1. C dot core-shell fluorescent silica nanoparticles, shown in schematic form (a) with the covalently bound TRITC dye within the particle core, (b) Scanning Electron Micrographs of 30 nm diameter C dot particles. Scale bar 50 nm. This image was kindly provided by Dr. Ulrich Wiesner and Andrew A. Burns.

individual fluorophores it contains) per particle fluorescence decay time than a single fluorophore. This makes them particularly useful for particle tracking experiments where collecting the maximum number of photons per particle per unit time is critical. Furthermore, this architecture is readily surface-functionalized to facilitate targeting or uptake in biological systems (Ow et al., 2005). Finally, the sol-gel synthesis (Brinker and Scherer, 1990) can be tailored to create particles with narrow particle size distributions and diameters from tens of nanometers up to microns, facilitating size-selective analyses (Ow et al., 2005).

Perhaps the most promising characteristic of C dots is that because they are composed primarily of silica, they are expected to be biologically inert and thus potentially non-toxic for research and biomedical applications. In this study, we evaluate biodistribution and toxicity of these particles and investigate their biomedical utility in a series of *in vivo* experiments.

4.3 Materials and Methods

Animals

Female ICR mice, 7-8 weeks, were purchased from Taconic (Hudson, NY) for the biodistribution and toxicity evaluation. Male SCID/NCr (BALB/C background), 6 weeks, were obtained from the National Cancer Institute (Bethesda, MD) for all other experiments. Six to ten weeks old FVB/N mice (inbred) or transgenic mice that carry GFP driven by chicken β-actin promoter (FVB.Cg-Tg(*ACTB-EGFP*)B5Nagy/J; Strain 003516; The Jackson Laboratory, Bar Harbor, ME) were used for bone marrow collection. All experiments were conducted under identical conditions, following recommendations of the Institutional Laboratory Animal Care and Use Committee of Cornell University.

C Dot Synthesis

Thirty nanometer diameter C dot particles were prepared based on the synthesis reported elsewhere (Herz et al., 2006). Briefly, an organic dye (Tetramethylrhodamine isothiocyanate or Oregon Green 488 isothiocyanate (TRITC or OG488) Invitrogen, Inc.) was dissolved in degassed ethanol (4.57 mM) and conjugated to 3-aminopropyltriethoxysilane (0.228 M) through the isothiocyanate group. This product is reacted with a pure silica precursor (tetraethoxysilane, TEOS, SigmaAldrich, Inc.) in the presence of deionized water (1.24 M) and ammonia (0.855 M) as a catalyst and allowed to react overnight to form dye-rich core particles. These cores are then coated with further TEOS (0.105M) added dropwise over the course of six hours to form the outer shell of the particle. The core-shell particles are allowed to react for a further 24 hours are then dialyzed (Pierce, 3,500 MWCO membrane) to 18.2 MΩ/cm deionized water and analyzed to determine size, concentration and photophysical properties (Ow et al., 2005).

Biodistribution and Toxicity Experiments

Thirty nanometer diameter particles were injected intravenously at 3.3×10^{-7} or 3.3×10^{-8} M in 200 µl of deionized water via the tail vein of mice anaesthetized with Avertin (2.5% v/v in 0.85% NaCl; 0.02 ml/g body weight). For each concentration, at least 3 mice were collected at one, three, seven, twenty-one and sixty days post-injection. As a control, mice were injected with distilled water and collected over the same time schedule. Mice were observed daily and subjected to careful pathological evaluation at the time of necropsy. Brain, thymus, lung, liver, kidney, adrenal gland, ovary, spleen, pancreas, intestine, heart, thigh muscle, and skin were fixed in phosphate-buffered 4% paraformaldehyde and representative specimens were further characterized by microscopic analysis of four micron thick paraffin sections stained

with hematoxylin and eosin following standard practices of toxicologic pathology assessment (Gad, 2007). For evaluation of C dot distribution sections were counterstained with nuclear stain DAPI. Quantitative assessment of fluorescence was performed by using custom image analysis software written using the IDL image analysis platform (Research Systems Incorporated, Boulder CO). C Dots (and cell nuclei) were located by threshholding the blue (and red) channels using the median image value plus five (two) times the image standard deviation. Non-zero regions are eroded, dilated and then enumerated. Each region of fluorescence in the C Dot channel is assigned to the particular nucleus to which it is closest. After collection of at least 5 images for each specimen, all data were expressed as a mean ± standard deviation.

Immunohistochemistry

Deparaffinized sections were exposed to 0.02% trypsin (0.05 M Tris-HCl, pH 7.8, with 1% calcium chloride, 30 min, 37°C) for antigen retrieval. After Avidin/Biotin blocking, samples were incubated with F4/80 antibodies (AbD Serotec, Raleigh, NC) for one hour at room temperature and subsequently treated with 0.3% H_2O_2 in methanol. Following incubation with the secondary biotinylated goat anti-rat antibodies (Vector Labs Inc., Burlingame, CA, 1:100, 30 min, room temperature) and Fluorescein Avidin D (Vector Labs; 3 μg/ml, 30 min, room temperature) the samples were counterstained with DAPI. Samples were mounted with GEL/MOUNT™ (Biomeda Corp. Foster City, CA), sealed with Clarion Mounting Medium (Biomeda Corp. Foster City, CA), and imaged by fluorescence microscopy (Carl Zeiss Axioskop 2).

In vivo capillary and macrophage labeling

Mice were prepared for imaging as previously described (Flesken-Nikitin et al., 2005). Briefly, mice were anesthetized with 3.5 % Isoflurane and placed on a heating pad throughout the experiment. Fur was removed by shaving and Nair® application. 200 µl of 0.33 µM particles were injected into the tail vein for endothelial blood vessel labeling and intradermally for macrophage labeling. The mice were maintained at 1.5 % Isoflurane for anesthesia and were imaged 1.5 hours after particle injection on a multiphoton microscope (Flesken-Nikitin et al., 2005). During imaging, the dorsal skin was immobilized to isolate the imaging area from body motion to facilitate high-resolution imaging.

Sentinel lymph node identification

Forty µl of 0.4 % trypan blue was injected intradermally in the right paw of an anaesthetized mouse. After five minutes, the skin was opened and the lymph node located. 70 µl of 0.33 µM C dots were injected intradermally at the same site on the paw. The lymph node was imaged by brightfield and fluorescence on an Olympus OV100 whole-mouse imaging system (Olympus America Inc., Melville, NY).

C Dot - TAT peptide conjugation

Oligopeptides of the active region of the TAT protein (residues 48-57) were purchased from Sigma-Genosys (The Woodlands, Texas, USA) with a cysteine residue at the C-terminus. To create the peptide-particle conjugates, 3-aminopropyltriethoxysilane (Gelest Inc., Morrisville, PA, USA) was reacted with N-(γ-maleimidobutryloxy)succinimide ester (GMBS, Pierce Inc, Rockford, IL, USA) in a 1:1.5 ratio in DMSO to yield a maleimide-silane. This product was reacted overnight onto the C dot surface in basic ethanol (0.1M NH_4OH). The maleimide-functionalized

particles were then reacted with a 100 times excess of TAT_{48-57} in ethanol to yield peptide-functionalized particles. Finally, the particles were dialyzed overnight to deionized water to remove unreacted peptide and ethanol and filtered through a sterile 0.22 μm PTFE filter.

Establishment of PCN2 and PCN2-EGFP prostate cancer cell lines

Cell line PCN2 was established from prostate carcinoma of 241-day-old *PB-Cre4, $p53^{loxP/loxP}Rb^{loxP/loxP}$* mouse (Zhou et al., 2006). PCN2 tumor cells were cultured in DMEM containing 10% FBS at 37°C in a humidified incubator with 5% CO_2. To prepare PCN2-EGFP cells, PCN2 cells were infected with the pLEGFP-N1 retroviral vector from Clontech (Palo Alto, CA) to introduce EGFP to the cells. Viral supernatant containing EGFP was generated by packaging cell line EcoPack2-293 (Clontech) according to manufacturer's protocols. 1×10^5 PCN2 cells were exposed to viral supernatant containing EGFP in a 6 cm dish at a multiplicity of infection of 1:1 in the presence of 8 μg/ml polybrene (Sigma, St. Louis, MO) for 24 hours. Subsequently, the viral supernatant was replaced with fresh medium. After further incubation for 24 hours, infected PCN2 cells were selected with 600 μg/ml G418 for 2 weeks and EGFP positive cells (PCN2-EGFP) were then sorted by FACS.

C dot labeling in cell culture

$1x10^6$ PCN2 cells were incubated with 1.66 picomol of either nascent or TAT-conjugated 30 nm C dots for two hours, washed three times with PBS, plated on slides and incubated overnight. The following day, the cells were incubated with a lipophilic fluorescent probe (DiO-C_{16} Molecular Probes, Eugene, OR) for plasma membrane staining, washed with PBS, counterstained with DAPI in some experiments, mounted as above on a Leica TCX-SP2 confocal microscope equipped with a 100x oil 1.40 NA

objective with separate excitation for the C dots and DiO-C_{16} (543 nm and 488 nm, respectively).

Isolation and labeling of bone marrow cells with TAT peptide-conjugated particles

Femoral and tibial bone marrow cells were collected from six to ten week old FVB/N or FVB.Cg-Tg(ACTB-EGFP)B5Nagy/J mice by flushing excised and cut leg bones with washing medium (DMEM including 2% FBS). The collected cells were washed twice and filtered through a 70 μm nylon filter (BD biosciences, San Jose, CA) to remove non-cellular material. Isolated bone marrow cells were incubated with TAT conjugated C dots for two hours at $1x10^5$ particles/cell. After incubation and washing, the cells were injected via the tail vein into FVB/N mice irradiated with a lethal dose (11 Gy) of X-rays to ensure removal of their own bone marrow cells. The mice were sacrificed by cervical dislocation 24 hours post-injection and tissue sections were analyzed as above.

Tracking metastatic and/or bone marrow cells

10^6 PCN2-EGFP cells were labeled with TAT-C dots as described for cell culture experiments but without labeling with DiO-C_{16} or DAPI. Following incubation with TAT-C dots for two hours and PBS washing cells were injected via the tail vein. For simultaneous tracking of two types of cells labeled with different color C dots, a mixture of PCN cells, $5x10^5$ cells, labeled with Oregon Green 488-based C dots (green) and bone marrow cells, $5x10^5$ cells, labeled with TRITC-based C dots (red) was injected into mice intravenously. The lung was collected 5 hours post-injection and imaged with multiphoton microscopy.

Statistical analyses

All statistical analyses in this study were done with InStat 3.06 and Prism 4.03 software (GraphPad, Inc., San Diego, CA). Means were compared by estimation of the two-tailed P with Mann-Whitney test. Statistical assessment of multiple samples was performed by one way ANOVA and linear regression as necessary.

4.4 Results

Before investigating biomedical applications of the C dots, we first examined the biodistribution and potential toxicity of C Dots in a mouse model system. No abnormal clinical signs were evident in mice exposed to tetramethylrhodamine (TRITC) dye-based 30 nm diameter core-shell C dots even at the highest technologically possible concentration of 0.33 μM administered in 200 μl of deionized water by tail-vein injection. The mice behaved normally throughout the experiment and showed no pathological alterations in any of the assessed tissues and organs.

Analysis of tissue samples revealed that the C dots were predominantly localized in the spleen, liver and lung (Figure 3.2a, b, 3.3, and 3.4) following their initial appearance in blood vessels throughout the body (Figure 3.5). The particles were mainly localized in the cells of the mononuclear phagocyte system such as F4/80 positive Kupffer cells in the liver (Figure 3.2d). The distribution pattern of C dots in the lung, liver and spleen was found to be time and concentration dependent as measured by a decrease in the number of cells with C dot fluorescence over time (Figure 3.2c, 3.3, and 3.4). At concentration 0.33 μM cells with TRITC-C dots became almost undetectable in the liver between 21 and 60 days post-injection (Figure 3.2c and 3.4). In order to confirm that the observed disappearance of particles was not due to the loss of their fluorescence intensity, we measured the emission of C dots incubated at 37ºC by spectrofluorometry over time relative to samples stored at 4ºC.

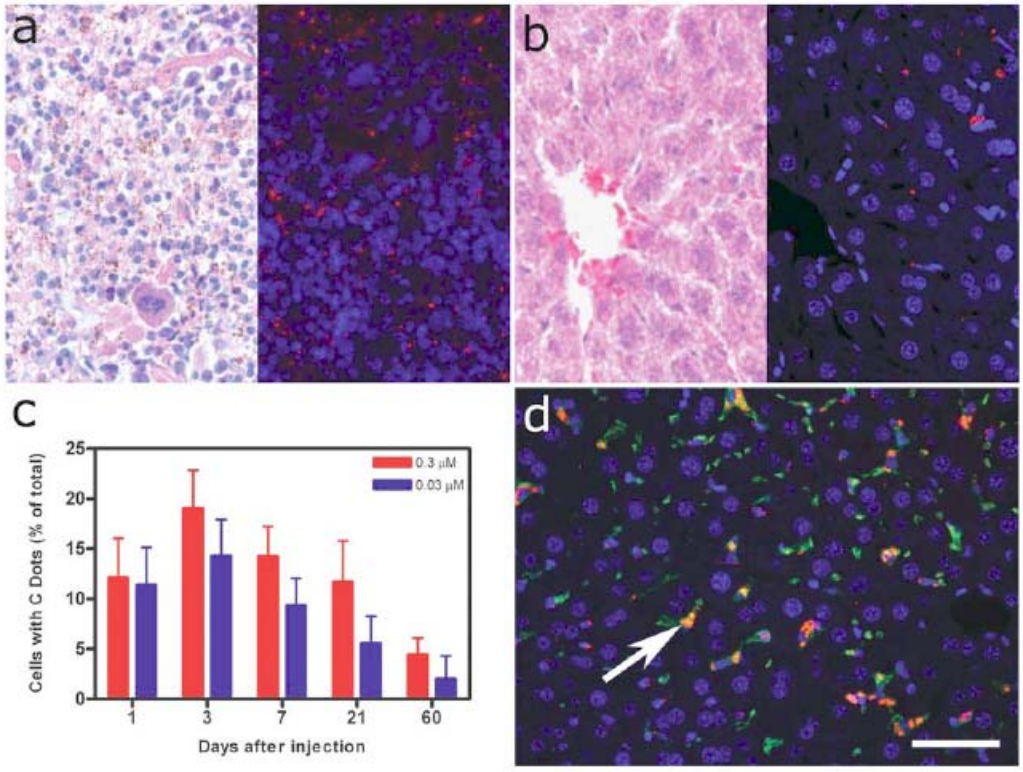

Figure 3.2. **Biodistribution of C dots following tail vein injection.** TRITC-C dots were found to localize predominantly in the spleen (a) and liver (b) with peak levels of particle fluorescence (red) occurring within the first week of intravenous injection (DAPI counterstain). Hematoxylin and Eosin stained parallel sections of spleen and liver show no pathological changes. The number of fluorescent cells (mean ± standard deviation) in the liver was monitored over time (c), showing that the C dots were almost cleared from over the course of approximately 60 days (red; 0.3 μM, blue; 0.03 μM 30 nm C dots). (d) Localization of the C dots within F4/80-positive Kupffer cells (arrow, green) of the liver. FITC Avidin D method. Scale bar: 50 μm.

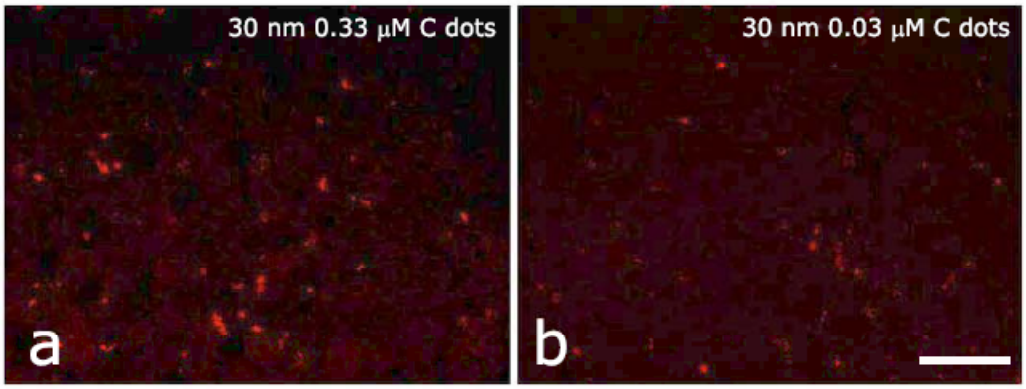

Figure 3.3. **Concentration dependent biodistribution of C dots injected intravenously.** Lung images 3 days after injection of (a), 0.33 μM of and (b), 0.3 μM of C dots. Images show number and intensity of TRITC-C dots in the lung. The scale bar indicates 50 μm.

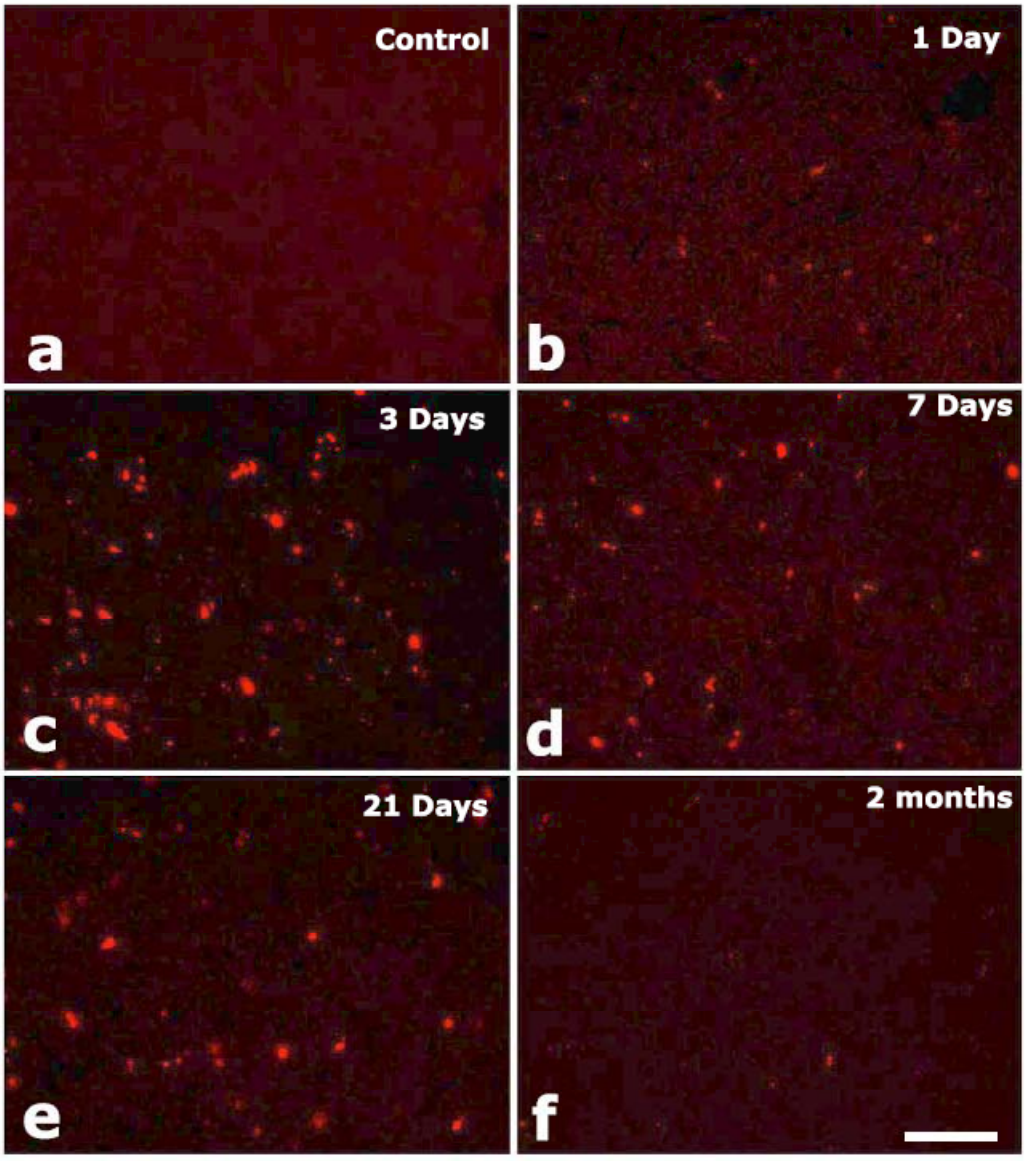

Figure 3.4. **Time dependent biodistribution of 30 nm C dot in the liver after intravenous injection.** (a) control was injected with distilled water, imaged one day post-injection, (b) 0.33 μM TRITC-C dots imaged one day post-injection, (c) three days post-injection, (d) seven days post-injection, (e) 21 days post-injection, and (f) 60 days post-injection. The scale bar indicates 50 μm.

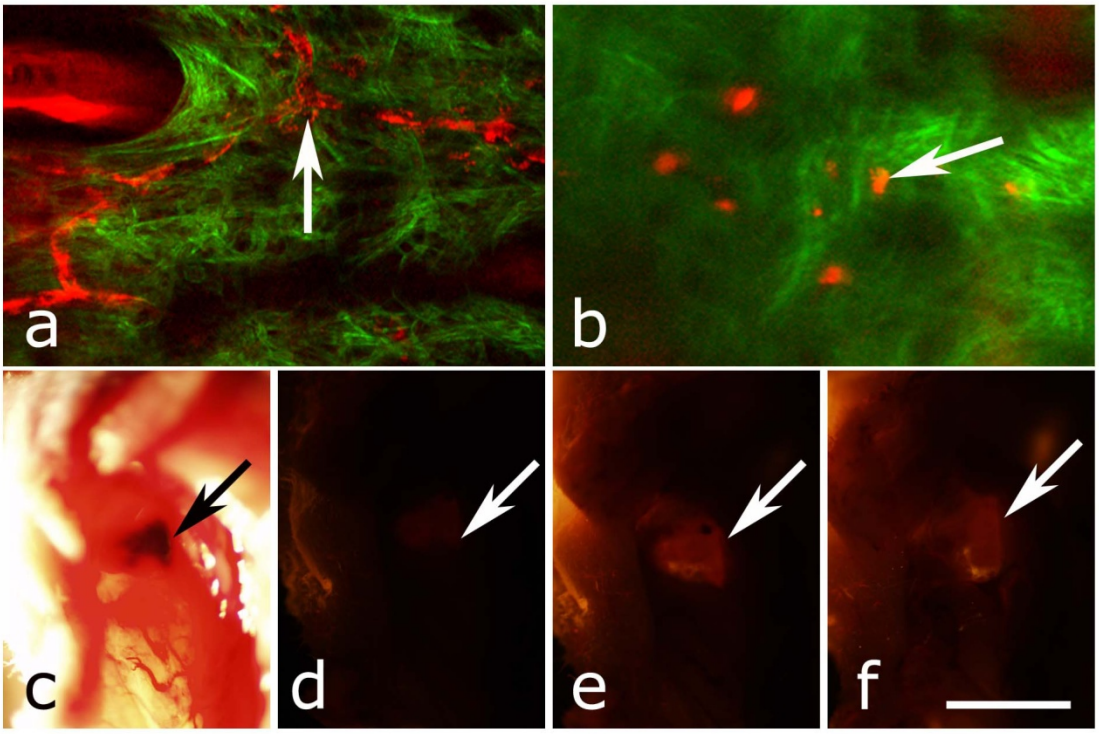

Figure 3.5. (a) Labeling of capillaries with C dots immediately following a tail vein injection of TRITC-C dots, fluorescent capillaries containing C dots (arrow) were clearly visible *in vivo* at the base of the dermis via a multiphoton microscopy. Here imaging was accomplished using 880nm excitation. Second harmonic generation from collagen fibrils is shown in green. Fluorescence emission (500-650 nm) is shown in red. The large red structure in the upper left hand corner is from an autofluorescent hair follicle. The skin was imaged in vivo using the temporary skin immobilizer as described in (Flesken-Nikitin et al., 2005). (b) Labeling of macrophages with C dots. Macrophages (arrow) were detected through the skin of a mouse following intradermal injection of C dots. (c - f) Sentinel lymph node mapping with C dots. The arrow indicates the auxiliary lymph node marked with trypan blue (c). Fluorescent images of the node were taken with the Olympus OV 100 system before (d) and at 1 (e) and 60 (f) minutes after administration of C dots injected at the same site as trypan blue. The scale bar: 75 μm (a), 50 μm (b), and 3 mm (c-f), respectively.

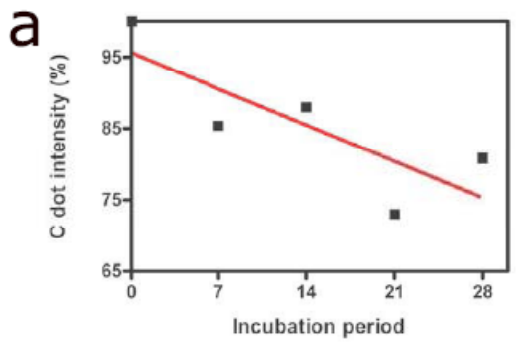

Incubation days	C dot intensity (%)
0	100
7	85
14	88
21	73
28	81

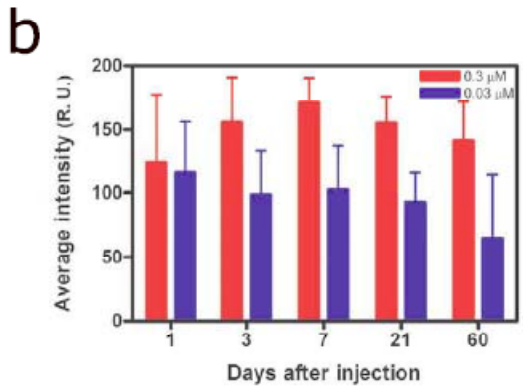

Figure 3.6. **The stability of C dot fluorescence intensity.** (a) The intensity of C dots that were incubated at 37°C *in vitro* only shows a 25% decrease over 4 weeks. The data were analyzed by linear regression (Slope; y= -0.7257x + 95.6, R^2=0.6536). (b) The average intensity of C dots in the liver was fairly stable and unchanged. The average intensity (mean ± standard deviation) indicates the average pixel value of C dots in cells with particles.

This experiment showed that although the particle fluorescence decreased slightly over time, this non-specific degradation was only ~25% per month and could not result in the net loss of fluorescence seen *in vivo* (Figure 3.6a). Although the particle size (30 nm diameter) is too large for excretion through the kidneys and urinary system (Choyke and Kobayashi, 2006), the localization of the particles within the mononuclear phagocyte system indicates that the particles may be scavenged and cleared by macrophages consistently with results from pulmonary silica particle exposure (Adamson et al., 1994; Lee and Kelly, 1992; Oberdorster et al., 2005). This possibility is in agreement with our observation that the average dot fluorescence per cell remained relatively constant (Figure 3.6b).

Having demonstrated the C dots to be a non-toxic and minimally invasive tool for *in vivo* experiments, we sought to demonstrate their capabilities for live animal imaging.

Multiphoton imaging (Figure 3.5a) of intravenously-injected C dots showed appreciable fluorescence within capillaries at the base of the dermis. In addition to intravenous injection, C dots were imaged following sub-cutaneous injection and found to localize within phagocytic cells within 30 minutes of injection (Figure 3.5b).

As a demonstration of the use of C dots as clinical tools for biomedicine, we next tested the particles as tracers for sentinel lymph node mapping. After intradermal injection of Trypan blue followed by TRITC-based C Dots into the mouse paw, the sentinel lymph node was marked by fluorescence in a whole-body imager from thirty seconds post-injection and remained visible up to one hour post-injection (Figure 3.5c-f, and 3.7).

The appeal of fluorescent silica nanoparticles as biological probes comes not only from their bright and stable fluorescence, but also the ability to tune the particle surface towards particular applications. For example, biological applications

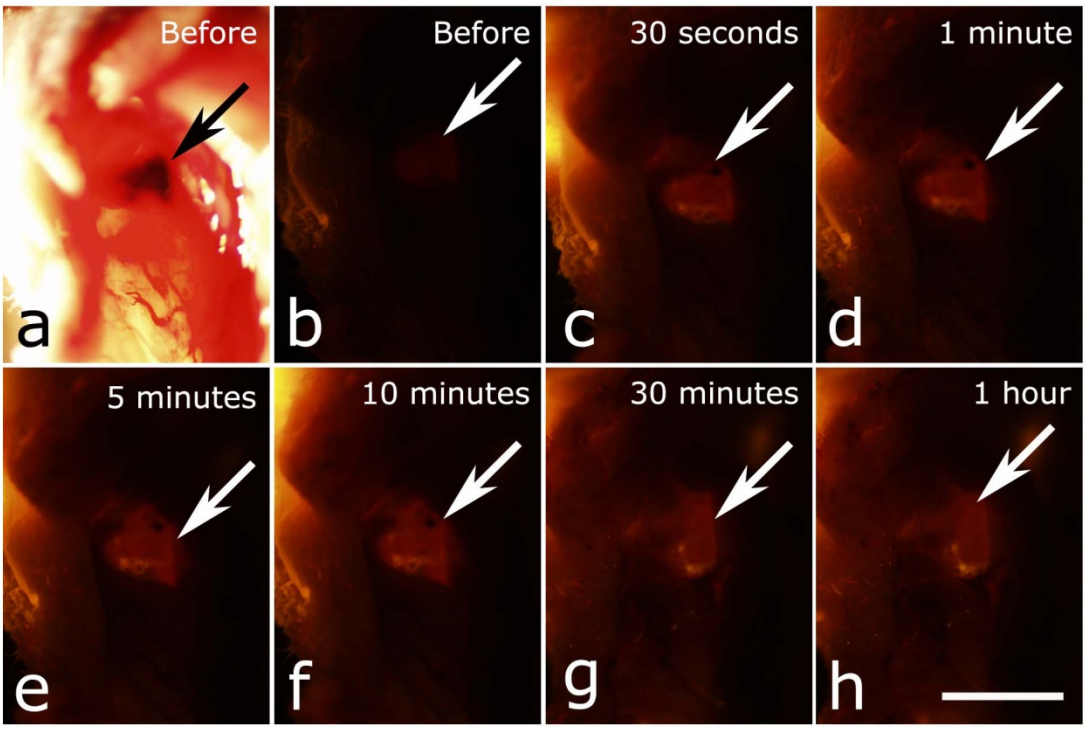

Figure 3.7. Sentinel lymph node mapping with C dots (supplementary images of Figure 3.5.c-f). (a) Identification of the lymph node with trypan blue, (b) before C dot injection, (c) 30 seconds after C dot injection, (d) one minute post-injection, (e) five minutes post-injection, (f) ten minutes post-injection, (g) 30 minutes post-injection, and (h) one hour post-injection. Arrows indicate the auxiliary lymph node. The scale bar indicates 3 mm.

frequently require the labeling of particular cells to facilitate imaging and tracing *in vivo*. Towards that end, cell-penetrating oligopeptides (*e.g.* HIV-1 TAT_{48-57} (Torchilin et al., 2001)) can be covalently bound to the particle surface to mediate cellular uptake (Santra et al., 2005b). We developed conjugation methods for functionalizing 30 nm TRITC-based C dots with TAT peptides. These functionalized particles were found to be readily endocytosed into intracellular vesicles in mouse prostate carcinoma cells (PCN2, Figure 3.8a), while bare particles showed minimal uptake under similar conditions (Figure 3.8b).

TRITC particle-labeled prostate carcinoma cells were introduced into the body intravenously to simulate the release of metastatic cells into the bloodstream by extravasation. Using the fluorescent C dot labels, in conjunction with GFP-expressing PCN2 cells, the cells were found to localize predominantly in the lung of the mouse, where they were imaged via multiphoton imaging (Figure 3.8). This application demonstrates the use of these particles as tags for the tracking and identification of metastatic cells towards a better understanding of the spread of cancer through the body.

This protocol was expanded to label primary bone marrow cells to demonstrate the versatility of TAT-peptide mediated particle uptake. We exposed TAT-conjugated TRITC-based C dots to freshly-harvested bone marrow cells from transgenic mice expressing GFP under the control of chicken β-actin promoter. We then administered the C Dot-labeled cells to irradiated chimeric mice lacking viable bone marrow cells and monitored the distribution of the cells in the body (Figure 3.8d-g). The TAT peptide-mediated labeling of these cells proved effective in tracking their fate following injection into the body, where they were found to localize predominantly in the bone marrow (e), liver (f), and spleen (g).

Figure 3.8. **Labeling and tracing cells with C dots.** PCN2 cells were incubated with TAT-conjugated (a) and bare silica (b) TRITC-C dots for 2 hours at 37 °C, stained with membrane-specific DiO-C_{16} lipophilic probe (green) and imaged by confocal fluorescence microscopy. The TAT-conjugated particles show efficient uptake into vesicles within the cytoplasm, when compared to the bare silica C dots (arrows). (c) Tumor cells expressing GFP (arrow) labeled with TRITC C dots (red) functionalized with TAT-peptide oligomers were imaged in the lung by multiphoton microscopy five hours after tail vein injection. Multiphoton microscopy bis accomplished using 880 nm excitation with two broad emission filters (380-550 nm, green and 550-650 nm, red). Note that non-specific autofluorescnce and second harmonic generation showing lung structure is also visible in the green channel. (d-g) Bone marrow cells (arrows) were collected from transgenic mice that carry GFP-driven by chicken β actin promoter, labeled with TAT-C dots (red) and imaged in bone marrow smear with DAPI labeling (d, e), the liver (f), and the spleen (g) 24 hours after tail vein injection of irradiated recipient mice. The bone marrow cells that contain TRITC-C dots are yellow (e), while those without C-dot labeling are green (d). (h) Metastatic tumor cells labeled with OG488 C dots (green, arrow) and bone marrow cells labeled with TRITC C dots (red, arrowhead) were detected in the lung by multiphoton microscopy. The scale bar indicates 25 μm (a and b), 75 μm (c and h), and 50 μm (d-g) respectively.

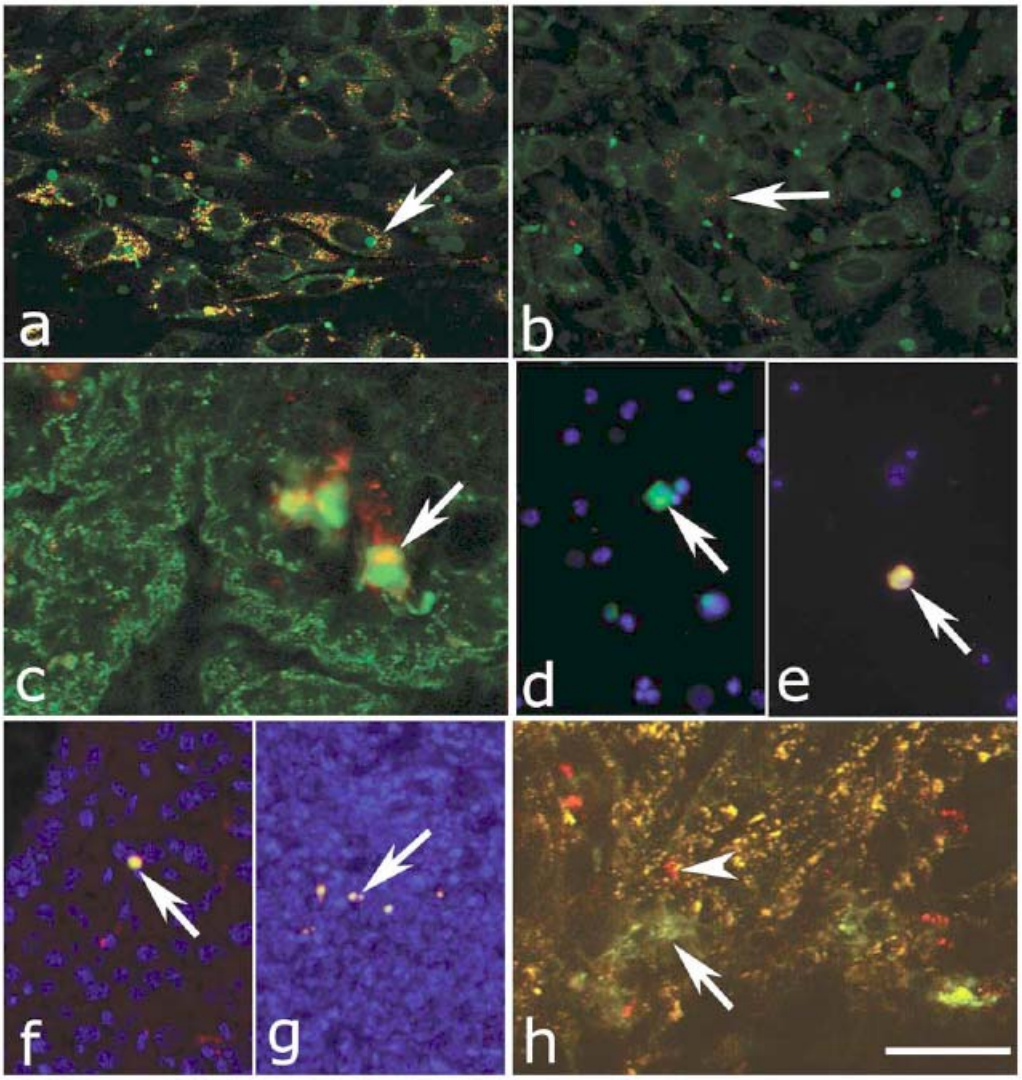
a
b
c
d
e
f
g
h

Finally, we investigated feasibility of labeling different cell types with C dots of different colors. TAT peptide-labeled Oregon Green 488 (OG488) and TRITC-based 30 nm C dots were incubated with PCN2 and bone marrow cells, respectively. Following mixing both cell types and tail vein injection of the combined solution, organs were harvested and imaged using multiphoton microscopy. Optical lung sections collected five hours post-injection showed that both cancer cells (green) and the bone marrow cells (red) can be easily detected (Figure 4.8h). Interestingly, both cell types are commonly found to be co-localized, indicating possible functional interactions between bone marrow and metastatic cells.

3.5 Discussion

Biological safety concerns are among the principle roadblocks on the way towards implementation of imaging nanoparticles into clinical practice. For example, the issue of QD toxicity caused by heavy metals (Cd, Pb, etc) has been raised and is of particular importance for long-term *in vivo* experiments. Recent studies have observed cytotoxicity in hepatocytes (a major target of Cd^{+2} injury), caused by the release of Cd^{+2} ions from the Cadmium selenide (CdSe) QD core due to oxidization by air or UV light (Derfus et al., 2004; Hoshino et al., 2004; Kirchner et al., 2005; Shiohara et al., 2004). Researchers have tried to combat this by applying surface coatings such as ZnS, polymers, or surfactants to reduce the release of heavy metals, but these treatments provide only partial protection to the core (Alivisatos et al., 2005). Additional research has shown that certain QD surface coatings (*e.g.* mercaptoundecanoic acid) can actually decrease cell viability in cell culture studies (Hoshino et al., 2004). These problems have prompted us to test if recently described bright core-shell silica nanoparticles (C dots) could be a feasible alternative to QDs in various biomedical imaging applications.

Available reports on toxicological effects of silica concentrate on pulmonary exposure (rather than intravenous) to simulate human exposure to particulates in air. Toxicological effects of colloidal (amorphous) silica are characterized fairly well as being less toxic than crystalline forms in experimental animals (Kelley and Lee, 1990; Oberdorster et al., 2005). However, there are studies suggesting that inhalation of materials such as colloidal silica by mice induces dose- and size-dependent pulmonary effects, with ultrafine (<100 nm) particles inducing greater lung inflammation and tissue damage than larger particles (Kaewamatawong et al., 2005). Generally, these effects were characterized by an accumulation of particles in alveolar macrophages, neutrophilic infiltration, and type II epithelial cell hyperplasia (Lee and Kelly, 1992; Lee and Kelly, 1993).

In our studies, we have found that 30 nm C dot silica nanoparticles administered by tail-vein injection (rather than inhalation) show no apparent toxicity in mice when compared with control populations, supporting the notion that colloidal (amorphous) silica is less toxic than crystalline silica. The discrepancy with the previous study by Kaewamatawong *et al.* (Kaewamatawong et al., 2005) is likely due to the different administration route of our particles. Thus, functional core-shell silica nanoparticles may represent a valuable materials platform for *in vivo* studies of fundamental biology as well as the development of clinical applications for the particles.

We chose to employ multiphoton microscopy for much of the *in vivo* imaging experiments because of its ability to image deeply in tissue and that it also allows for simultaneous collection of morphological information from intrinsic tissue emitters and collagen second harmonic (Zipfel et al., 2003). In addition, the localized excitation eliminates photobleaching outside of the focal plane compared to single photon wide field or confocal microscopy (Zipfel et al., 2003). This allowed us to

determine the location and trafficking of the particles within the circulatory system as well as within the tissue of the mouse with high signal-to-noise, and may be useful in the future for imaging of, *e.g.*, tumor vasculature or ischemia.

One area where the development of nanoscale tools is of particular interest is cancer research and diagnosis (Santra et al., 2005a). The convergence of sensitive and stable imaging agents(Burns et al., 2006a) with advancements in multiphoton (Zipfel et al., 2003) and whole-body imaging can facilitate studies of both fundamental cancer biology as well as potentially advancing clinical techniques. For example, early detection of cancer dramatically increases survival rates and the use of targeted multifunctional nanoparticle assays with advanced imaging techniques may decrease the detection limit for tumor size to allow treatments to be targeted to tumors before they pose a major threat to the patient.

As well, these particles may allow for greater sensitivity in clinical applications such as sentinel lymph node mapping which has been proven to be an effective method for diagnosis of tumor metastasis and is currently the protocol of choice to determine the likely site of tumor progression (Jakub et al., 2003). In this approach a dye or other tracer is injected in the tumor locale, and visualized as it drains into the lymphatic basin. The sentinel lymph node is the node which collects this tracer and can then be removed for biopsy. Further analysis of the node reveals whether or not any metastatic cells have also drained into the node and provides oncologists with an effective means to monitor the spread of the cancer through the body. Our study demonstrates that the bright and stable fluorescence of the 30 nm C dots make them excellent imaging agents for the identification of sentinel lymph nodes.

Nanoparticle-based probes also facilitate studying fundamental cancer biology. For example, fluorescence imaging provides an excellent tool for following the fate of

metastatic cells as they leave the tumor milieu (Voura et al., 2004). By surface-functionalizing the C dots with cell-penetrating peptides (Santra et al., 2005b; Torchilin et al., 2001), we were able to internally label the cells through particle uptake and track the metastatic prostate carcinoma cells through the body. This method may be employed in the future to study the trafficking of different cancer cells and to determine their response to therapeutic interventions.

One of the rapidly developing areas of metastasis research is understanding of interactions between metastatic and bone marrow cells (Kaplan et al., 2005; Ren et al., 2008). To test for such interactions, we developed a multi-color labeling experiment using different colored TAT-conjugated C dots to label prostate cancer cells and bone marrow cells *in vivo*. We then injected both particles and were able to detect their co-localization by multiphoton microscopy. This work demonstrates versatility of TAT-C dots as tools for the labeling of various cell types and their particular suitability to study interactions between metastatic and bone marrow cells.

In this paper, we have demonstrated the safety, efficacy and utility of fluorescent core-shell silica nanoparticles (C dots) for biomedical applications from research to clinically relevant tools for oncology and beyond. These experiments point to the use of these particles as an appealing alternative to QDs for a variety of *in vivo* applications including immunolabeling, targeted imaging, and cell tracking. Moreover, recent work has shown that the C dot architecture can be built upon further to develop core-shell particles incorporating multiple dye species. One application of these particles is the creation of quantitative ratiometric sensors for analytes such as pH (Burns et al., 2006b) which could be of interest for probing the growth of tumors *in vivo*. In the future, the modular nature of the core-shell architecture may allow creation of multifunctional silica particles, a concept referred to as “lab on a particle” (Burns et al., 2006a), incorporating, *e.g.*, imaging, drug delivery, targeting, and sensing

capabilities into a single probe. In turn, this may lead to the production of highly-integrated and functional nanoparticle platforms for molecular medicine.

REFERENCES

Adamson, I. Y., Prieditis, H., and Bowden, D. H. (1994). Enhanced clearance of silica from mouse lung after instillation of a leukocyte chemotactic factor. Exp Lung Res *20*, 223-233.

Akerman, M. E., Chan, W. C., Laakkonen, P., Bhatia, S. N., and Ruoslahti, E. (2002). Nanocrystal targeting in vivo. Proc Natl Acad Sci U S A *99*, 12617-12621.

Albini, A. (1998). Tumor and endothelial cell invasion of basement membranes. The matrigel chemoinvasion assay as a tool for dissecting molecular mechanisms. Pathol Oncol Res *4*, 230-241.

Alivisatos, A. P., Gu, W., and Larabell, C. (2005). Quantum dots as cellular probes. Annu Rev Biomed Eng *7*, 55-76.

Ballou, B., Lagerholm, B. C., Ernst, L. A., Bruchez, M. P., and Waggoner, A. S. (2004). Noninvasive imaging of quantum dots in mice. Bioconjug Chem *15*, 79-86.

Brinker, C. J., and Scherer, G. W. (1990). Sol-Gel Sceinc: The Physics and Chemistry of Sol-Gel Processing. (Boston, MA, USA, Harcourt Brace Jovanovich).

Burns, A., Ow, H., and Wiesner, U. (2006a). Fluorescent core-shell silica nanoparticles: towards "Lab on a Particle" architectures for nanobiotechnology. Chem Soc Rev *35*, 1028-1042.

Burns, A., Sengupta, P., Zedayko, T., Baird, B., and Wiesner, U. (2006b). Core/Shell Fluorescent Silica Nanoparticles for Chemical Sensing: Towards Single-Particle Laboratories. Small *2*, 723-726.

Choyke, P., and Kobayashi, H. (2006). Functional Magnetic Resonance Imaging of the Kidney using Macromolecular Contrast Agents. Abdominal Imaging *31*, 224-231.

Derfus, A. M., Chan, W. C. W., and Bhatia, S. N. (2004). Probing the cytotoxicity of semiconductor quantum dots. Nano lette *4*, 11-18.

Ferrari, M. (2005). Cancer nanotechnology: opportunities and challenges. Nat Rev Cancer *5*, 161-171.

Flesken-Nikitin, A., Williams, R. M., Zipfel, W. R., Webb, W. W., and Nikitin, A. Y. (2005). Use of multiphoton imaging for studying cell migration in the mouse. Methods Mol Biol *294*, 335-345.

Gad, S. C., ed. (2007). Animal Models in Toxicology, Second edn (Boca Raton, CRC Press).

Gao, X., Yang, L., Petros, J. A., Marshall, F. F., Simons, J. W., and Nie, S. (2005). In vivo molecular and cellular imaging with quantum dots. Curr Opin Biotechnol *16*, 63-72.

Guan, K., Nayernia, K., Maier, L. S., Wagner, S., Dressel, R., Lee, J. H., Nolte, J., Wolf, F., Li, M., Engel, W., and Hasenfuss, G. (2006). Pluripotency of spermatogonial stem cells from adult mouse testis. Nature *440*, 1199-1203.

Herz, E., Burns, A., Lee, S., Sengupta, P., Bonner, D., Ow, H., Liddell, C., Baird, B., and Wiesner, U. (2006). Fluorescent core-shell silica nanoparticles: an alternative radiative materials platform. Paper presented at: Colloidal Quantum Dots for Biomedical Applications (San Jose, CA, USA, SPIE).

Hirsch, L. R., Stafford, R. J., Bankson, J. A., Sershen, S. R., Rivera, B., Price, R. E., Hazle, J. D., Halas, N. J., and West, J. L. (2003). Nanoshell-mediated near-infrared thermal therapy of tumors under magnetic resonance guidance. PNAS *100*, 13549-13554.

Hoshino, A., Fujioka, K., T., O., Suga, M., Sasaki, Y. F., Ohta, T., Yasuhara, M., Suzuki, K., and Yamamoto, K. (2004). Physicochemical Properties and Cellular Toxicity of Nanocrystal Quantum Dots Depend on Their Surface Modification. Nano Lett *4*, 2163 - 2169.

Jakub, J. W., Pendas, S., and Reintgen, D. S. (2003). Current status of sentinel lymph node mapping and biopsy: facts and controversies. Oncologist *8*, 59-68.

Kaewamatawong, T., Kawamura, N., Okajima, M., Sawada, M., Morita, T., and Shimada, A. (2005). Acute pulmonary toxicity caused by exposure to colloidal silica: particle size dependent pathological changes in mice. Toxicol Pathol *33*, 743-749.

Kaplan, R. N., Riba, R. D., Zacharoulis, S., Bramley, A. H., Vincent, L., Costa, C., MacDonald, D. D., Jin, D. K., Shido, K., Kerns, S. A.*, et al.* (2005). VEGFR1-positive haematopoietic bone marrow progenitors initiate the pre-metastatic niche. Nature *438*, 820-827.

Kelley, D. P., and Lee, K. P. (1990). Pulmonary response to Ludox colloidal silica inhalation exposure in rats. Toxicologist *10*, 202A.

Kim, S., Lim, Y. T., Soltesz, E. G., De Grand, A. M., Lee, J., Nakayama, A., Parker, J. A., Mihaljevic, T., Laurence, R. G., Dor, D. M.*, et al.* (2004). Near-infrared fluorescent type II quantum dots for sentinel lymph node mapping. Nat Biotechnol *22*, 93-97.

Kirchner, C., Liedl, T., Kudera, S., Pellegrino, T., Munoz Javier, A., Gaub, H. E., Stolzle, S., Fertig, N., and Parak, W. J. (2005). Cytotoxicity of colloidal CdSe and CdSe/ZnS nanoparticles. Nano Lett *5*, 331-338.

Lakowicz, J. R. (2006). Principles of Fluorescnec Spectroscopy (New York, Springer-Verlag).

Larson, D. R., Zipfel, W. R., Williams, R. M., Clark, S. W., Bruchez, M. P., Wise, F. W., and Webb, W. W. (2003). Water-soluble quantum dots for multiphoton fluorescence imaging in vivo. Science *300*, 1434-1436.

Lee, K. P., and Kelly, D. P. (1992). The pulmonary response and clearance of Ludox colloidal silica after a 4-week inhalation exposure in rats. Fundam Appl Toxicol *19*, 399-410.

Lee, K. P., and Kelly, D. P. (1993). Translocation of particle-laden alveolar macrophages and intra-alveolar granuloma formation in rats exposed to Ludox colloidal amorphous silica by inhalation. Toxicology *77*, 205-222.

Medintz, I. L., Uyeda, H. T., Goldman, E. R., and Mattoussi, H. (2005). Quantum dot bioconjugates for imaging, labelling and sensing. Nat Mater *4*, 435-446.

Michalet, X., Pinaud, F. F., Bentolila, L. A., Tsay, J. M., Doose, S., Li, J. J., Sundaresan, G., Wu, A. M., Gambhir, S. S., and Weiss, S. (2005). Quantum dots for live cells, in vivo imaging, and diagnostics. Science *307*, 538-544.

Nagasaki, Y., Ishii, T., Sunaga, Y., Watanabe, Y., Otsuka, H., Kataoka, K. (2004). Novel Molecular Recognition via Fluorescent Resonance Energy Transfer Using a Biotin-PEG/Polyamine Stabilized CdS Quantum Dot. Langmuir *20*, 6396-6400.

Neuhauser, R. G., Shimizu, K. T., Woo, W. K., Empedocles, S. A., Bawendi, M. G. (2000). Correlation between Fluorescence Intermittency and Spectral Diffusion in Single Semiconductor Quantum Dots. Physical Review Letters *85*, 3301-3304.

Oberdorster, G., Maynard, A., Donaldson, K., Castranova, V., Fitzpatrick, J., Ausman, K., Carter, J., Karn, B., Kreyling, W., Lai, D., *et al.* (2005). Principles for characterizing the potential human health effects from exposure to nanomaterials: elements of a screening strategy. Part Fibre Toxicol *2*, 8.

Ow, H., Larson, D. R., Srivastava, M., Baird, B. A., Webb, W. W., and Wiesner, U. (2005). Bright and stable core-shell fluorescent silica nanoparticles. Nano Lett *5*, 113-117.

Portney, N. G., and Ozkan, M. (2006). Nano-oncology: drug delivery, imaging, and sensing. Anal Bioanal Chem *384*, 620-630.

Ren, Y. X., Finckenstein, F. G., Abdueva, D. A., Shahbazian, V., Chung, B., Weinberg, K. I., Triche, T. J., Shimada, H., and Anderson, M. J. (2008). Mouse

mesenchymal stem cells expressing PAX-FKHR form alveolar rhabdomyosarcomas by cooperating with secondary mutations. Cancer Res *68*, 6587-6597.

Santra, S., Dutta, D., Walter, G., and Moudgil, B. (2005a). Fluorescent Nanoparticle Probes for Cancer Imaging. Technology in Cancer Research and Treatment *4*, 593-602.

Santra, S., Dutta, D., Walter, G. A., and Moudgil, B. M. (2005b). Fluorescent nanoparticle probes for cancer imaging. Technol Cancer Res Treat *4*, 593-602.

Shiohara, A., Hoshino, A., Hanaki, K., Suzuki, K., and Yamamoto, K. (2004). On the cyto-toxicity caused by quantum dots. Microbiol Immunol *48*, 669-675.

Stroh, M., Zimmer, J. P., Duda, D. G., Levchenko, T. S., Cohen, K. S., Brown, E. B., Scadden, D. T., Torchilin, V. P., Bawendi, M. G., Fukumura, D., and Jain, R. K. (2005). Quantum dots spectrally distinguish multiple species within the tumor milieu in vivo. Nat Med *11*, 678-682.

Torchilin, V. P., Rammohan, R., Weissig, V., and Levchenko, T. S. (2001). TAT peptide on the surface of liposomes affords their efficient intracellular delivery even at low temperature and in the presence of metabolic inhibitors. Proc Natl Acad Sci U S A *98*, 8786-8791.

Voura, E. B., Jaiswal, J. K., Mattoussi, H., and Simon, S. M. (2004). Tracking metastatic tumor cell extravasation with quantum dot nanocrystals and fluorescence emission-scanning microscopy. Nat Med *10*, 993-998.

Wang, F., Tan, W. B., Zhang, Y., Fan, X., and Wang, M. (2006). Luminescent nanomaterials for biological labelling. Nanotechnology *17*, R1-R13.

Zhou, Z., Flesken-Nikitin, A., Corney, D. C., Wang, W., Goodrich, D. W., Roy-Burman, P., and Nikitin, A. Y. (2006). Synergy of p53 and Rb deficiency in a conditional mouse model for metastatic prostate cancer. Cancer Res *66*, 7889-7898.

Zipfel, W. R., Williams, R. M., and Webb, W. W. (2003). Nonlinear magic; multiphoton microscopy in the biosciences. Nat Biotech *21*, 1369-1377.

CHAPTER 4

Conclusion and future prospects

4.1. Mouse model of soft tissue sarcoma and its application for histogenesis and pathogenesis studies

By using conditional inactivation of *p53* and *Rb* tumor suppressor genes in dermal connective tissue we established a new mouse model of soft tissue sarcoma (STS). After subcutaneous injection of Ad*CMVCre*, mice with floxed *p53* and *Rb* mainly developed undifferentiated pleomorphic sarcomas (UPS), also known as malignant fibrous histiocytomas (MFH), which are the common human STS. Sarcomas in this temporally and spatially controlled mouse model morphologically closely resemble human STS and contain the most common genetic alterations, that is of *p53* and *Rb* mutations, typical for human STS. Generation of this model has addressed a lack of accurate animal systems to study STS with complex genotypes and UPS in particular.

Our model is very useful for future exploration of the molecular mechanism of sarcomagenesis associated with *p53* and *Rb* deficiency.

Our mouse model demonstrates that a development of STS is a result of cooperation of *p53* and *Rb* inactivation. Several recent reports support this notion. It has been shown that osteosarcoma development is dependent on the loss of *p53* and potentiated by the loss of *Rb* using a mouse model with *Osterix*-Cre-mediated deletion of *p53* and *Rb* (Berman et al., 2008; Walkley et al., 2008). Their acceleration effect has also been reported in another sarcoma model induced by *Prx1*-Cre expression in mesenchymal cells of mouse embryonic limbs (Lin et al., 2009). Importantly, our model allows studying roles of p53 and Rb in adult dermal connective tissue cells.

We found that the sarcomas in our model overexpress Cxcr4 that is thought to be correlated with poor progression in a variety of malignancies (Muller et al., 2001; Oda et al., 2006; Strahm et al., 2008; Taichman et al., 2002). We have confirmed this observation with a human sarcoma tissue array, which shows high expression in UPS compared to dermatofibrosarcoma or fibrosarcoma. A recent work with a large series of human STS also has shown that CXCR4 expression in STS, including UPS, was significantly higher than that in normal tissues and higher levels of expression correlated with poorer prognosis (Oda et al., 2009). This observation further confirms the close resemblance of our model with human STS. Importantly, since it has been reported that CXCR4 is negatively regulated by P53 in breast cancer (Mehta et al., 2007), our model may be very valuable for evaluation of similar molecular mechanism in STS. Such studies may uncover a link between inactivation of *p53* and the cancer progression, including metastasis.

Since MFH identified as a neoplasm containing cells with features of fibroblast and macrophage/histiocyte differentiation (Kauffman and Stout, 1961; O'Brien and Stout, 1964; Ozzello et al., 1963), the issue of its cell of origin has been controversial. Recent studies have mainly supported a view that this type of STS originates from fibroblasts or mesenchymal stem/progenitor cells (Fu et al., 1975; Hoffman and Dickersin, 1983; Mackall et al., 2002; Nikitin, 1993; Takeya et al., 1995). Consistent with this notion, by using bone marrow transplantation chimera model, we demonstrated that sarcomas, UPS/MFH originate from local resident connective tissue cells. Importantly, our observation does not support an earlier study (Li et al., 2007) indicating that STS may arise from bone marrow derived cells directly. In their model, STS, mostly fibrosarcomas, spontaneously developed in aged mice 18 to 24 months after bone marrow transplantation. Unfortunately, direct comparison of these neoplasms with our model is complicated because genetic

alterations initiating sarcomas described by Li et al. are unknown. Furthermore, morpho-functional similarities between sarcomas observed in both studies remain unclear. Future research should determine if all dermal MSC are maintained locally or bone marrow-derived cells contribute to their replenishment.

Using such properties as the plastic adherence and the low level of Sca-1 expression, we isolated dermal MSC and demonstrated their increased transformation potential, as comported to more differentiated connective tissue cells of the dermis, after inactivation of *p53* and *Rb*. The importance of this observation is threefold: (1) dermal mesenchymal stem cells can be isolated by the plastic adherence and Sca-1^{low} fraction, (2) transformation induced by inactivation of *p53* and *Rb* with Ad*CMVCre* occurs preferentially in dermal MSC, (3) these transformed MSC may be a cell of origin of STS. Several studies have reported that sarcomas originate from MSC (Li et al., 2007; Matushansky et al., 2007; Tolar et al., 2007). However, since bone marrow MSC were used in those experiments, their relevance to natural course of the disease has been uncertain.

As described above, our mouse model closely resembles human STS according to a number of morphological and molecular features. We anticipate that use of comparative oncogenomic approach suggests many clues to pathogenesis of human STS. By genome wide gene expression profiling and array comparative genomic hybridization, we may be able to identify potential critical genes and pathways and explore molecular mechanisms essential for sarcomagenesis. Recently, Matushansky et al. (Matushansky et al., 2007) has indicated that UPS/MFH may develop from human MSC transformed via inhibition of Wnt signaling. This suggests that genes associated with Wnt pathway may be selective candidates for further studies.

We demonstrated that UPS/MFH contains a large number of infiltrating macrophages which are derived from bone marrow cells according to bone marrow

transplantation chimera model. However, the role and mechanism of macrophage infiltration in sarcomagenesis remain unclear. This is of particular interest because it has been reported that in many cancers, neoplastic cells produce various chemokines which recruit many inflammatory cells, including macrophages, which, in turn, may facilitate tumor growth or cancer metastasis (Bingle et al., 2002). It has been reported that human derived MFH cells produced monocyte chemoattractant protein-1 (MCP-1) that is released by tumor cells as well as fibroblasts, endothelial cells, and macrophages (Takeya et al., 1995; Takeya et al., 1991). Checking MCP-1 expression in our sarcomas will be a good starting point in this study. Besides MCP-1, other chemokines including macrophage-colony stimulating factor (M-CSF or CSF-1) and vascular endothelial growth factor (VEGF) will be additional candidates to study the mechanism of macrophage infiltration and its roles in sarcoma development.

In order to isolate dermal MSC we used two main characterization of MSC, their plastic adherence and the low level of Sca-1 expression. The development of fluorescence activated cell sorting (FACS) technique and specific cells surface markers allow for an advanced cell based analysis and isolation of pure cell population. Unlike hematopoietic stem cells, cell surface markers for isolation of MSC have not been studied well. Although several markers including Sca-1, c-kit, CD29, CD49a and CD44 have been suggested for MSC isolation (Baddoo et al., 2003; Sun et al., 2003), there are no standard markers established. Therefore, identification and testing of additional candidate markers is required for further enrichment of dermal MSC. Moreover, further development of MSC differentiation assays may provide important clues towards explaining diversity of STS histological patterns.

Given increasing appreciation of potential contributions of *p53* and *Rb* in regulation of stem cells, it will be of a particular interest to study their roles in MSC.

As the first steps, analyses of senescence, apoptosis, proliferation and self-renewal of MSC after inactivation of *p53* and *Rb* will be performed.

Finally, we believe that our STS model can serve as a valuable tool for identification of valid therapeutic targets and development and testing of novel therapeutic approaches. For example, our model would allow preclinical testing of STS treatment by Cxcr4-siRNA administration.

4.2 Applications of core-shell silica nanoparticles in biomedicine and for in vivo imaging study of sarcoma origin

In chapter 3, we described several successful applications of fluorescent core-shell silica nanoparticles (known as C dots) as a powerful imaging tool in biomedicine. Overall in the study, we showed C dots have no apparent toxicity in mice and can be used as a valuable tool in imaging or labeling blood vessels and macrophage and mapping sentinel lymph nodes. Furthermore, C dots can be efficiently functionalized for particular applications, such as TAT-peptide conjugation for enhanced cell penetration, with their ability to tune the particle surface. We finally showed the feasibility of labeling different cell types with multiple colors of C dots.

These data indicate that C dots can be replaced with quantum dots, which are commercially available and widely used in many imaging applications in biomedicine, with non-toxicity, and high sensitivity, resolution, and stability. One of the advantages of C dots is their feasible tunability of the particle surface. This allows increasing targeting selectivity and multifuctionality in therapeutic strategies. In particular, these nanoprobes will improve cancer imaging technologies, starting with the effective early detection of cancer and metastasis lesions and the proficient therapeutic target efficiency to cancer lesions. Beyond cell labeling, targeting imaging and cell tracking, C dots will represent an effective tool in the new advanced nanomedicine with the

modular nature of the C dots architecture that allows highly integrated and functional nanoparticles platforms.

We have successfully visualized blood vessels and individual cells marked with C dots in the dermis of mice *in vivo* through a multiphoton microscopy. Based on these observations, we expect that the *in vivo* imaging will allow monitoring behavior of connective tissue cells after inactivation of *p53* and *Rb*. These studies will provide more clues regarding cellular origin of sarcoma to clarify the correlation between tumor cells and macrophages. In order to further test the hypothesis that UPS/MFH originates from MSC, several *in vivo* imaging experiments will be applied with a variety of fluorescent markers. First of all, chimeric mice carrying $p53^{loxP/loxP}$ and $Rb^{loxP/loxP}$ that contain RFP-expressing bone marrow cells derived from donor transgenic RFP mice can be administrated with Ad*CMVCre-GFP* to induce sarcomas. A chronic-transparent window (skin-flap), where virus was injected, will be visualized by the optical approach with a multiphoton microscopy. This experiment will show the behavior of adenovirus-targeted cells and macrophages individually or their interactions at the stage of tumor initiation. The second approach will be the imaging of macrophage motility towards sarcoma cells orthotopically injected into mouse dermis. Following labeling dermal resident macrophages with red-color C dots by intradermal injection, sarcoma cells labeled with green-color C dots will be administrated into the dermis nearby where macrophages are labeled. Additionally, we might be able to observe that macrophage could be located nearby visualized blood vessels marked with red-color C dots injected intravenously. Macrophages are known to be a stimulant of angiogenesis in tumor progress (Condeelis and Segall, 2003; Jain et al., 2002). Their association could provide us a key in how macrophage affect in sarcoma development.

Furthermore, monitoring reductions in tumor size or metastasis after treatment of tumors by therapeutic agents labeled with fluorescent nanoparticles, for example, injection of CXCR4-siRNA labeled with C dots, by the whole body imaging will provide us visualized cancer treatments which deliver some clues to prevent side effects in early stage.

REFERENCES

Baddoo, M., Hill, K., Wilkinson, R., Gaupp, D., Hughes, C., Kopen, G. C., and Phinney, D. G. (2003). Characterization of mesenchymal stem cells isolated from murine bone marrow by negative selection. J Cell Biochem *89*, 1235-1249.

Berman, S. D., Calo, E., Landman, A. S., Danielian, P. S., Miller, E. S., West, J. C., Fonhoue, B. D., Caron, A., Bronson, R., Bouxsein, M. L., *et al.* (2008). Metastatic osteosarcoma induced by inactivation of Rb and p53 in the osteoblast lineage. Proc Natl Acad Sci U S A *105*, 11851-11856.

Bingle, L., Brown, N. J., and Lewis, C. E. (2002). The role of tumour-associated macrophages in tumour progression: implications for new anticancer therapies. J Pathol *196*, 254-265.

Condeelis, J., and Segall, J. E. (2003). Intravital imaging of cell movement in tumours. Nat Rev Cancer *3*, 921-930.

Fu, Y. S., Gabbiani, G., Kaye, G. I., and Lattes, R. (1975). Malignant soft tissue tumors of probable histiocytic origin (malignant fibrous histiocytomas): general considerations and electron microscopic and tissue culture studies. Cancer *35*, 176-198.

Hoffman, M. A., and Dickersin, G. R. (1983). Malignant fibrous histiocytoma: an ultrastructural study of eleven cases. Hum Pathol *14*, 913-922.

Jain, R. K., Munn, L. L., and Fukumura, D. (2002). Dissecting tumour pathophysiology using intravital microscopy. Nat Rev Cancer *2*, 266-276.

Kauffman, S. L., and Stout, A. P. (1961). Histiocytic tumors (fibrous xanthoma and histiocytoma) in children. Cancer *14*, 469-482.

Li, H., Fan, X., Kovi, R. C., Jo, Y., Moquin, B., Konz, R., Stoicov, C., Kurt-Jones, E., Grossman, S. R., Lyle, S., *et al.* (2007). Spontaneous expression of embryonic factors

and p53 point mutations in aged mesenchymal stem cells: a model of age-related tumorigenesis in mice. Cancer Res *67*, 10889-10898.

Lin, P. P., Pandey, M. K., Jin, F., Raymond, A. K., Akiyama, H., and Lozano, G. (2009). Targeted mutation of p53 and Rb in mesenchymal cells of the limb bud produces sarcomas in mice. Carcinogenesis *30*, 1789-1795.

Mackall, C. L., Meltzer, P. S., and Helman, L. J. (2002). Focus on sarcomas. Cancer Cell *2*, 175-178.

Matushansky, I., Hernando, E., Socci, N. D., Mills, J. E., Matos, T. A., Edgar, M. A., Singer, S., Maki, R. G., and Cordon-Cardo, C. (2007). Derivation of sarcomas from mesenchymal stem cells via inactivation of the Wnt pathway. J Clin Invest *117*, 3248-3257.

Mehta, S. A., Christopherson, K. W., Bhat-Nakshatri, P., Goulet, R. J., Jr., Broxmeyer, H. E., Kopelovich, L., and Nakshatri, H. (2007). Negative regulation of chemokine receptor CXCR4 by tumor suppressor p53 in breast cancer cells: implications of p53 mutation or isoform expression on breast cancer cell invasion. Oncogene *26*, 3329-3337.

Muller, A., Homey, B., Soto, H., Ge, N., Catron, D., Buchanan, M. E., McClanahan, T., Murphy, E., Yuan, W., Wagner, S. N., *et al.* (2001). Involvement of chemokine receptors in breast cancer metastasis. Nature *410*, 50-56.

Nikitin, A. Y., Rajewsky, M. F., Pozharisski, K. M. (1993). Development of malignant fibrous histiocytoma induced by 7,12-dimethylbenz[a]anthracene in the rat: characterization of early atypical cells. Virchows Arch B Cell Pathol Incl Mol Pathol *64*, 151-159.

O'Brien, J. E., and Stout, A. P. (1964). Malignant fibrous xanthomas. Cancer *17*, 1445-1455.

Oda, Y., Tateishi, N., Matono, H., Matsuura, S., Yamamaoto, H., Tamiya, S., Yokoyama, R., Matsuda, S., Iwamoto, Y., and Tsuneyoshi, M. (2009). Chemokine receptor CXCR4 expression is correlated with VEGF expression and poor survival in soft-tissue sarcoma. Int J Cancer *124*, 1852-1859.

Oda, Y., Yamamoto, H., Tamiya, S., Matsuda, S., Tanaka, K., Yokoyama, R., Iwamoto, Y., and Tsuneyoshi, M. (2006). CXCR4 and VEGF expression in the primary site and the metastatic site of human osteosarcoma: analysis within a group of patients, all of whom developed lung metastasis. Mod Pathol *19*, 738-745.

Ozzello, L., Stout, A. P., and Murray, M. R. (1963). Cultural characteristics of malignant histiocytomas and fibrous xanthomas. Cancer *16*, 331-344.

Strahm, B., Durbin, A. D., Sexsmith, E., and Malkin, D. (2008). The CXCR4-SDF1alpha axis is a critical mediator of rhabdomyosarcoma metastatic signaling induced by bone marrow stroma. Clin Exp Metastasis *25*, 1-10.

Sun, S., Guo, Z., Xiao, X., Liu, B., Liu, X., Tang, P. H., and Mao, N. (2003). Isolation of mouse marrow mesenchymal progenitors by a novel and reliable method. Stem Cells *21*, 527-535.

Taichman, R. S., Cooper, C., Keller, E. T., Pienta, K. J., Taichman, N. S., and McCauley, L. K. (2002). Use of the stromal cell-derived factor-1/CXCR4 pathway in prostate cancer metastasis to bone. Cancer Res *62*, 1832-1837.

Takeya, M., Yamashiro, S., Yoshimura, T., and Takahashi, K. (1995). Immunophenotypic and immunoelectron microscopic characterization of major constituent cells in malignant fibrous histiocytoma using human cell lines and their transplanted tumors in immunodeficient mice. Lab Invest *72*, 679-688.

Takeya, M., Yoshimura, T., Leonard, E. J., Kato, T., Okabe, H., and Takahashi, K. (1991). Production of monocyte chemoattractant protein-1 by malignant fibrous histiocytoma: relation to the origin of histiocyte-like cells. Exp Mol Pathol *54*, 61-71.

Tolar, J., Nauta, A. J., Osborn, M. J., Panoskaltsis Mortari, A., McElmurry, R. T., Bell, S., Xia, L., Zhou, N., Riddle, M., Schroeder, T. M., *et al.* (2007). Sarcoma derived from cultured mesenchymal stem cells. Stem Cells *25*, 371-379.

Walkley, C. R., Qudsi, R., Sankaran, V. G., Perry, J. A., Gostissa, M., Roth, S. I., Rodda, S. J., Snay, E., Dunning, P., Fahey, F. H., *et al.* (2008). Conditional mouse osteosarcoma, dependent on p53 loss and potentiated by loss of Rb, mimics the human disease. Genes Dev *22*, 1662-1676.